

Emilie Lundvall and Egil Monsås

# Dramsvegen Panorama – Modal dynamics in tall CLT buildings

Extraction of modal properties by means of frequency domain decomposition and finite element modeling with discrete connections

Master's thesis in Civil- and environmental Engineering

Supervisor: Kjell Arne Malo

Co-supervisor: Saule Tulebekova

June 2022



Emilie Lundvall and Egil Monsås

# **Dramsvegen Panorama – Modal dynamics in tall CLT buildings**

Extraction of modal properties by means of frequency domain decomposition and finite element modeling with discrete connections

Master's thesis in Civil- and environmental Engineering  
Supervisor: Kjell Arne Malo  
Co-supervisor: Saule Tulebekova  
June 2022



Norwegian University of Science and Technology  
Faculty of Engineering  
Department of Structural Engineering





## MASTER THESIS 2022

SUBJECT AREA: <b>Timber Structures, dynamics</b>	DATE: <b>June 9th 2022</b>	NO. OF PAGES: <b>72 + 12 (Appendix)</b>
---	-------------------------------	--

TITLE: <b>Dramsvegen Panorama – Modal analysis in tall CLT buildings</b> Extraction of modal properties by means of <i>frequency domain decomposition</i> and finite element modeling with discrete connections <b>Dramsvegen Panorama – Modalanalyse i høye massivtrehus</b> Bestemmelse av modale egenskaper ved bruk av <i>frequency domain decomposition</i> og elementmetodemodellering ved bruk av diskrete forbindelser	
BY:  Emilie Lundvall  Egil Monsås	 

SUMMARY: <p>Due to the environmental benefits of timber as a building material, there has in the last decade or so, been a significant rise in popularity and interest in timber for construction of tall buildings. One popular timber product for modern buildings is <i>cross laminated timber</i>, CLT. This is a relatively new material, and the number of tall CLT-buildings are very limited. Consequently, the dynamic properties of CLT structures and how to model them accurately and practically is not thoroughly understood.</p> <p>The main goal of this thesis is therefore to investigate the modal properties of two CLT-buildings in Tromsø by using an operational modal analysis (OMA) -procedure called frequency domain decomposition (FDD). Python and MATLAB scripts for processing of raw data and performing the FDD algorithms.</p> <p>In addition to this, a parametric finite element model was developed in Abaqus. This model uses discrete parts for walls and connector springs to model the interaction between CLT elements. The properties of the connectors are controlled by two global parameters that control stiffness, and two parameters that control viscous damping values.</p> <p>Through model updating, the models are able to reproduce the measured frequencies and damping ratios. However, due to differences in the optimized connector parameters for the two buildings, there are doubts about the predictive capability of this modeling approach, especially in its current implementation.</p>
---

RESPONSIBLE TEACHER: <b>Prof. Kjell Arne Malo</b>
SUPERVISOR(S): <b>Prof. Kjell Arne Malo and PhD student Saule Tulebekova</b>
CARRIED OUT AT: <b>Department of Structural Engineering, NTNU</b>



## Preface

This thesis marks the conclusion of the five year master program *Civil and Environmental Engineering* NTNU in Trondheim. It is written for the timber group at the Department of Structural Engineering, and was written over a time period of 20 weeks in the spring of 2022.

The work on the project has been interesting and rewarding. We have learned a lot about the advantages and disadvantages of building with CLT, as well as gaining in-depth knowledge of modeling in Abaqus with python scripting, and how to carry out a dynamic analysis from experimental acceleration data.

We would like to thank our supervisor prof. Kjell Arne Malo and co-supervisor, PhD. candidate Saule Tulebekova for invaluable input and guidance throughout the process, as well as the Department of Structural Engineering at NTNU for providing the acceleration data.

**Emilie Lundvall & Egil Monsås**

Trondheim, June 2022





## Abstract

Due to the environmental benefits of timber as a building material, there has in the last decade or so, been a significant rise in the popularity and interest in timber for construction of tall buildings. One popular timber product in modern projects is *Cross laminated timber*, CLT. This is a relatively new *engineered wood product*, and the number of tall CLT-buildings are very limited. Consequently, the dynamic properties of CLT-structures and how to model the buildings accurately and practically is not thoroughly understood.

The main goal of this thesis is therefore to investigate the modal properties of two CLT-buildings in Tromsø by using an *operational modal analysis* (OMA) -procedure called *frequency domain decomposition* (FDD). Acceleration data from the two buildings taken in the spring of 2021 was made available, and from this, the natural frequencies, mode shapes and damping ratios are found.

In addition to this, a parametric finite element model was developed in Abaqus, by using discrete fasteners called *connectors* to model the joints between the CLT-plates. The stiffness of the connections are controlled by two global parameters: *axial stiffness ratio* (ASR) and *sliding stiffness ratio* (SSR). Damping in the connections is implemented by defining two global viscous damping values, similar to the stiffness parameters, where one covers damping in the axial deflection of connections, and the other covers damping in the sliding of connections.

A parameter optimization of the models is performed to investigate the performance and validity of the modeling scheme. Each model is run with different combinations of ASR and SSR, in order to match the results from the data analysis as closely as possible. This led to the conclusion that the modeling approach is able to reproduce the desired frequencies for both buildings. However, the use of the method to *predict* the dynamic properties of a building is more uncertain, because the interchange of the optimized stiffness ratios of the two buildings does not yield very good results.



## Sammendrag

Som følge av miljøfordelene ved å bygge med trevirke har det de siste ti årene vært en betydelig økning interessen for å bygge høyhus i tre. Et av materialene som har gjort det mulig å bygge såpass høyt, er krysslaminert trevirke (CLT). Dette er et relativt nytt massivtre-produkt, og antallet høye bygninger laget av CLT er derfor begrenset. På grunn av dette er kjennskapen til de dynamiske egenskapene fortsatt usikre, og hvordan man best skal modellere slike bygg er heller ikke fullstendig utforsket.

Hovedmålet med denne masteroppgaven er derfor å undersøke de dynamiske egenskapene til to CLT-bygg i Tromsø ved å bruke en *operasjonell modal analyse* (OMA) kalt *frekvensdomene dekomposisjon* (FDD). De to bygningene ble utstyrt med akselerometre, og akselerasjonsdata ble samlet inn våren 2021. Disse målingene er analysert, og ut i fra dette er de *naturlige frekvensene*, *svingeformene* og *dempningsforholdene* funnet.

I tillegg er en parametrisk elementmodell utviklet i Abaqus ved å bruke diskrete festemidler kalt *connectors* til å modellere sammenføyningene mellom CLT-elementer. Stivheten i disse connectorene kontrolleres av to globale parametre: *aksialt stivhets-forholdstall* (ASR) og *glidnings-stivhetsforholdstall* (SSR). Damping i forbindelser dekkes ved å definere to globale dempingsparametre for viskøs damping i forbindelser. Én dekker damping i aksialdeformasjon i festemidler, den andre dekker damping for glidning i forbindelser.

En parameteroptimalisering av modellene er også gjennomført for å studere hvordan modellen responderer på ulike parametersammensetninger, samt for å vurdere validiteten til modelleringsteknikken. Hver av modellene ble kjørt med ulike sammensetninger av ASR og SSR, for å få resultatene så like de målte verdiene som mulig. Dette førte til konklusjonen at modelleringsteknikken klarer å reprodusere de ønskede modale verdiene for begge bygningene. Samtidig tyder det på at det å skulle bruke metoden for å *predikere* de modale egenskapene til andre bygg er mer usikker, ettersom det å bytte om på de optimaliserte stivhets-forholdstallene for de to bygningene ikke fører til gode resultater.



# Acronyms

**ASR** Axial stiffness ratio

**CLT** Cross-laminated timber

**DFT** Discrete fourier transform

**DOF** Degree of freedom

**DSP** Digital signal processing

**EMA** Experimental modal analysis

**FDD** Frequency domain decomposition

**FEM** Finite element modeling

**IFT** Inverse fourier transform

**MAC** Modal assurance criterion

**MDOF** Multi- degree of freedom

**OMA** Operational modal analysis

**PSD** Power spectral density

**RMS** Root mean square

**SDOF** Single degree of freedom

**SSR** Sliding stiffness ratio

**SVD** Single value decomposition

# List of Figures

- 1.1 Assembly of a CLT plate . . . . . 2
- 1.2 Damping and frequency trends of a selection of tall timber buildings [12] . 3
- 1.3 Dramsvegen panorama . . . . . 4
- 1.4 Dramsvegen panorama . . . . . 4
- 2.1 Cell structure in wood . . . . . 7
- 2.2 Common axis system in timber . . . . . 7
- 2.3 Displacement patterns of CLT-panels . . . . . 9
- 2.4 Damping influence on amplitude . . . . . 10
- 2.5 Free harmonic vibration of damped systems [27] . . . . . 12
- 2.6 General rayleigh damping curve . . . . . 13
- 2.7 Aliasing . . . . . 15
- 2.8 Common band-pass filter types . . . . . 16
- 2.9 Illustration of butterworth filter . . . . . 17
- 2.10 Zero-phase filtering . . . . . 18
- 2.11 Detrending of a signal with a spurious trend . . . . . 19
- 2.12 Zero-centering of a signal with an initial offset . . . . . 20
- 2.13 Example spectrum . . . . . 21
- 2.14 MDOF system spectrum . . . . . 24
- 2.15 Narrow range around identified modes . . . . . 25
- 2.16 Auto-correlation around peaks . . . . . 26
- 2.17 Plot of logarithmic decrement estimate . . . . . 27
- 2.18 A conventional shell element with four nodes. . . . . 29
- 3.1 Flowchart of the data pre-processing and breakdown . . . . . 30
- 3.2 Signal vs noise . . . . . 33
- 4.1 Model overview . . . . . 34
- 4.2 Origin of CLT-stiffness . . . . . 36
- 4.3 Connector stiffness setup . . . . . 37
- 4.4 The CLT plate studied, here with 5 discrete boundary conditions . . . . . 39
- 4.5 Discretization error . . . . . 40

4.6	Mass distributions . . . . .	42
4.7	Investigation regarding choice of mesh density . . . . .	45
5.1	SML3: PSD . . . . .	49
5.2	SML3: Computed mode shapes by FDD, plots . . . . .	50
5.3	SML3: damping ratio estimates . . . . .	51
5.4	SML3: Boxplot . . . . .	52
5.5	SML3: Rayleigh damping . . . . .	53
5.6	SML5: PSD . . . . .	54
5.7	SML5: Computed mode shapes by FDD, plots . . . . .	55
5.8	SML5 damping ratio estimates . . . . .	56
5.9	SML5: Boxplot . . . . .	57
5.10	SML5: Rayleigh damping . . . . .	58
5.11	SML3: FEM mode-shapes . . . . .	59
5.12	SML3: Stiffness parameter optimization . . . . .	60
5.13	SML5: FEM mode-shapes . . . . .	62
5.14	SML5: Stiffness parameter optimization . . . . .	63

# List of Tables

- 4.1 Estimated stiffness of a single connector. (One connector every 300mm) . . . 38
- 4.2 Influence of discrete vs. continuous boundary conditions on the deformation. 40
- 4.3 Material properties used in the model . . . . . 43
- 5.1 SML3: Modal frequencies . . . . . 49
- 5.2 SML3: Computed mode shapes by FDD, grouped by sensors . . . . . 50
- 5.3 SML3: Computed mode shapes by FDD, grouped by axes . . . . . 50
- 5.4 SML3: Damping ratios from FDD . . . . . 51
- 5.5 SML3: Rayleigh damping coefficients . . . . . 53
- 5.6 SML5: Modal frequencies . . . . . 54
- 5.7 SML5: Computed mode shapes by FDD, grouped by sensors . . . . . 55
- 5.8 SML5: Computed mode shapes by FDD, grouped by axes . . . . . 55
- 5.9 SML5: Damping ratios from FDD . . . . . 56
- 5.10 SML5: Rayleigh damping coefficients . . . . . 58
- 5.11 SML3: Frequency optimized models . . . . . 60
- 5.12 SML3: Damping optimized model . . . . . 61
- 5.13 SML5: Frequency optimized models . . . . . 63
- 5.14 SML5: Damping optimized model . . . . . 64
- 6.1 Measured frequency vs prediction . . . . . 66



# Contents

1	Introduction . . . . .	1
1.1	Background . . . . .	1
1.2	Dramsvegen Panorama . . . . .	3
1.3	Previous Work . . . . .	5
1.4	Project Description . . . . .	6
2	Theory . . . . .	7
2.1	Timber Structures . . . . .	7
2.1.1	Material Structure of Wood . . . . .	7
2.1.2	Material Properties of Timber . . . . .	7
2.2	Structural Dynamics . . . . .	9
2.2.1	Equation of Motion . . . . .	9
2.2.2	Natural Frequencies and Modes . . . . .	10
2.2.3	Damping . . . . .	11
2.3	Operational Modal Analysis . . . . .	14
2.3.1	Data Pre-processing . . . . .	14
2.3.2	Natural Frequencies by Peak Picking . . . . .	21
2.3.3	Frequency Domain Decomposition . . . . .	23
2.4	Finite Element Modeling . . . . .	27
2.4.1	Meshing . . . . .	28
2.4.2	Shell Elements . . . . .	28
3	Data Analysis . . . . .	30
3.1	Pre-processing . . . . .	31
3.2	FDD . . . . .	32
3.3	Post-processing . . . . .	33
4	Modeling . . . . .	34
4.1	Defining the Geometry . . . . .	35
4.2	Connections . . . . .	35
4.2.1	Stiffness Ratios in Connections . . . . .	36
4.2.2	Damping in Connections . . . . .	40

4.3	Foundation . . . . .	41
4.4	Mass . . . . .	41
4.5	Loads . . . . .	43
4.6	Materials . . . . .	43
4.7	Analysis Steps . . . . .	44
4.8	Meshing . . . . .	44
4.9	Parameter Optimization . . . . .	46
	4.9.1 Frequency Optimization . . . . .	46
	4.9.2 Damping Optimization . . . . .	47
5	Results . . . . .	48
5.1	Empirical Results . . . . .	48
	5.1.1 SML3 . . . . .	49
	5.1.2 SML5 . . . . .	54
5.2	Modeling Results . . . . .	59
	5.2.1 SML 3 . . . . .	59
	5.2.2 SML 5 . . . . .	62
6	Discussion . . . . .	65
6.1	Analysis of Measurements . . . . .	65
	6.1.1 Comparison of Pre-processing Schemes . . . . .	66
6.2	Comparison of Empirical Results With Other Structures . . . . .	66
6.3	Modeling . . . . .	67
	6.3.1 Comments on Mode Shapes . . . . .	67
	6.3.2 The Modeling Approach . . . . .	68
	6.3.3 Modeling Floors as a Single, Continuous Part . . . . .	68
	6.3.4 The Use of Connectors . . . . .	69
	6.3.5 Frequency Optimization . . . . .	69
	6.3.6 Damping Optimization . . . . .	70
7	Conclusions and Further Work . . . . .	71
7.1	Conclusions . . . . .	71
	7.1.1 Data analysis by FDD . . . . .	71
	7.1.2 Modeling with discrete connectors . . . . .	71
7.2	Further Work . . . . .	72
	7.2.1 Data analysis . . . . .	72
	7.2.2 Modeling . . . . .	72
<b>Appendices</b>		<b>76</b>
<b>A Mass Configuration</b>		<b>A.1</b>
A.1	Estimation of Outer Wall Dead Mass . . . . .	A.2

A.2	SML3 Mass Calculations . . . . .	A.3
A.2.1	Mass Configuration 1 . . . . .	A.3
A.2.2	Mass Configuration 2 . . . . .	A.3
A.3	SML5 Mass Calculations . . . . .	A.4
A.3.1	Mass Configuration 1 . . . . .	A.4
A.3.2	Mass Configuration 2 . . . . .	A.4
<b>B</b>	<b>Parameter Optimization Results</b>	<b>B.1</b>
B.1	SML3 . . . . .	B.2
B.1.1	Mass Configuration 1 . . . . .	B.2
B.1.2	Mass Configuration 2 . . . . .	B.3
B.2	SML5 . . . . .	B.4
B.2.1	Mass Configuration 1 . . . . .	B.4
B.2.2	Mass Configuration 2 . . . . .	B.5
<b>C</b>	<b>Damping Optimization Results</b>	<b>C.1</b>
C.1	SML3 . . . . .	C.2
C.2	SML5 . . . . .	C.2

# 1 Introduction

## 1.1 Background

Timber is a versatile building material with very good environmental properties. Because of this the use of timber, especially in bigger structures, has become a lot more popular in the last twenty years.

Historically, there has been heavy restrictions put on the use of timber in large structures, due to its combustibility [1]. Because of persevering concerns about fires in the past few centuries, timber has been disfavored or even banned to use in larger structures or in densely populated areas. As a consequence brick and later reinforced concrete and steel structures has been the dominating building materials for tall and/or urban structures. In the last 20 years however, there has been many studies exploring the fire behaviour of timber, causing the restrictions to gradually lift[2].

One of the driving forces behind the renewed interest in timber is the increased focus on the environmental impact in the construction sector. The sector as a whole is responsible for 23 % of the global emissions, in addition to consuming huge amounts of non-renewable energy from oil and gas [3]. Timber is renewable, in addition to the fact that the production process demands small amounts of energy compared to cement and steel production. In choosing timber instead, the carbon emissions decrease significantly [4]. Growing support from the public and politicians alike provides a powerful tailwind for the development of timber and wood techniques, both in construction and in the material fabrication processes.

Another factor contributing to the rise in popularity is the development of new engineered wood products like glulam (glued laminated timber), CLT (cross laminated timber) or OSB (oriented strand boards). This has opened up new possibilities allowing engineers to tailor fit the properties of the product to the specified requirements, drastically increasing the applicability of wood-based materials in construction.

## Cross-Laminated Timber (CLT)

*Cross-laminated timber* or CLT, is an engineered wood product, consisting of orthogonal (typically 3 - 7) layers of timber planks glued and pressed into a solid, massive plate element. The planks used are the side-boards left over from sawmilling, taking advantage of the fact that this is where the log has the best material properties, and making sure that there is less waste from the timber production [6].

The resulting plates has a very good strength-to-weight ratio, and are able to carry loads in two directions, making them suitable for both wall- and floor elements. An advantage of using CLT is the fact that the elements are prefabricated, and modern CNC-machining (Computer Numerical Control) allow for complex routings, edge joints, ventilation openings and other types of geometry to be quickly and precisely machined into the elements in the factory, allowing for technical installations to be completed faster. In addition to this, the low density reduces the overall bearing requirements of the building and its foundation. This makes the transportation, handling, and installation easier, which in turn decreases the need for on site infrastructure during construction, and results in a short erection time [7].

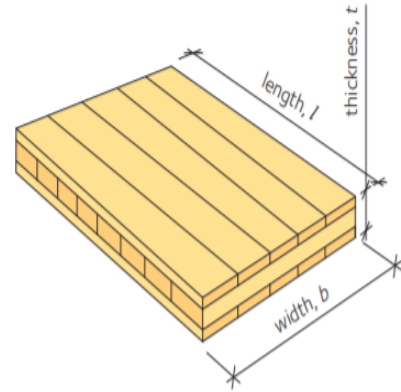


**Figure 1.1:** Assembly of a CLT plate [5]

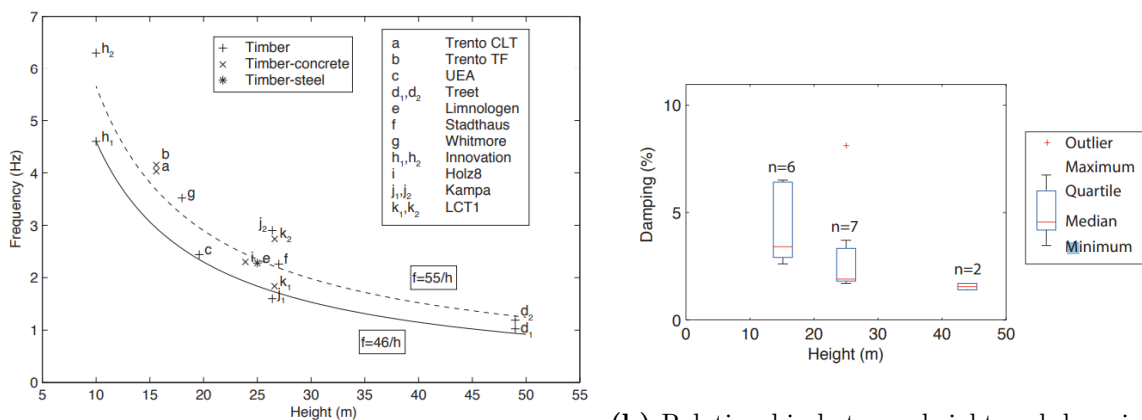
## Dynamics in Timber Buildings

CLT buildings typically have low mass and medium-low stiffness. This in combination with the high in-plane stiffness of the panels as well as the capacity of the connections to resist deformations with little impact on their strength, leads to excellent seismic properties [8]. This allows the buildings to withstand and survive earthquake to a much higher degree than many brick or stone buildings [9]. However, this also means that timber buildings are susceptible to wind-induced motions [10]. While this is not typically a safety concern, excessive swaying motions in buildings can make inhabiting them uncomfortable. This is one of the major limiting factors for how tall it is possible to build with timber today [10].

As timber buildings get taller and taller, it is crucial that engineers have good knowledge of dynamics in such buildings, to be able to predict the dynamic behaviour accurately. That way, the material can be utilized more efficiently, reliably, and safely. Timber as a high rise building material is a relatively new concept, and the dynamic properties are not yet fully understood.

**State of The Art: Dynamics in Timber Buildings** A state of the art study performed in 2018 by researchers at the *American institute of civil engineering*, reviewed damping results for CLT-shear frame buildings, of which the tallest was only 6 storeys tall [11]. In this study the 6-storey building had a damping ratio of approx 2 – 4%, but their data reveals a clear trend of lower damping ratios for taller buildings.

A paper published in 2016 at the *International Network on Timber Engineering Research*-conference presents a collection of measured frequency and damping values of tall timber buildings from various locations [12]. These buildings were built with various techniques, some with solid CLT-shear structures, some with more traditional column-beam frames and some with a combination. See Figure 1.2 for plots of the aggregated data.



(a) Relationship between height and base frequency ratio

(b) Relationship between height and damping

**Figure 1.2:** Damping and frequency trends of a selection of tall timber buildings [12]

A lot of work is currently being done in this field, for instance the European DynaTTB project[13].

## 1.2 Dramsvegen Panorama

The two buildings studied in this thesis are Smørbukklia 3 and 5 in Tromsø, henceforth referred to as SML3 and SML5. They are a part of a student housing development called 'Dramsvegen Panorama', and is owned by the Arctic Student Welfare Organization. They provide students with services like childcare, different sports and exercise possibilities, and student housing [14]. Some of the inhabitants in the buildings in question has reported uncomfortable swaying on the upper floors. Samskipnaden has therefore contacted NTNU in order to examine this behaviour.



**Figure 1.3:** Dramsvegen Panorama student housing. The two buildings in question are located to the right [14].

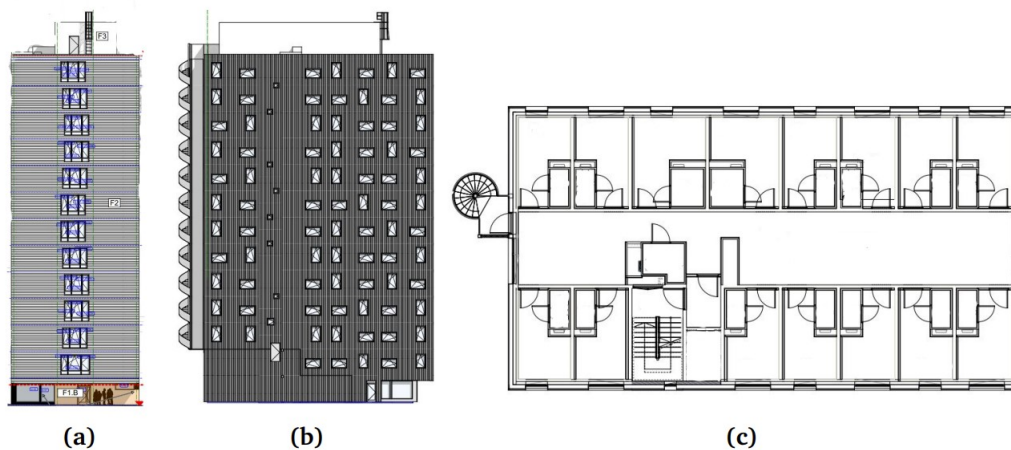


**Figure 1.4:** Illustrations of SML3 provided by Amax consultAB. Figure a) shows the south-east facing facade, b) the south-west facade, and c) shows a floor plan for the floors 3-13. SML5 has a very similar construction

Both buildings are built on bedrock, and are constructed in a very similar manner, with concrete storeys on the bottom and CLT-plates in the upper storeys. They have a very regular, almost rectangular, shape which makes them very well suited for this type of analysis because it is possible to cross compare the results in order to verify them further.

SML3 is the tallest of the two buildings, with thirteen storeys amounting to a height of the main section of 39 metres, and a footprint of approx.  $14m \times 25m$ . The building process was finished in February 2021 [15]. The first two storeys are made of reinforced concrete, and the upper eleven storeys of CLT-plates of varying thicknesses. A continuous elevator shaft and stairwell runs through the entirety of the building. On floor 3-13, there are 15 apartments spread around a common area with a kitchen and living room, as shown in figure 1.4, and the lower floors has fewer apartments because they contain storage spaces, bicycle parking and a technical room. In total there are 179 apartments.

SML5 has a footprint of approx.  $14m \times 25m$  over ten storeys with a total height of the main section of 30 metres, and was finished in August 2017 [16]. This building also has a base of reinforced concrete, with three concrete storeys and seven made of CLT. The placement of the apartments is very similar to SML3, and there are 124 apartments in total. There is also an elevator shaft and stairwell that runs through this building.

### 1.3 Previous Work

As a part of the ongoing project in Tromsø, two master theses were written in the spring of 2021. This thesis is a continuation of the work done, and so the following sections is a short summary of each thesis in order to understand what this thesis is based upon.

#### **Lervik & Kristansen: Assessing Wind Induced Dynamic Properties of Two Tall CLT Buildings in Tromsø**

Lervik and Kristiansen performed on-site measurements of the two buildings in Trømsø, and evaluated the results by operational modal analysis to find the dynamic properties [17]. The buildings were instrumented with four accelerometers and one anemometer each, to measure the accelerations of the buildings and the wind velocities. The accelerometers were placed strategically in the building in order to obtain the best possible results. The measurements were taken during operation, which limited the placement of the accelerometers, but in return the measured values represent the actual behaviour of the building.

Some of the measured data was evaluated by an output-only *operational modal analysis* (OMA) called *Data-Driven Stochastic Subspace Identification* (DD-SSI). This is a method for analysing acceleration data, where only the output, (the response of the structure) is known, and the input (load) is unknown. From this, it is possible to acquire the natural frequencies and mode shapes as well as the damping ratios. As a result of insufficient time, Lervik & Kristiansen didn't get to analyze the majority of the data. This made it difficult to procure good results for both the mode-shapes and the damping ratios.



## Elstrand & Os: A Parametric Study of Connection Modeling in Tall CLT Structures

In their master thesis, Elstrand and Os made a numerical model of the two CLT-buildings in Smørbukklia in Abaqus. After a literature study, they came to the conclusion that a lot of the uncertainty concerning the modeling of CLT-buildings stems from inadequate knowledge of how the connections in between plates influence the overall behaviour of the building [18]. To account for this, they modeled the connections by defining "connection zones" along the element edges. These zones has a reduced thickness, while the other material parameters are the same as the original element except for the density, which is increased to make sure that the mass matrix remains unchanged. The biggest advantage of this method is that the walls are modelled as one continuous plate instead of many CLT-elements, which eases the modeling process.

This modeling technique was then evaluated by performing both a sensitivity analysis and a parameter update in Simulia Isight. The former was to determine which parameters influence the overall results, while the latter was performed to optimize the model based on measured frequencies. The conclusion was that this way of modeling makes it possible to hit a wide range of frequencies, only by changing the thickness fractions of the connection zones in the horizontal (wall-to-floor) and vertical (wall-to-wall) in both x- and z-direction.

### 1.4 Project Description

The work done in this thesis can be split into three separate but interconnected parts:

- The analysis of the acceleration data measured by Lervik & Kristiansen in the spring 2021 [17]. By using an operational modal analysis called *frequency domain decomposition* estimations of the natural frequencies, mode shapes and damping ratios were extracted.
- The development of a parametric FEM-model inspired by the one Elstrand & Os made in the spring of 2021 [18]. As discussed in section 1.3, they used a reduced thickness around the joints to model connections, whereas in this thesis the connections are modeled using discrete fasteners called *connectors*.
- A parametric optimization in which the models were optimized against the target values obtained in the data analysis. This was done to explore the model response from different inputs and to verify that the models are able to reproduce the actual behaviour of the physical buildings.

## 2 Theory

In the autumn 2021, as a part of the subject TKT4550, a preliminary project for this thesis was conducted. Considerable parts of the theory section in this thesis is taken from the project report, with permission from our supervisor.

### 2.1 Timber Structures

#### 2.1.1 Material Structure of Wood

Wood is an organic material that consists of about 50% carbon, 6% hydrogen and 44% oxygen. Together these three elements form cellulose, hemicellulose and lignin, which are the building blocks that form the cell structure shown in figure 2.1. The cellulose fibres, often called microfibrils form cell walls in a tube shaped form, in what is called a tracheid-cell. The lignin is what binds the cell walls together, and acts like an adhesive matrix [5].

Due to this structure, the material properties of wood is very dependent on which direction the load is applied in, making the material anisotropic. To be able to describe the behaviour of wood it is therefore necessary with 12 different engineering constants, which is very computationally heavy.

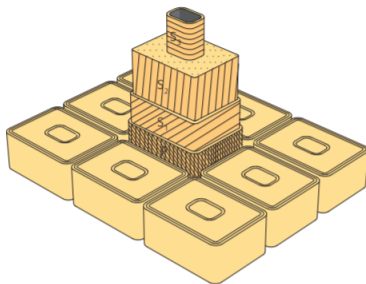


**Figure 2.1:** Cell structure in wood [5]

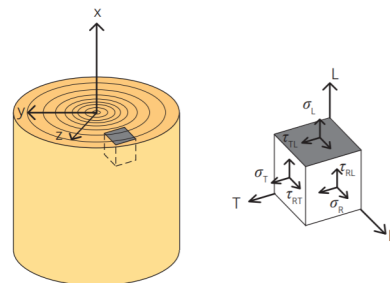


**Figure 2.2:** Common axis system in timber [5]

#### 2.1.2 Material Properties of Timber

The directions it is common to work with when modeling timber are the longitudinal, radial and tangential (L, R and T as shown in 2.2). Strength-wise, T and R are in the same range of magnitude relative to the L-direction which is about ten times stronger than the other two [19].

For simplicity, the properties in R and T directions are averaged, and in practice we are left with the 0- (parallel to grain) and 90-direction (perpendicular to grain) [20]. This reduces the problem into 3 planes of symmetry, known as an *orthotropic* material [21].

To describe the relations between the strains and stresses in the different directions, we use Hooke's law formulated on matrix form:

$$\boldsymbol{\varepsilon} = \mathbf{C}\boldsymbol{\sigma} \quad \text{or} \quad \boldsymbol{\sigma} = \mathbf{K}\boldsymbol{\varepsilon} \quad (2.1)$$

Where  $\boldsymbol{\sigma}$  denotes stress,  $\boldsymbol{\varepsilon}$  denotes strain,  $\mathbf{C}$  is the compliance matrix, and  $\mathbf{K}$  is the stiffness matrix.

The compliance matrix,  $\mathbf{C}$ , for an orthotropic material is given as [21]:

$$\begin{bmatrix} \varepsilon_{11} \\ \varepsilon_{22} \\ \varepsilon_{33} \\ \gamma_{23} \\ \gamma_{31} \\ \gamma_{12} \end{bmatrix} = \begin{bmatrix} S_{11} & S_{12} & S_{13} & 0 & 0 & 0 \\ S_{21} & S_{22} & S_{23} & 0 & 0 & 0 \\ S_{31} & S_{32} & S_{33} & 0 & 0 & 0 \\ 0 & 0 & 0 & S_{44} & 0 & 0 \\ 0 & 0 & 0 & 0 & S_{55} & 0 \\ 0 & 0 & 0 & 0 & 0 & S_{66} \end{bmatrix} \begin{bmatrix} \sigma_{11} \\ \sigma_{22} \\ \sigma_{33} \\ \tau_{23} \\ \tau_{31} \\ \tau_{12} \end{bmatrix}, \quad (2.2)$$

or expressed with engineering constants:

$$\begin{bmatrix} \varepsilon_{11} \\ \varepsilon_{22} \\ \varepsilon_{33} \\ \gamma_{23} \\ \gamma_{31} \\ \gamma_{12} \end{bmatrix} = \begin{bmatrix} \frac{1}{E_1} & \frac{-\nu_{12}}{E_1} & \frac{-\nu_{13}}{E_1} & 0 & 0 & 0 \\ & \frac{1}{E_2} & \frac{-\nu_{23}}{E_2} & 0 & 0 & 0 \\ & & \frac{1}{E_3} & 0 & 0 & 0 \\ & & & \frac{1}{G_{23}} & 0 & 0 \\ & \text{sym} & & & \frac{1}{G_{31}} & 0 \\ & & & & & \frac{1}{G_{12}} \end{bmatrix} \begin{bmatrix} \sigma_{11} \\ \sigma_{22} \\ \sigma_{33} \\ \tau_{23} \\ \tau_{31} \\ \tau_{12} \end{bmatrix} \quad (2.3)$$

where  $E$  is the young's modulus,  $G$  is the shear modulus, and  $\nu$  is Poisson's ratio. The numbers in the sub-indexes indicate what direction the value refers to.

From this, the stiffness-matrix can be found by inverting the compliance-matrix:

$$\begin{bmatrix} \varepsilon_{11} \\ \varepsilon_{22} \\ \varepsilon_{33} \\ \gamma_{23} \\ \gamma_{31} \\ \gamma_{12} \end{bmatrix} = \begin{bmatrix} \frac{1-\nu_{23}\nu_{32}}{E_2E_3D} & \frac{\nu_{12}+\nu_{31}\nu_{23}}{E_2E_3D} & \frac{\nu_{31}+\nu_{21}\nu_{32}}{E_2E_3D} & 0 & 0 & 0 \\ & \frac{1-\nu_{13}\nu_{31}}{E_1E_3D} & \frac{\nu_{32}+\nu_{12}\nu_{31}}{E_1E_3D} & 0 & 0 & 0 \\ & & \frac{1-\nu_{12}\nu_{21}}{E_1E_2D} & 0 & 0 & 0 \\ & & & G_{23} & 0 & 0 \\ & \text{sym} & & & G_{31} & 0 \\ & & & & & G_{12} \end{bmatrix} \begin{bmatrix} \sigma_{11} \\ \sigma_{22} \\ \sigma_{33} \\ \tau_{23} \\ \tau_{31} \\ \tau_{12} \end{bmatrix} \quad (2.4)$$

**Deflection in CLT** Lateral deflection patterns of CLT panels include a combination of bending- and shear deformation of the panel material, as well as sliding and rocking of the panels as a whole (see Figure 2.3). The dominating deformation patterns are the sliding and rocking [22].

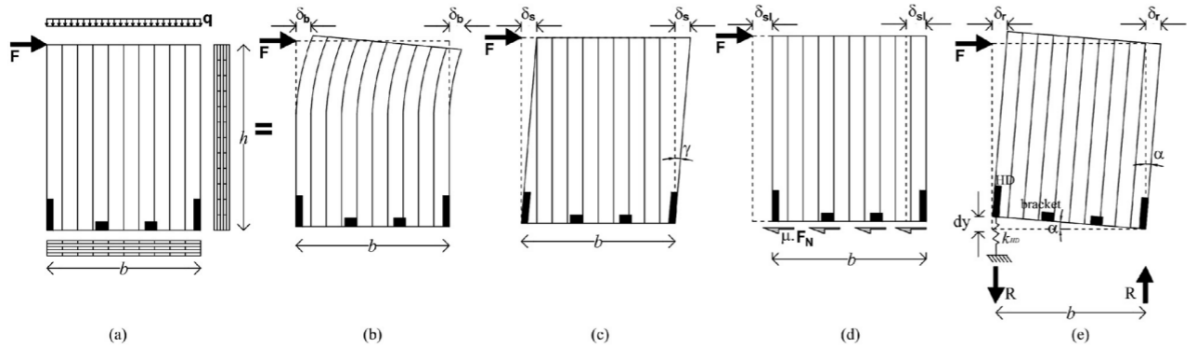


**Figure 2.3:** Displacement patterns of CLT-panels. a) Bending, b) Shear, c) Sliding and d) Rocking [22]

## 2.2 Structural Dynamics

### 2.2.1 Equation of Motion

The equation of motion for a single degree of freedom system is given as

$$f_I + f_d + f_s = p(t) \quad (2.5)$$

where  $f_I$  is the inertia force caused by the mass resisting the acceleration, from Newtons second law of motion  $F = Ma$ . The damping force  $f_d$  is the sum of the structural and material damping, or in other words the energy dissipation of the system.  $f_s$  is the stiffness force derived from the spring stiffness relation:  $F = kx$  where  $k$  is the stiffness of the spring, while  $x$  denotes the distance from equilibrium position.

To make (2.5) applicable to a multi-degree of freedom (MDOF) system, the equation is presented in matrix form, where each element in the matrices and vectors are related to the DOFs of the system. With *viscous damping*, this leads to the classic equation of motion:

$$\mathbf{M}\ddot{\mathbf{u}}(t) + \mathbf{C}\dot{\mathbf{u}}(t) + \mathbf{K}\mathbf{u}(t) = \mathbf{P}(t) \quad (2.6)$$

Here  $\mathbf{M}$ ,  $\mathbf{C}$  and  $\mathbf{K}$  denotes the mass-, damping-, and stiffness matrices respectively.  $\mathbf{P}$  is the force vector acting on the structure, and  $\mathbf{u}(t)$  is a vector containing the displacement of each degree of freedom as a function of time.

### 2.2.2 Natural Frequencies and Modes

The natural frequencies of a structure refers to the frequency the structure oscillates at in free vibration, e.g. when there is no outer load applied. A phenomenon called *resonance* occurs when the load frequency reaches the structures natural frequency. At resonance, the amplitude increases and increases while the load is acting, which may lead to failure, and is why this is such an important property in structural dynamics [24].

Figure 2.4 shows how the vibration amplitude of a structure depends on the frequency ratio, which is defined by  $\beta = \omega/\omega_n$ , where  $\omega$  is the load frequency and  $\omega_n$  is the natural frequency of the structure. When the two frequencies are equal ( $\beta = 1$ ), this is where the peak is located in the graph, as expected.

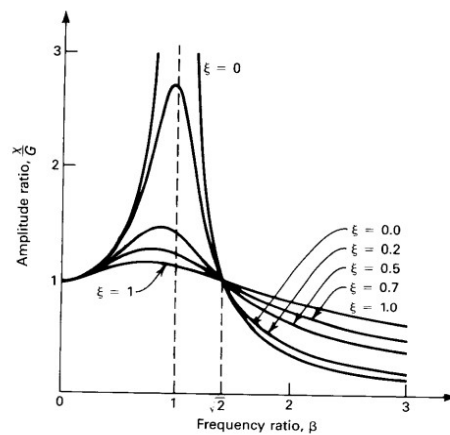


**Figure 2.4:** Response amplitude from different damping ratios and load frequencies, note resonance as  $\beta \rightarrow 1$  [23].

Each structure has several resonant frequencies relating to different vibration modes, often referred to as *mode shapes*. A mode shape is a dimensionless deflection pattern that describes how the different degrees of freedom (DOFs) are excited in relation to each other[24]. The mode shapes depends upon the *distribution* mass and stiffness of the structure, more so than the global mass and stiffness.

To find the natural frequencies and mode shapes of a system, it is necessary to find the eigenmodes and eigenvalues. This is done by solving the eigenvalue problem of the undamped system:

$$(\mathbf{K} - \omega_n^2 \mathbf{M}) \Phi = \mathbf{0} \quad (2.7)$$

where  $\omega_n$  is the natural frequency and  $\Phi$  are the mode shapes that describes the different vibration modes of the system. For the non-trivial solutions, the determinant is zero:

$$\det(\mathbf{K} - \omega_n^2 \mathbf{M}) = 0 \quad (2.8)$$

After solving (2.8) for the natural frequencies, and substituting them in (2.7), the mode shapes  $\Phi$ , can be found.

The eigenvectors of an undamped system are orthogonal in relation to each other by nature. Because of this, it is possible to describe all other displacement modes with a linear combination of these, by using the superposition principle. Because of this, it is possible to generalize the system matrices by pre-multiplying them with the transposed mode vector, and post-multiplying by the regular mode vector as follows [25]:

$$\Phi^T M \Phi \ddot{\mathbf{y}} + \Phi^T C \Phi \dot{\mathbf{y}} + \Phi^T K \Phi \mathbf{y} = \Phi^T \mathbf{p}(t) \quad (2.9)$$

To simplify the notation, the generalized matrices are denoted with a tilde:

$$\begin{aligned} \tilde{M} &= \Phi^T M \Phi \\ \tilde{C} &= \Phi^T C \Phi \\ \tilde{K} &= \Phi^T K \Phi \end{aligned} \quad (2.10)$$

These generalized mass and stiffness matrices has the advantage that they are diagonalized; all the non-zero terms are located along the diagonal. This means that the entire system is uncoupled, and each linear equation can be solved separately which reduces the computation time significantly.

The damping matrix however, is not a part of the eigenvalueproblem, and is therefore usually impossible to orthogonalize. This means that for a general case, (2.9) is not possible to solve analytically to find the modal solutions, only explicit numerical solutions exist.

### 2.2.3 Damping

The damping behaviour of built structures is very complex. It is the result of a combination of factors [23]:

- The internal friction within the material
- The friction that appears in the connections
- Energy dissipation that happens as the vibration propagates

A common representation of the damping in structures is viscous damping. This means that the damping is assumed to be proportional to velocity:

$$f_d = c\dot{u}(t) \quad (2.11)$$

The formulation of this type of damping was originally based on the study of damping in liquids. It has been shown that viscous damping is not completely accurate for solids, because the internal friction within liquids and solids behave differently [26]. However, viscous damping models are still widely used, owing to their convenience and the fact that it has sufficient accuracy in many cases [23].

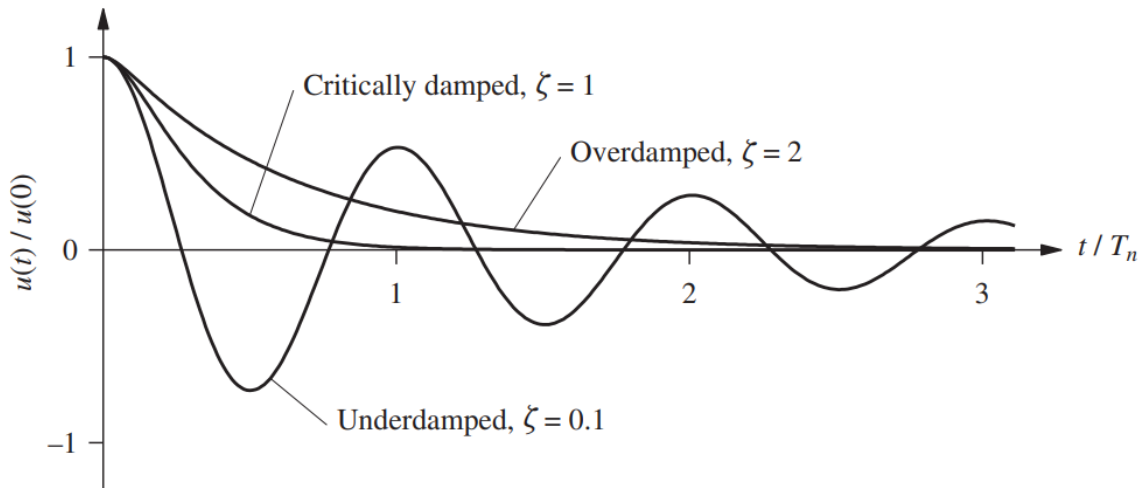


**Figure 2.5:** Free harmonic vibration of damped systems [27]

Figure 2.5 shows the free vibration response of a system with different levels of damping, denoted by the damping ratio  $\zeta$ . Underdamped systems are systems that will oscillate back and forth in free vibration some number of times before coming to a rest. Buildings, bridges, and the like are almost always underdamped, except for very rare exceptions [27], and thus civil engineers are usually only concerned with underdamped systems.

The introduction of damping to a under damped system introduces a frequency shift equal to [27]:

$$\omega_d = \omega_n \sqrt{1 - \zeta^2} \quad (2.12)$$

## Rayleigh damping

As mentioned, the damping matrix,  $[\tilde{\mathbf{C}}]$ , makes the dynamic calculations more complicated because of the fact that it is not possible to orthogonalize. A possible workaround of this problem is to approximate it as a linear combination of  $[\tilde{\mathbf{M}}]$  and  $[\tilde{\mathbf{K}}]$ ; see equation (2.13). Figure 2.6 shows an example of a general Rayleigh damping profile. Because the modal mass- and stiffness matrices are diagonal, this creates a diagonal damping matrix. The result is a MDOF system essentially being broken down into a series of SDOF-systems that is possible to solve separately.

$$\mathbf{C} = \alpha\mathbf{M} + \beta\mathbf{K} \quad (2.13)$$

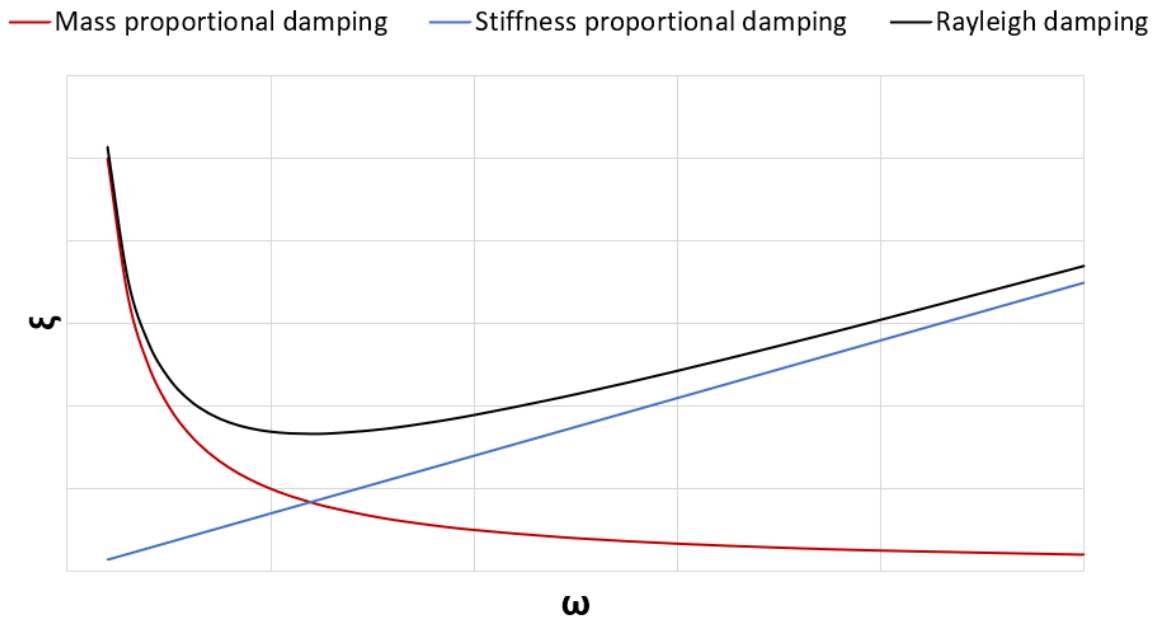


**Figure 2.6:** General rayleigh damping curve

$\alpha$  and  $\beta$  are coefficients that are found by use of the estimated modal damping ratios. By substituting  $C_n$  with the linear combination in equation (2.13), and keeping in mind that  $\omega_n^2 = K/M$ , we get:

$$\zeta_n = \frac{C_n}{C_{critical}} = \frac{C_n}{2M_n\omega_n} = \frac{\alpha}{2\omega_n} + \frac{\beta}{2}\omega_n \quad (2.14)$$



Using two different measured damping ratios at two different natural frequencies, this becomes a system of equations with two equations and two unknowns, which leads to the following expressions:

$$\begin{aligned}\alpha &= \frac{2\omega_m\omega_n(\zeta_m\omega_n - \zeta_n\omega_m)}{\omega_n^2 - \omega_m^2} \\ \beta &= \frac{2(\zeta_n\omega_n - \zeta_m\omega_m)}{\omega_n^2 - \omega_m^2}\end{aligned}\tag{2.15}$$

When combining the expressions in (2.15) and (2.13), the Rayleigh damping matrix can be found. If multiple identified modes and damping ratios found, a different approach can be used, such as optimizing across the entire set, e.g. choosing an  $\alpha$  and  $\beta$  that minimizes the root mean squared error (RMS) between the Rayleigh curve and measured values.

## 2.3 Operational Modal Analysis

The process of determining the modal properties of a structure in normal operation, *operational modal analysis* (OMA), is a subfield in structural dynamics that allows engineers to estimate important structural properties such as natural frequencies, mode shapes and the associated modal damping ratios. In OMA the excitation force is assumed to be stochastic and white-noise like, unlike *experimental modal analysis* (EMA), where the input load is known and defined, for instance when a building is forced to vibrate with a shaking contraption.

Central to all OMA-related tasks is the collection, processing and analysis of data. Typically this is done by installing accelerometers in different locations of a structure and logging the acceleration response. This data is then processed and analysed to determine the dynamic properties.

### 2.3.1 Data Pre-processing

Real world signal data is messy or *noisy*, i.e. it is subject to many sources of noise that disturb the signal. This noise can be physical, e.g. vibrations from people moving around, from machines such as HVAC systems and the like; or it can be digital, such as electric or magnetic noise disturbing the sensors directly or the cables that connect them.

For the digital sampling of the analog signal, an analog filter must be applied prior to the analog-to-digital conversion [28]. This is usually installed on the actual hardware that does the monitoring and logging.

In order to achieve meaningful and efficient calculations, proper *digital signal processing* (DSP), is necessary. In DSP a series of steps pre-processing of the raw signal data are performed to prepare the data for analysis. Which steps are needed, and the appropriate parameters involved will depend on the signal data and which type of analysis the engineer plans to perform.

**Down Sampling** In OMA, signals are typically *over-sampled*, which means that the sampling rate is much higher than what is strictly necessary for the analysis in question. While this does increase the storage space required for the raw data as well as requiring some extra pre-processing steps to handle larger files, over-sampling does have some advantages. Firstly, high quality data at high sampling rates is available in case it is needed in the future. More importantly, when pre-processing the data with *digital down-sampling*, there is less noise in the resulting data than it would have been if sampled at the lower rate directly [28].

Down-sampling is a process that applies some function to the raw data which converts the raw-data into *processed signal data* sampled into a lower sampling rate. This increases computational speed and reduces memory usage compared to the initial over-sampled data. As long as the downsampled rate is high enough to sufficiently cover the frequency-range of interest, there will be little to no impact on the accuracy of the analysis done on the data [29]. A well-known "law" in digital signal theory is known as the *Nyquist's theorem*, and it states that for any process with a given frequency  $f$ , a minimum digital sampling rate of  $2f$  is required to properly describe said process [28].

## Aliasing

The process of down-sampling is not as straightforward as picking every  $n$ -th point in the data set. Doing so would cause higher frequency components to be interpreted as spurious lower frequency components, a phenomenon commonly known as aliasing [28]. These spurious frequency components are indistinguishable from the real signal and would thus compromise the quality of the analysis. So, prior to down-sampling, there should be applied a digital filter function that can remove all frequencies that can cause aliasing.

After passing the signal through anti-aliasing filters, it is then passed through a decimation

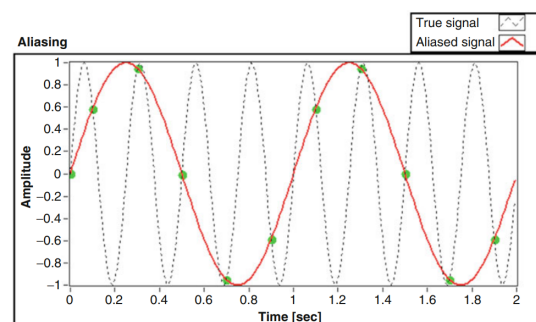


**Figure 2.7:** How aliasing can occur when down sampling [29]

function, the most common of which being the *polyphase quadrature filtering*. This function is extensively used in all kinds of signal processing involving compression, such as audio processing. The method involves subdividing the signal spectrum into multiple sub-bands which are handled independently and the outputs are summed to yield the down-sampled (or up-sampled if needed) signal [30].

### Frequency filtering

For the digital filtering and preparation of signal data, various digital frequency filters exists, and most DSP-frameworks have built in functions for the different filtering tasks. See Figure 2.8 for an illustration of the frequency response of some common filtering functions.

Prior to down-sampling, to combat the aforementioned aliasing-problem, a low-pass filtering function is applied to remove high frequency components. In accordance with the Nyquist-theorem, at least the frequencies that are 50% of the target down-sample rate should be filtered out. In practice however, it is recommended to keep the filter limit comfortably below the *Nyquist frequency*:  $f_{Nyquist} = \frac{f_s}{2}$ , e.g.  $0.8f_{Nyquist}$ . In other words, for a signal down-sampled from 400Hz to 20Hz, processes with frequency up to approx.  $0.8\frac{20}{2} = 8\text{Hz}$  can be analysed with reasonable accuracy.

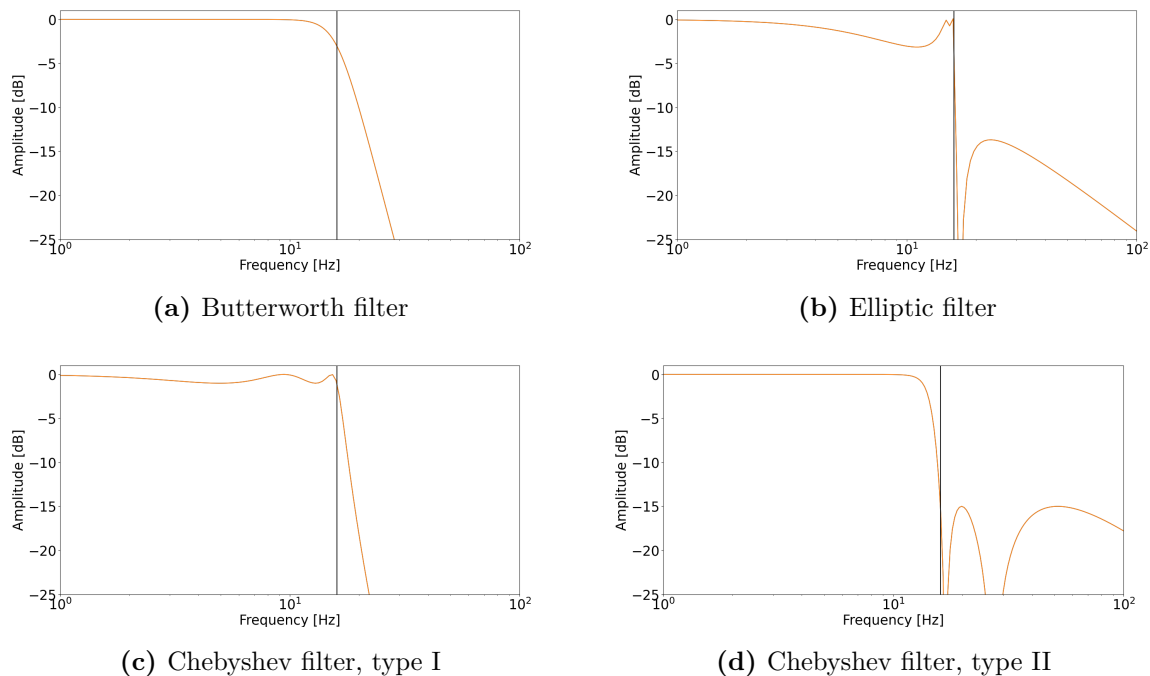
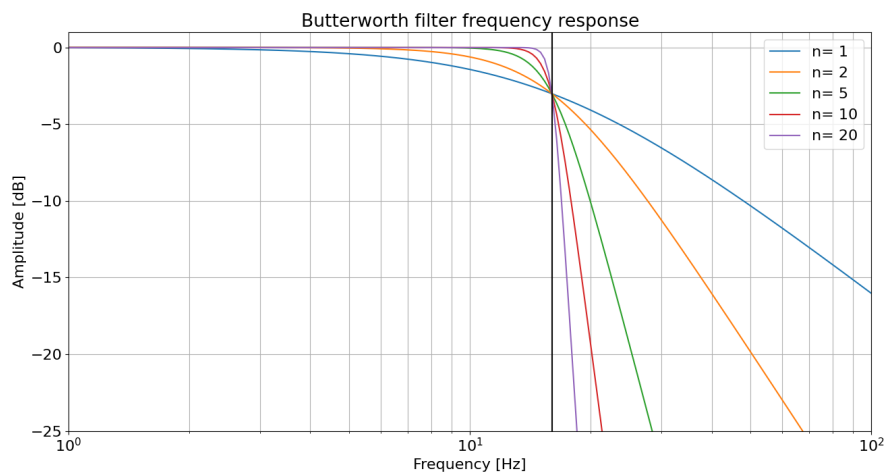


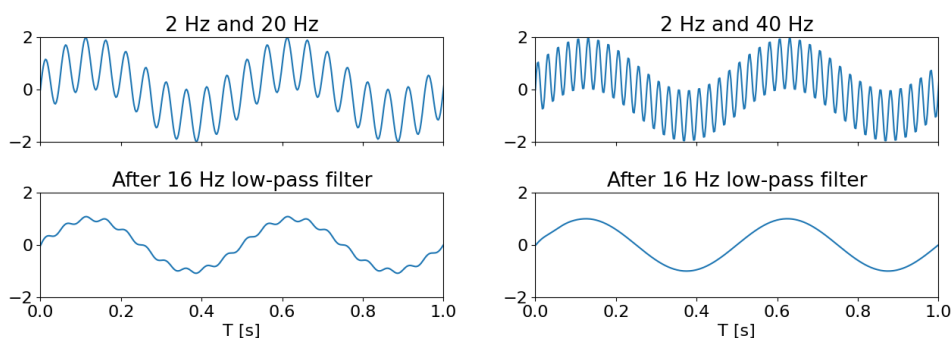
**Figure 2.8:** Common band-pass filter types

As can be observed Figure 2.8, the elliptic and Chebyshev filters have quite noticeable side-effects in the spectrum, where different frequencies receive different levels of amplification in a rippling fashion rather than having a smooth decay. Furthermore, with the exception of chebyshev type II, they also do not have a maximum amplitude across the frequency band of interest (known as the passband). For OMA, this is especially undesirable as the ripples could interfere with the frequency peaks associated with modes.

The Butterworth filter however, has a flat maximum amplitude across nearly the entire passband, and a smooth decay above the cut-off frequency, which makes this filter ideal for OMA purposes. The Butterworth filter can be designed with a higher order, which would create a sharper decay, see Figure 2.9. As can be observed in the figure, the amplitude decay will start at some distance to the chosen cut off frequency, depending on the order of filter chosen. This should be taken into account when choosing both cut off frequency and filter order, to ensure that the filter does not affect the frequencies of interest.



(a) Frequency response Butterworth filters of different orders



(b) Frequency components closer to the cutoff survive to a small extent  
(c) Frequency components far above the cut-off are removed entirely

**Figure 2.9:** Different butterfilter orders and the effects of a 5th order forward-backward (effective 10th order) filter on two different frequency components

Normally, bandpass-filtering induces a phase shift in the filtered signal, while the general shape and amplitude is preserved [29]. In the context of FDD, depending on the severity of the phase shift, it can lead to significantly negative consequences on the accuracy analysis. This happens when either end of the filtered signal is included in the analysis, causing spurious frequency components to appear. This can be negated in one of two ways.

One option is to truncate the ends of the filtered signal in order to exclude them from the analysis. The other method is to pass the same filtering function in both directions by first applying the filter like normal, and then flipping the signal and apply the filter once again. This filtering procedure removes the phase-shift in the signal and essentially doubles the order of the filter. See Figure 2.10 for an illustration of the phase shift phenomenon and remedy.

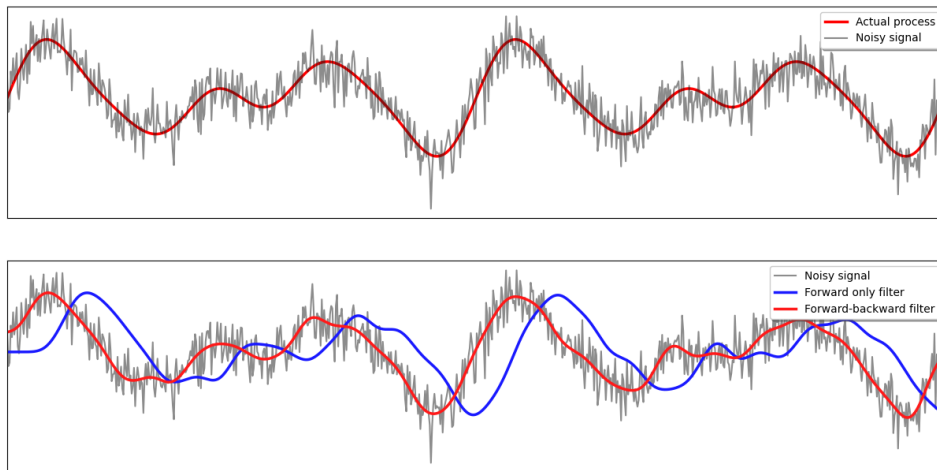


**Figure 2.10:** Comparison of forward-only and forward-backward filtering

It is not usually necessary to remove low frequency components with a high-pass filter, when performing OMA, but it is possible and not uncommon to apply a filter like this as well.

## Detrending

A spurious trend is when a time-series' mean is trending away from the mean of the physical process being measured. This will distort the spectral estimate of the process by magnifying the lower frequencies [29]. It is therefore important to remove any such trend from the signal.

To detrend a signal a low order regression of the signal, such as a line, is used:

$$x_{detrended,i} = x_{trended,i} - mi, \quad (2.16)$$

where  $m$  is the slope of the regression line  $y = mi + c$ , and  $x$  is the signal in question.

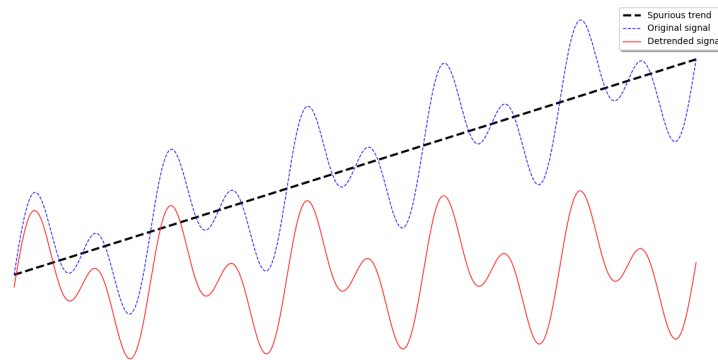


**Figure 2.11:** Detrending of a signal with a spurious trend

## Offsets

A signal offset is when the *signal mean* is different to the mean of the underlying process that was measured. Depending on the type of analysis which is to be performed on the data, it might be necessary to remove any offsets. In other words: when considering zero-centered processes such as structural acceleration, it is important that the signal data also oscillates about zero.

For zero-centered processes a discrete signal  $s$  with a measurement offset can be easily removed by subtracting the mean of the signal, as illustrated in figure 2.12

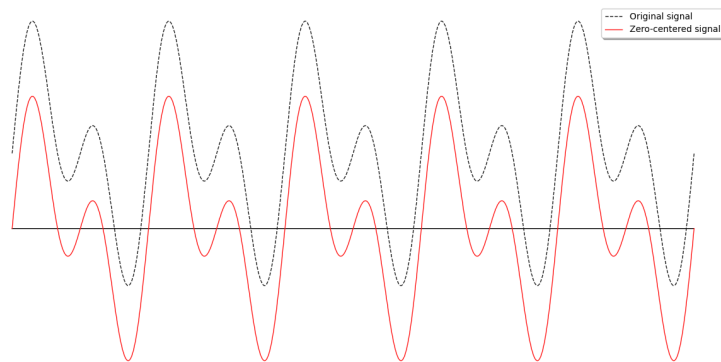


**Figure 2.12:** Zero-centering of a signal with an initial offset

$$x_{zero-centered,i} = x_{offset,i} - \frac{1}{N} \sum_0^N x_{offset,i} \quad (2.17)$$

### 2.3.2 Natural Frequencies by Peak Picking

A structure subjected to ambient white noise excitation will respond strongly near its natural frequencies [29]. Through this phenomenon, natural frequencies can be determined by analysing the *power spectral density* (PSD), of the response. The value of the PSD at a given frequency is related to how much the frequency component contributes to the total signal [31]. When plotting the PSD over the frequency range, this is known as a periodogram. The modes and associated frequencies will appear as local peaks on the periodogram, and can be visually determined by the engineer performing the analysis.

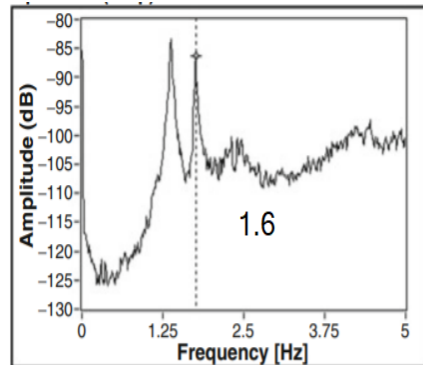


**Figure 2.13:** Signal periodogram with two clear natural frequency peaks [29]

By inspection of the periodogram in figure 2.13, two clear natural frequency peaks at 1.3 Hz and 1.7 Hz can be identified. There might be natural frequencies at 2.5 Hz and 4.4 Hz as well, but further analysis is needed to determine the less pronounced peaks [29].

### Discrete Fourier Transform

The *discrete Fourier transform* (DFT) of a signal is the frequency domain decomposition of the time series. It is used to give an estimate of the real PSD of the signal by taking the square absolute of the DFT.

For discrete signals  $x = [x_0, x_1 \dots x_{N-1}]$ , the discrete fourier transform  $X = [X_0, X_1 \dots X_{N-1}]$ , is given by [32]:

$$X_k = \frac{1}{N} \sum_{n=0}^{N-1} x_n \exp^{-\frac{i2\pi}{N}kn} \quad (2.18)$$

The resulting fourier transform of the signal will have a frequency resolution of  $df = \frac{f_s}{N}$ . For example, a fourier transform of a 20 Hz signal with 1000 data points will have a frequency resolution of  $df = 20$  mHz

### Windowing

For finite signals, the DFT introduces errors because each end of the signal ends abruptly, which the DFT interprets as spurious frequency components known as *leakage* [28]. To combat this effect, a windowing function is applied to the signal. This reduces the influence of the signal's ends on the result when computing the DFT, while the middle of the signal



is given more influence. The most common of these windowing functions is known as a *Hamming window* [33].

$$W(n) = 0.54 - 0.46\cos\left(2\pi\frac{n}{N}\right) \quad (2.19)$$

The Hamming window  $\mathbf{W}$ , is applied to the finite time series before computing the filtered DFT,  $A$ :

$$A(n) = \frac{1}{N} \sum_{j=0}^{N-1} x(j)W(j) \exp\frac{-i2jn}{N} \quad (2.20)$$

To compensate for the reduction of amplitude by the windows, a correction factor,  $U$ , is applied to the filtered DFT,  $A$ , and gives a filtered periodogram  $I$ :

$$I(f_n) = \frac{1}{U}|A|^2, \quad (2.21)$$

where

$$\text{frequency } f_n = n/N, n = 0, 1 \dots N$$

$$U = \sum_{j=0}^{L-1} W(j)^2$$

For a sufficiently long time series, the resulting DFT yields a reasonably accurate estimate of the frequency composition [29].

### Welch's Method

Welch's method is a technique for estimation of the PSD of finite signals in which the signal is divided into multiple overlapping segments. A windowing function is applied, and the DFT is computed for each of the segments. The estimate of the process PSD,  $\hat{P}$  is then computed as the ensemble average of the segment periodograms  $I_k$  [34]:

$$\hat{P}(f_n) = \frac{1}{K} \sum_{k=1}^K I_k(f_n), \quad (2.22)$$

where  $K$  is the number of segments.

In addition to yielding less noisy periodogram estimates, Welch's method also gives a more uniform distribution of influence from the signal on the DFT computation, giving more accurate estimates of the PSD.

### 2.3.3 Frequency Domain Decomposition

*Frequency domain decomposition* or FDD, is performed by studying the the estimate of the PSD matrix of the output signal for a process. Since this is an OMA-based technique, the input does not need to be known, but is assumed to be a stationary white-noise-like excitation.

The general idea of FDD is that around a structure's natural frequencies, its motion is dominated by a single vibration mode, namely the mode associated with the natural frequency at hand. By studying small frequency ranges around the frequency peaks, it is possible to compute estimates of mode shapes and damping ratios of single modes.

Consider the general relationship for a stochastic input-output process.

$$[\hat{G}_{yy}] = [A][\hat{G}_{qq}][A]^H, \quad (2.23)$$

where

$[\hat{G}_{yy}]$  is the output PSD,

$[\hat{G}_{qq}]$  is the input PSD, and

$[A] = [a_1, a_2 \dots]$  is the mode shape matrix.

Here, only the left hand side is known. This is the ouput PSD-estimate computed from *in situ* measurements.  $\hat{G}_{yy}$  can be broken down by *single value decomposition* or SVD, giving

$$[\hat{G}_{yy}(j\omega_i)] = [U_i][\Sigma_i][V_i]^H, \quad (2.24)$$

where

$[U_i] = [u_{i1}, u_{i2} \dots]$  and  $[V] = [v_{i1}, v_{i2} \dots]$  are the left and right singular matrices

$[\Sigma]$  contains scalar values along its diagonal

For an n-channel signal,  $[\Sigma]$  is an  $n \times n \times m$  matrix, where m is the number of points per channel in the original PSD. Each step along the diagonal represent one higher order of spectral analysis. If the first element along the diagonal is extracted,  $\{\sigma_1\} = \{\Sigma_{[1,1,1]}, \Sigma_{[1,1,2]} \dots \Sigma_{[1,1,m]}\}$ . This gives a one-dimensional vector with length  $m$ . This vector is equivalent to the first order spectrum of the multi-channel signal data, ie. the modal spectrum for a MDOF system.

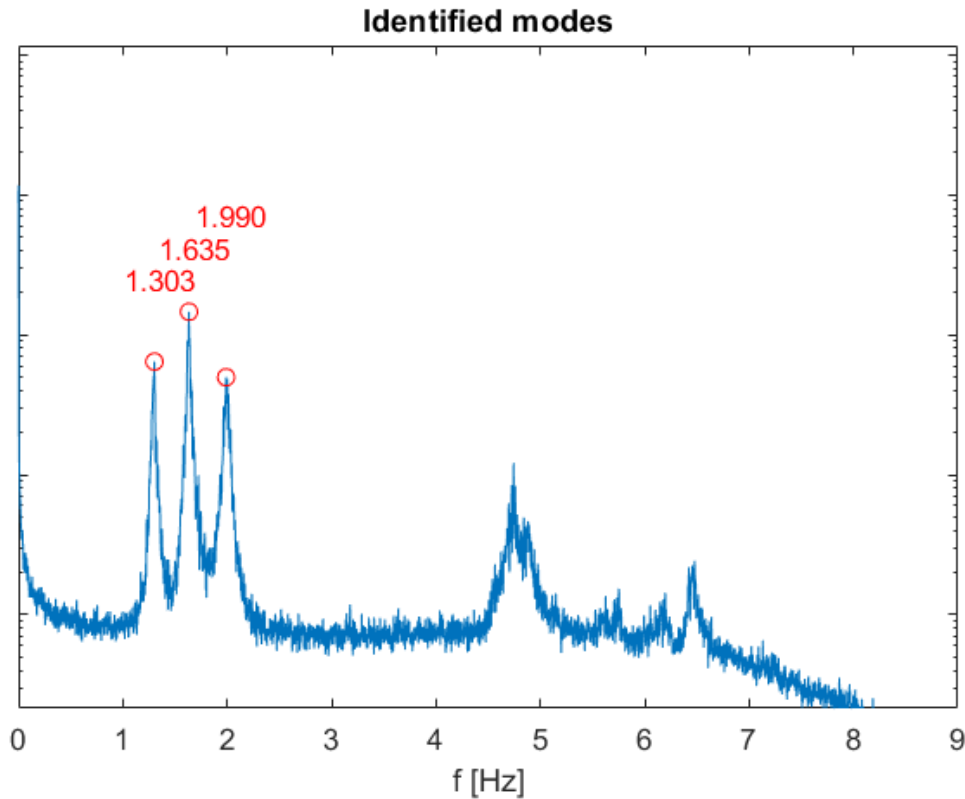


**Figure 2.14:** Plot of the 1st order modal spectrum  $\{\sigma_1\}$ , with first 3 modes identified

In FDD theory,  $u_{i1}$  and  $v_{i1}^H$  approximate the mode shapes near mode-peaks in the frequency domain [29]. Equation (2.24) then becomes:

$$[\hat{G}_{yy}(\omega)] \approx \{\sigma_{k1}\}\{u_{k1}\}\{u_{k1}\}^H, \quad \omega \rightarrow \omega_k \quad (2.25)$$

Then, a narrow range around the mode peaks must be defined. This is commonly done with the MAC-criterion:

$$MAC(\{u_j\}, \{\hat{\phi}_k\}) = \frac{|\{u_j\}^H \{\hat{\phi}_k\}|^2}{(\{u_j\}^H \{u_j\})(\{\hat{\phi}_k\}^H \{\hat{\phi}_k\})}, \quad MAC \in [0, 1], \quad (2.26)$$

Initially starting at a given mode peak, we "walk" up the frequency range, continually computing MAC-values between the mode shape at the given frequency and the mode shape at the mode peak. As mode shape-estimates drift further apart with different frequencies, the MAC-value (starting at 1) will be gradually lower as the gap widens. When the MAC-value falls below some rejection threshold chosen by the user, the upper bound for the frequency range is found. The process is equivalent for finding the lower bound. In FDD, the rejection threshold is usually set to around 0.8 [29]. The user must also inspect the computed frequency ranges to confirm that the frequency sub-ranges are appropriately sized, and adjust the rejection threshold if necessary.

It is not strictly necessary to use the MAC criterion to define the range. In fact, any scheme that yields a reasonably sized range around the peak; wide enough to include ample information, and narrow enough that other modes or the *noise floor* does not appear in the range will do.

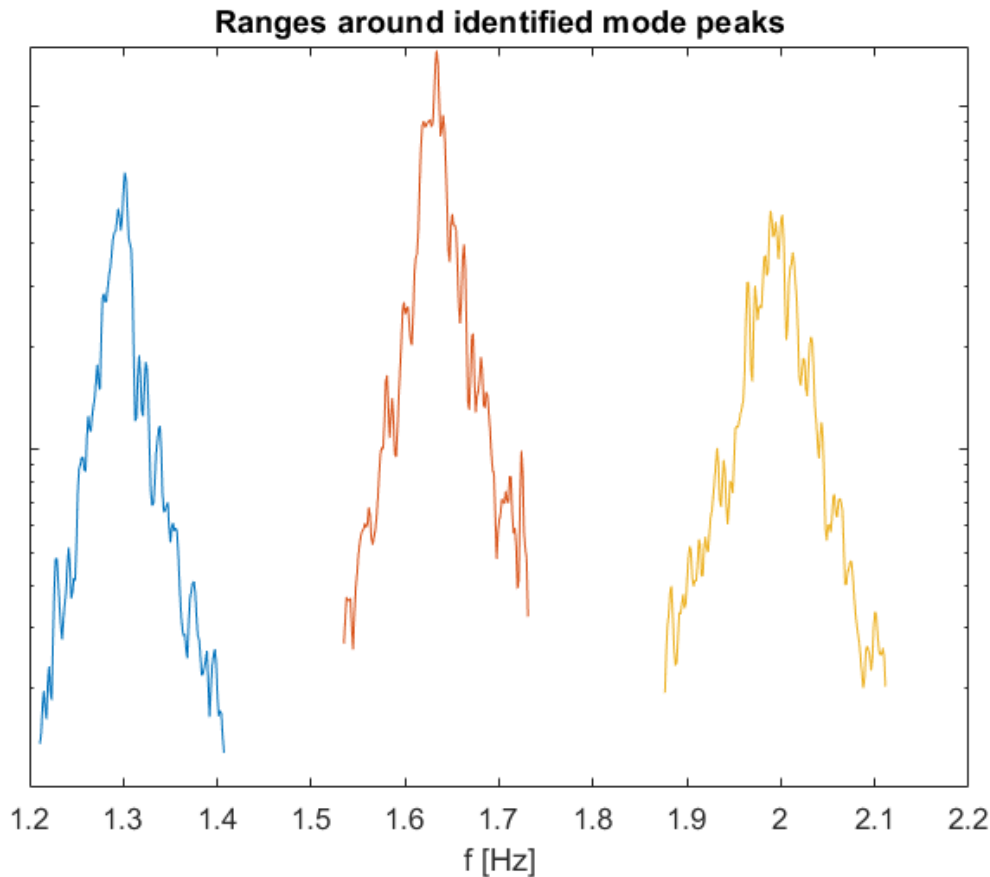


**Figure 2.15:** By the MAC-criterion, narrow ranges around identified modes is defined

An *inverse Fourier transform* (IFT) of the vector  $\{\sigma_1\}$  for the sub-interval found around mode  $k$ , will approximately yield an auto-correlation function for a SDOF system. This auto-correlation function will, for a small range of time-offsets near 0, have a decaying function envelope [35].

Extracting the peaks of the auto-correlation functions in this initial range, can be done by defining some appropriate rejection criteria. One convenient approach is to normalize the auto-correlation function such that it swings between 0 and 1, and then include all the peaks from the first until the envelope drops below a threshold, for example 0.4. This threshold can be tweaked up or down to better fit the data at hand.

After finding the peaks to include in the analysis, see Figure 2.16, the logarithmic decrement is computed on said peaks [35]:

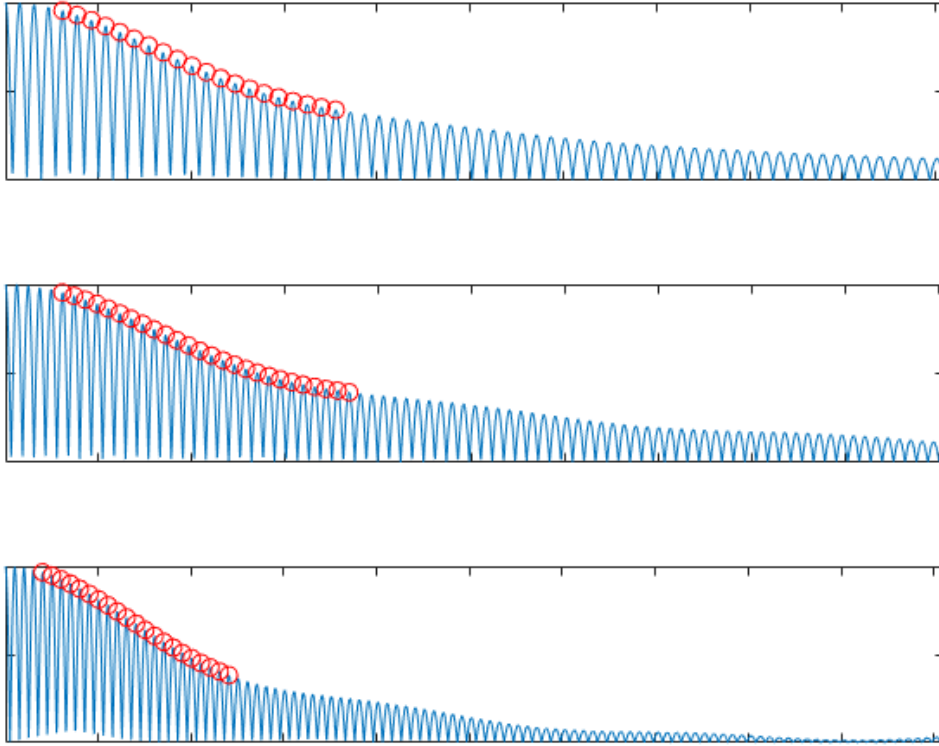


**Figure 2.16:** Normalized auto-correlation around mode peaks. Red rings mark the peaks that comply with a user-specified criteria.

$$\delta_k = \frac{2}{k} \ln\left(\frac{r_0}{r_k}\right), \quad (2.27)$$

where  $r_0$  and  $r_k$  are the 1st and k-th peak of the correlation function respectively.

Computing the logarithmic decrement for different numbers of included peaks yield the  $\delta$ -vector  $\{\delta\} = \{\delta_0, \delta_1 \dots \delta_n\}$ .

Manipulating (2.27), gives the function  $Y = k\delta_k + 2\ln(|r_k|)$ , which, when plotted against  $k$ , should approximate a straight line for processes with fairly constant damping ratios [35], see Figure 2.17. The slope of a linear regression on this function is the estimated average logarithmic decrement  $\bar{\delta}$  for the mode.

Finally, using  $\bar{\delta}$ , the damping ratio estimate  $\hat{\zeta}$  can then be computed with the formula [35]:

$$\hat{\zeta} = \frac{\bar{\delta}}{\bar{\delta}^2 + 4\pi^2} \quad (2.28)$$

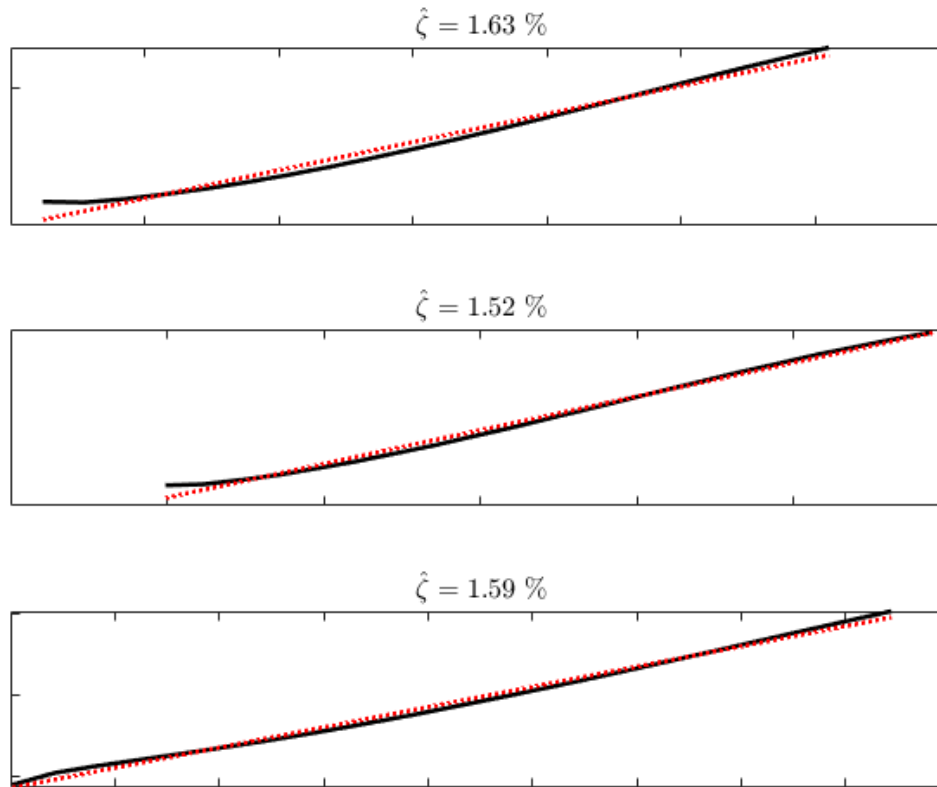


**Figure 2.17:** Plot of the logarithmic decrement estimate  $Y = k\delta_k + 2\ln(|r_k|)$ , along with the linear regression lines and computed damping ratios by (2.28).

## 2.4 Finite Element Modeling

Finite element modeling is a numerical analysis method that is widely used in different engineering fields such as electromagnetism, machine- and structural design. The approach of the method is to subdivide the geometry of the structure into finite elements, and assigning them 'material properties' by the use of shape functions. The shape functions describe the behaviour of the elements, and should enforce both compatibility and equilibrium for a successful result [36].

When applying loading and boundary conditions to the structure, this approach will lead to an approximation of how the structure behaves in real life.

The two main considerations when developing a finite element model is what type of elements to use, and how to subdivide the geometry into finite elements, also known as meshing. In order to obtain an accurate solution, it is crucial that the engineer has a thorough understanding of the expected behaviour of the system, to be able to assess the quality of the results [36].

### 2.4.1 Meshing

When meshing a structure, there is always a choice between the accuracy of the solution and how long computation time is available. A very dense mesh leads to a more accurate solution, but this also causes the CPU cost to become very high. A compromise between the two is to have a relatively dense mesh where there are high stress gradients, and a coarser mesh where the stress levels are more constant [36]. When refining the mesh in this way, it is important to use gradual transitions in element size, as sudden changes in the mesh can cause an ill-conditioned stiffness matrix, which is very difficult to solve.

In the finite element method, there are also errors related to the individual finite elements that are important to be aware of. The behaviour of each element is described by displacement interpolation polynomials, and these sometimes cause errors to occur when the polynomials chosen cannot accurately represent the actual behaviour of the material described [37].

One such error is called *parasitic shear*, and is caused by incomplete interpolation polynomials. This causes false normal strains to appear in the shear strain expressions, and is difficult to avoid when using a standard formulation technique. The solution is to use reduced numerical integration when solving the system. However, this may lead to what is called *spurious zero-energy modes*, or *hourglass-modes*. This is because the reduced integration removes the strain-modeling terms that belong in the strain energy expression, which leads to what appears to be extra rigid body modes [37]. These spurious modes leads to a singularity in the stiffness matrix, making it impossible to invert, which is why these modes should be avoided [38].

The final source of error related to individual elements is *shear locking*, which dominates in elements where the thickness is small compared to the width and height. The elements ability to represent the condition of zero transverse shear strains decreases when the thickness does, which affects the elements ability to retain a sufficient amount of element DOFs to represent all the deformation modes. Shear locking occurs when the only solution that satisfies the zero transverse shear strains condition is the one that implies zero nodal displacements altogether [39].

### 2.4.2 Shell Elements

The choice of what element-type to use in the modeling of a structure is dependent on what type of loading and stress distribution the elements are exposed to. In the case of a CLT- structure that consists mainly of massive wall- and floor plates, a good choice is to use *shell elements*. These are capable of carrying loads both in- and out of plane, and has a small thickness compared to the height and width of the elements, which fits the

characteristics of the CLT-plates.

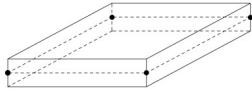


**Figure 2.18:** A conventional shell element with four nodes.

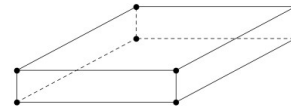


**Figure 2.19:** A continuum shell element with eight nodes.

In Abaqus, there is a choice between *conventional stress/displacement* shell elements and *continuum* shell elements. The conventional shells are defined by a reference plane with four nodes, and are assigned thickness from its' section. The continuum shells on the other hand, discretize the entire 3D body with eight nodes, but cannot represent the rotational DOFs [40]. Because the conventional shells have less nodes, the computation time is shorter, which makes them preferable as long as they provide sufficient accuracy.

The simplest form of the conventional shell elements is the S4 element in Abaqus. This is a very robust general purpose element, and can be used as both a thick- and thin plate element. It also has the advantage that it is resistant to both transverse shear locking and unconstrained hourglass modes [41].



### 3 Data Analysis

This section presents how the data analysis was performed and the choices taken both in the pre- and post-processing of the data, as well as in the *frequency domain decomposition*, in order to obtain the natural frequencies, mode shapes and damping ratios of the two buildings studied. See Figure 3.1 for a breakdown of the pre-processing of the data records.

It would have been possible to use existing software to apply the following techniques, but these programs are often expensive and does not allow direct control of the steps in the procedure. As an alternative, original scripts was developed using the theory presented in subsection 2.3. The scripts along with the MATLAB modules, are included in the digital appendix.

In this chapter, the following naming convention is used:

- Time record: the original 6 hr signal data records
- Time series: smaller partitions of the time records treated independently
- (Time) segment: smaller partitions of a time series, strictly in the context of computation of PSD by Welch’s method.

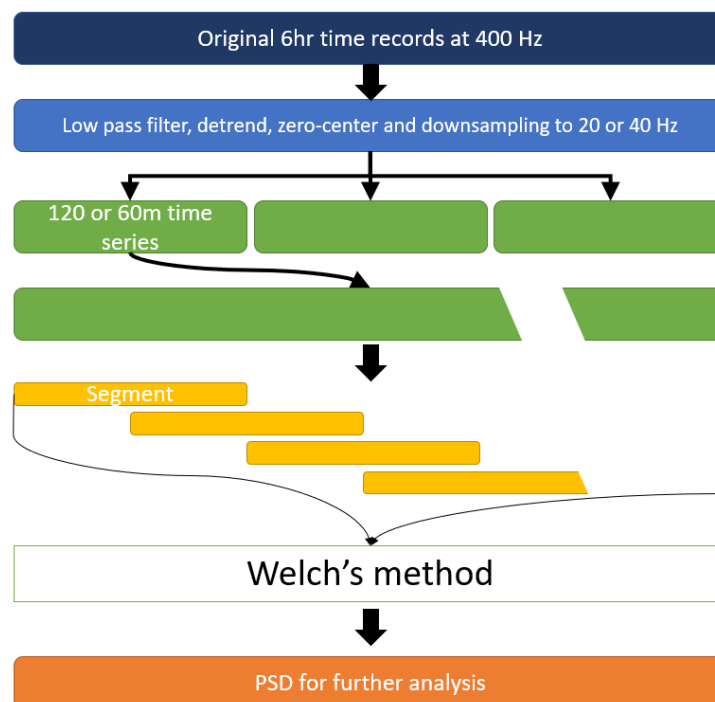


**Figure 3.1:** Flowchart of the data pre-processing and breakdown

### 3.1 Pre-processing

For the purpose of pre-processing of raw measurement data, a python script `preprocess.py` was prepared. The script relies heavily on the DSP-library `scipy.signal 1.8.0` [30], as well as the math library `numpy 1.22` [42]. In addition, 3rd party libraries `nptmids 1.4.0` [43] and `scipy.io 1.8.0` [30] were used for handling the various file formats in relation to opening and saving data. The most important functions used for processing of the data are summarized below:

- `scipy.signal`
  - `butter()`, creates the butterworth filtering parameters
  - `sosfiltfilt()`, applies the two sided digital filter to the data
  - `decimate()`, downsamples the data
  - `detrend()`, removes any spurious trend in the data if it exists
- `numpy`
  - `mean()`, used to compute the mean of the signals for the purpose of zero-centering

In an attempt to reduce the risk of systemic errors introduced by possible unfortunate choices of record length or decimation factors, four different sets of pre-processed data were produced on the same raw-data. Two different time series lengths of *60min* and *120min*, and two different down-sampled frequencies of 20Hz and 40Hz were chosen.

Prior to the down-sampling, all of the data was passed through a 5th order two-sided butterworth low pass filter at a frequency of  $0.4f_{downsampled}$ , ie. at 8Hz and 16Hz for the 20Hz and 40Hz data respectively. While `decimate()` does contain an anti-aliasing filter, manually applying a low pass filter prior to decimation provides greater control and a more powerful anti-aliasing of the data.

Next, the filtered data was down-sampled (decimated). It is not recommended to decimate with factors larger than 13 [30], and thus, for the files to be decimated from 400Hz down to 20Hz, this was done by decimating them twice, first at 2x and then at 10x.

### 3.2 FDD

For performing the FDD algorithm, a MATLAB module **FDD.m** and a script **FDDscript.m** was created. No external libraries were used, but functions inside the *Digital signal processing toolbox* [44] in MATLAB r2021a were used extensively.

The most important built-ins used in the prepared MATLAB module are:

- `cpsd()`, for computing the cross-spectral PSD-matrix
- `svd()`, for computing the SVD of the cross-spectral matrix
- `ifft()`, for computing the autocorrelation function from the SVD
- `findpeaks()`, to identify the peaks of the auto-correlation function for the purpose of computing the logarithmic decrement
- `polyfit()`, for linear regression of the delta array,

The pre-processed data consisting of a series of 6hr recordings were divided into multiple, shorter time-series. Various sources gives different recommendations regarding length of time series in connection with OMA. As a good rule of thumb, a recommended minimum time series length of  $T_s \geq \frac{10}{\zeta f_{min}}$  [28], which would suggest a time series  $T_s$ , of 1000 seconds if damping  $\zeta$  is 1% and the 1st fundamental mode  $f_{min}$ , is  $1Hz$ .

When using Welch's method for the PSD calculation however, the use of longer time series allow for taking the ensemble average of several sub-segments without sacrificing frequency-resolution in the PSD-estimate. This has the advantage that it leads to more stable and accurate results. In conclusion, it is often advantageous to use longer time series than the recommended minimum, especially when using the FDD-algorithm for damping estimations.

In order to investigate the validity of the chosen time series length, the OMA analysis was performed on the entire dataset with two different choices of time series length, namely 60 and 120 minutes. In the end, a time segment of  $\frac{T_s}{10}$  was chosen in the computation of the PSD. With a 50% overlap, this yielded 19 segments over which the ensemble average is taken.

### 3.3 Post-processing

By defining a convenient ratio for modal excitation such as  $S = \frac{Amp_{Mode_{peak}}}{Amp_{Noise_{floor}}}$ , a threshold can be set to quickly filter out data points that come from time segments deemed to be of too low excitation to yield reliable results (see Figure 3.2). After inspecting the scatter plots of the results in Figure 5.3 and Figure 5.8, a threshold of  $S > 20$  was chosen.

After the aforementioned signal amplitude threshold-filtering, some sporadic data points with obviously false damping ratio estimates might remain. These are handled by excluding the estimates outside of the [5 95]th percentile range.

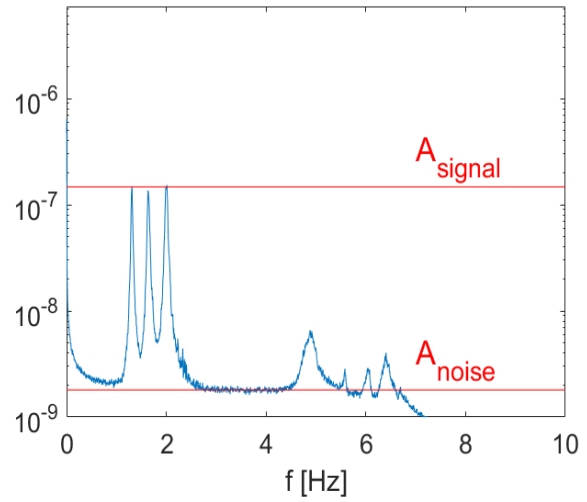
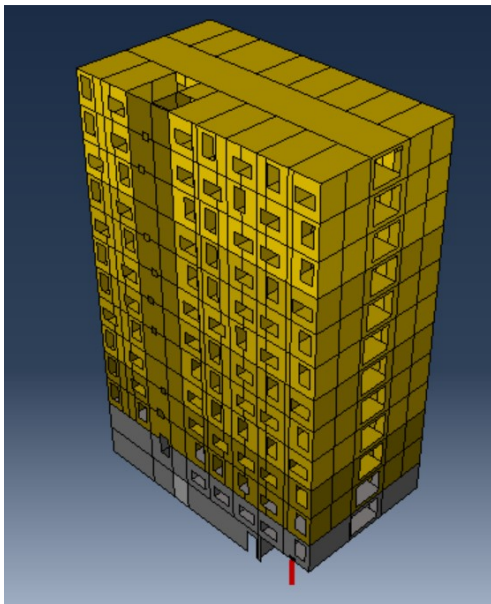


**Figure 3.2:** Signal to noise amplitude. In this plot, modes 1, 2, 3 have a ratio of approx. 100

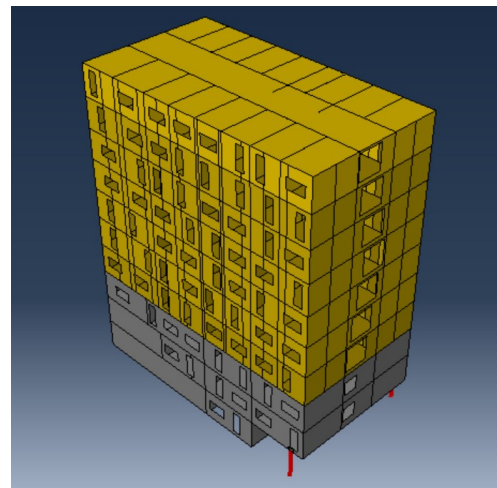
## 4 Modeling

This section describes the choices taken and methods used when developing the finite element model. The software used to build the parametric models of the two buildings is *Simulia Abaqus 2019*, along with *Python version 2.7* and *Microsoft Excel*. The parameters and information used to build the model is stored in an Excel workbook, which serves as a convenient way to store/modify the necessary parameters. The scripts and excel workbooks are made available in the digital appendix.

The scripts and input files are written and structured with recyclability in mind, and should be reasonably easy to understand and use in other projects. Adding or modifying the functionalities of the model is should be somewhat simple for someone with experience in python programming and Abaqus.



(a) SML3



(b) SML5

**Figure 4.1:** Screen shots of the two models. The color grey indicates concrete elements, the red indicates steel, while the yellow indicates CLT. The darker the shade, the thicker the section.

## 4.1 Defining the Geometry

SML3 and SML5 are quite simple and regular in their design:

- Rectangular floor plans
- Facades are flat planes, with the exception of an overhang (supported by columns) on the ground floors
- Windows and openings, while they do alternate rotations and placements slightly, follow a regular grid
- The bearing walls follow an orthogonal grid and the pattern is repeated every storey, with exception of the concrete walls in the first few storeys
- The structural system is almost entirely comprised of CLT

The floors were assumed to have a rigid diaphragm effect, which means that they have a rigid body motion and does not deform during loading. For low frequency modes this should be a valid assumption [45].

Due to the simple geometry, modeling the walls were done by defining the start and end point in terms of which axes these points lie on. The next step is defining the target width of elements. CLT walls were given a target maximum width of 2500mm, as this is essentially the maximum width that is usually transported on Norwegian roads. The script then computed the width necessary to cover the entire span of the wall with an integer number of parts. Finally, the array of wall parts was constructed.

Concrete walls were modeled as one single element from start to finish, as it was assumed that site-cast concrete is used for these buildings, as opposed to pre-cast concrete.

The walls and floors then have openings such as doors and windows cut out from their geometry. The openings were positioned in accordance with drawings and plans made available for this thesis' work as accurately as possible.

## 4.2 Connections

The interactions between elements in Abaqus can be defined in several different ways. In this thesis the connections were modeled using discrete *connectors* spaced at some interval. This is a component in Abaqus that uses discrete springs and damper dashpots, which when combined into a single element is called *connectors*. They provide a realistic modeling of connections, as well as giving direct control of the stiffness in a given direction for a set of connectors. This allows the analysis to discuss parameters such as 'stiffness

per unit length' along a joint, which is easier to convert to a physical parameter than the reduced thicknesses from the previous models.

To ease the modeling process, connectors were used for both the concrete and the CLT storeys. To account for the fact that the concrete walls are continuous, and not plates connected by discrete fasteners like the CLT walls, the connectors in the concrete walls were given infinite stiffness.

#### 4.2.1 Stiffness Ratios in Connections

The connector stiffnesses were defined as a ratio of the stiffness of the elements they connect, instead of manipulating the numerical values directly because this is more convenient. For this to work it is necessary to find a representative stiffness value for a CLT-plate. To do this, all connectors related to the same section type were grouped together and given the same stiffness values. The geometry of the panels are taken into account by defining a characteristic height and width of a cross section by using the average height and width of all plates with the cross section in question. Because all the storeys are 3000m tall, and all the CLT-walls have a target width of 2500mm, the characteristic sizes were not very disparate between different cross-sections.

$$\begin{bmatrix} m_x \\ m_y \\ m_{xy} \\ v_{xz} \\ v_{yz} \\ n_x \\ n_y \\ n_{xy} \end{bmatrix} = \begin{bmatrix} D_{11} & D_{12} & 0 & 0 & 0 & 0 & 0 & 0 \\ D_{21} & D_{22} & 0 & 0 & 0 & 0 & 0 & 0 \\ 0 & 0 & D_{33} & 0 & 0 & 0 & 0 & 0 \\ 0 & 0 & 0 & D_{44} & 0 & 0 & 0 & 0 \\ 0 & 0 & 0 & 0 & D_{55} & 0 & 0 & 0 \\ 0 & 0 & 0 & 0 & 0 & D_{66} & D_{67} & 0 \\ 0 & 0 & 0 & 0 & 0 & D_{76} & D_{77} & 0 \\ 0 & 0 & 0 & 0 & 0 & 0 & 0 & D_{88} \end{bmatrix} \cdot \begin{bmatrix} K_x \\ K_y \\ K_{xy} \\ \gamma_{xz} \\ \gamma_{yz} \\ \epsilon_x \\ \epsilon_y \\ \gamma_{xy} \end{bmatrix}$$

**Figure 4.2:** The origin equations used for computing the stiffness of connectors [46]

The basis of the equations used for the calculations of the stiffness of connectors are shown in figure 4.2, where

$$\begin{aligned} D_{66} &= E_{0,mean} \cdot h_x \\ D_{77} &= E_{0,mean} \cdot h_y \\ D_{67} &= D_{76} = 0 \\ D_{88} &= 0.75 \cdot G_{0,mean} \cdot h_{clt} \end{aligned}$$

Along a joint between two CLT-panels, the following equations were used to control the stiffness values of a single connector (see Figure 4.3 for an illustration of what  $k_{\perp}$  and  $k_{\parallel}$  refer to):

$$k_{i,\perp} = ASR \frac{E_{0,mean,CLT} * l_k * h_{\parallel}}{d_k * n_{connectors}} \quad (4.1)$$

$$k_{i,\parallel} = SSR \frac{G_{0,mean,CLT} * 0.75 * l_k * h}{d_k * n_{connectors}}, \quad (4.2)$$

where

- ASR (axial stiffness ratio) and SSR (sliding stiffness ratio) are the chosen stiffness ratios perpendicular and parallel to the joint respectively
- $E_{0,mean,CLT}$  and  $E_{G,mean,CLT}$  are the representative stiffness properties of CLT plates
- $l_k$  is the length of a characteristic joint for a given cross section (in this model: approx.  $3m$  for vertical joints and  $2.5m$  for horizontal joints)
- $d_k$  is the depth of the panel in the plane in the direction perpendicular to the joint, ie. for a joint along the top edge of a plate, this would be the height of the panel
- $h$  and  $h_{\parallel}$  are the total thickness of a plate and the total thickness of lamellas parallel with the force, respectively
- $n_{connectors}$  is the number of connectors along the joint

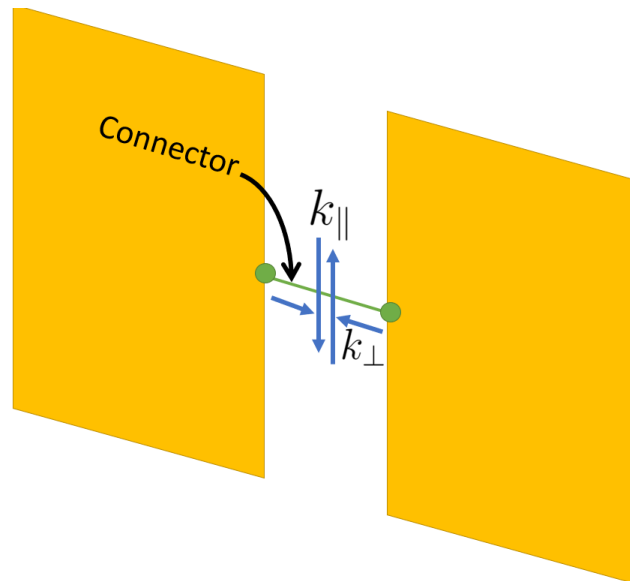


**Figure 4.3:** Illustration of the stiffness directions of a single connector. Multiple connectors are spaced evenly along joints.



Using the following values:

- $E_{0,mean} = 11000$  MPa
- $G_{0,mean} = 690$  MPa
- $height_{char} = 3000$  mm,  $width_{char}=2500$  mm
- $ASR = SSR = 1$

, a set of stiffness values for a single connector associated with a given section type was estimated, as presented in Table 4.1. Manipulating ASR or SSR will simply scale the associated stiffnesses to be used. Note that this table uses fixed values for  $height_{char}$  and  $width_{char}$ , while the approach used in the modeling script computes the actual characteristic values for these. However, as the storeys are all 3000mm tall and the target width for the walls is set to 2500mm, the actual difference from the values in Table 4.1 and the computed values used in the model is relatively small.

**Table 4.1:** Estimated stiffness of a single connector. (One connector every 300mm)

Section	$h_{vert}$ $h_{hor}$		Along top/bot		Along sides	
	[mm]		$k_{\perp}$	$k_{\parallel}$	$k_{\perp}$	$k_{\parallel}$
			[N/mm]			
180-7Ply	120	60	122 222	8 625	72 000	10 162
160-7Ply	120	40	122 222	7 667	48 000	9 033
150-7Ply	110	40	112 037	7 118	48 000	8 468
140-7Ply	80	60	81 481	6 708	72 000	7 904
130-7Ply	100	30	101 852	6 229	36 000	7 339
120-7Ply	90	30	91 667	5 750	36 000	6 775
100-7Ply	80	20	81 481	4 792	24 000	5 645
80-7Ply	60	20	61 111	3 883	24 000	4 516

This approach ensures that one value for ASR and one for SSR controls the stiffness of every connector in the model, while each joint is still related to the stiffness of the CLT-plates they attach.

### Impact on Effective Stiffness from Discretization of Connections

In reality, the connections between CLT-plates are held together by a combination of contact-friction in between the plates and discrete fasteners such as screws, hold-downs or angle brackets. For physical CLT-panels, compressive forces are transferred by the contact-force between abutting elements. Contact forces are very difficult and expensive to model in FEM [47]. Therefore, in the modeling approach used in this thesis, the contact-force must also be transmitted with connectors. However, this leads to a loss of stiffness in the connection due to stress concentrations in the zones near the boundaries. A higher density of connectors reduce this effect but increases modeling complexity and cost.

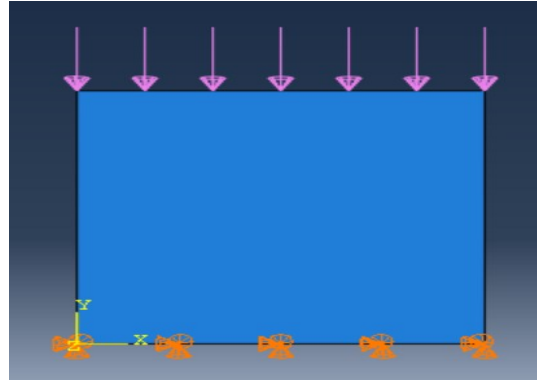


**Figure 4.4:** The CLT plate studied, here with 5 discrete boundary conditions

On the other hand, in reality, the tensile stress in connections are entirely captured with connectors. Again, because of stress distributions near joints, increasing connector density beyond the real connector density would give an increase in apparent stiffness for the same reasons.

In short:

- An excessively high density of connectors will overestimate tensile stiffness in joints and have a high computational cost
- An excessively low density of connectors will underestimate compressive stiffness in joints but have a low computational cost

For these reasons, a compromise between cost and accuracy for both compressive and tensile forces is desired, ideally with a reasonably realistic density of connectors.

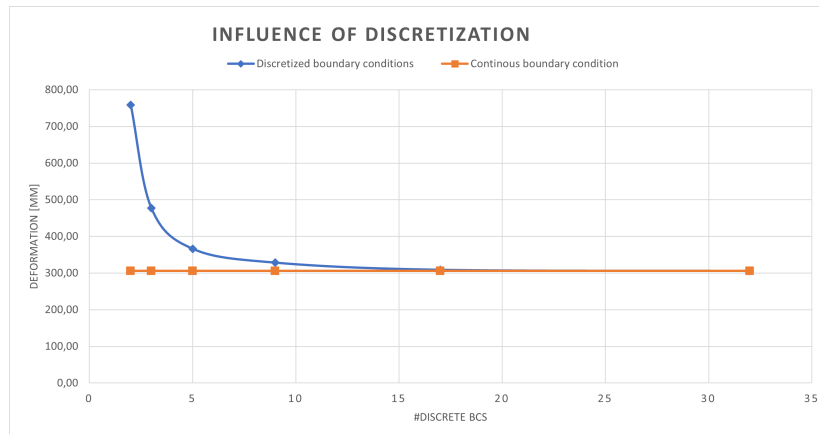
To investigate this effect, a simple test was executed in Abaqus CAE. A  $3 \times 3 \text{ m}^2$  CLT-plate shown in figure 4.4, was modeled by the same principles as the ones in SML3 and SML5: a S4 shell element with an orthotropic section material called *CLT 160:5Ply*, equivalent to the one used in the actual model. A shell edge load with magnitude  $10 \text{ kN}$  was applied along the top edge, and several different constellations of boundary conditions were applied to inspect the influence of the boundary conditions on the deformations of the plate. The results are displayed in table 4.2.

Figure 4.5 displays how increasing the number of discrete boundary conditions makes the displacements converge towards the continuous solution, as is expected. At 17 discrete

points, the error between the two solutions is 0.01, which indicates that it is possible to approximate the continuous joints in the real structure with discrete fasteners without disturbing the stress distribution too much.

**Table 4.2:** Influence of discrete vs. continuous boundary conditions on the deformation.

Boundary condition	Displacement [mm]
Continuous	305,60
2 discrete points	758,40
3 discrete points	476,90
5 discrete points	366,10
9 discrete points	328,30
17 discrete points	308,70
32 discrete points	305,70



**Figure 4.5:** Graph displaying the influence of discretization on the displacements compared to a continuous boundary condition.

From the results of this investigation, a connector density of  $c/c$  300mm was chosen, equivalent to 11 discrete points in Table 4.2, resulting only a minor drop in compressive stiffness, while keeping a realistic connector density.

#### 4.2.2 Damping in Connections

Damping in connections is implemented by defining two global viscous damping parameters, one for axial deformation in connections and one for sliding deformation in the connections.

The viscous damping values, unlike the stiffness distribution in connectors, does not take the cross-sections the connector is attached to into consideration, and is not scaled with the stiffness of the connector either.

### 4.3 Foundation

Both SML3 and SML5 are built directly on bed-rock, with the first two floors having solid concrete load-bearing walls.

The bedrock upon which the concrete walls are cast is thought to have sufficient stiffness and strength that the foundation can be modeled by translationally locking the nodes of the concrete walls that are in contact with the bedrock.

As the terrain is slightly sloped, the concrete walls in 1. and 2. floor are partly submerged under some back-filled soil. This puts a slight ground-spring action on the below-terrain wall area. However, as the stiffness contribution from the abutting soil is massively dwarfed by the structural stiffness of the concrete walls, this will have no significant effect on the overall stiffness of the structure, and is for that reason neglected from the model.

### 4.4 Mass

In their thesis, Lervik & Kristiansen performed fairly detailed estimates of the mass of SML3 and SML5, lumped by storeys [17], see Figure 4.6. To preserve some degree of comparability and to avoid doing double-work, these calculations serve as the basis for mass distributions in this thesis' models.

Two different mass configurations were tested:

- Mass configuration 1, where the dead mass from outer wall cladding, windows and so on, is smeared across outer walls. The rest of the dead mass is smeared across floors.
- Mass configuration 2, where dead mass is only smeared across floors

See Appendix A for the calculations for dead mass distribution. The result from the mass calculations were added as non structural mass distributed evenly across the area of the respective parts. Then, as there was some slack in some of the area estimates in the calculations, the dead-mass inputs were evenly adjusted until the exact target total mass was reached.

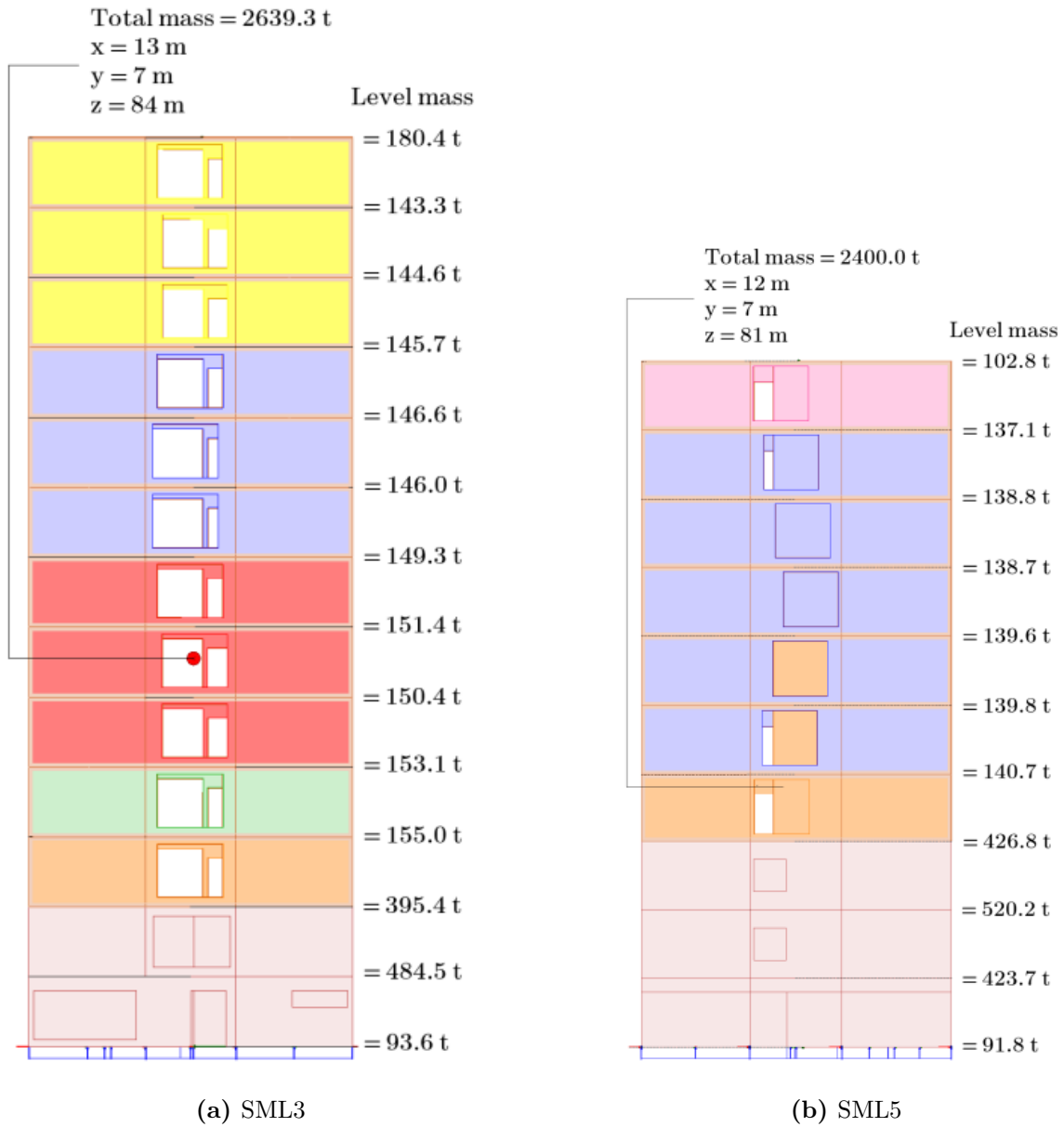


Figure 4.6: Mass distributions as calculated by Lervik & Kristiansen [17]

## 4.5 Loads

As the goal is to find the modal properties, only the global gravitational load of  $9810 \frac{mm}{s^2}$  is necessary. No other external loads or ground springs are included in the model.

## 4.6 Materials

The following assumptions are made for the material properties:

- All timber-elements are comprised of Nordic spruce boards with C24 quality
- Concrete elements are cast with B45 quality

**Table 4.3:** Material properties used in the model

	Density [ $kg/m^3$ ]	$E_1$ [MPa]	$E_2$ [MPa]	$E_3$ [MPa]	$\nu_{12}$	$\nu_{13}$	$\nu_{23}$	$G_{12}$ [MPa]	$G_{13}$ [MPa]	$G_{23}$ [MPa]
C24	420	11000	370	370	0.5	0.6	0.6	690	690	50

(a) Timber properties used in the model [48]

	$E_{0,mean}$ [MPa]	$G_{0,mean}$ [MPa]
CLT with C24 only	11000	690

(b) Timber properties used in the model for the purpose of computing the connector stiffnesses [5]

	Density [ $kg/m^3$ ]	$E$ [MPa]	$\nu$
B45	2300	34000	0.2

(c) Concrete properties used in the model [49]

	Density [ $kg/m^3$ ]	$E$ [MPa]	$\nu$
S355	7850	210000	0.3

(d) Steel properties used in the model [50]

## 4.7 Analysis Steps

To extract the modal properties of the model in Abaqus, both a modal frequency- and complex frequency step was used in addition to the required initial step. The modal frequency step extracts the natural frequencies and mode shapes of the undamped structure by solving the eigenvalue problem presented in section 2.2.2, by use of the Lanczos method. After this, the complex frequency step, which is a subspace projection method, uses the extracted eigenmodes as a subspace to find the complex natural frequencies and mode shapes. This step is necessary to include the effects of damping in the analysis, and to find the damping ratios of the structure.

## 4.8 Meshing

Before optimizing the model, a preliminary series of analyses were performed in order to determine appropriate mesh density, that is, the minimum mesh density that yields sufficiently accurate modal estimates. As the 3 fundamental modes are the most important for the context of this analysis, the impact of varying mesh densities was evaluated by the effect it had on these modes.

A sample configuration of the connector-model of SML3 was used. Note that as this step was performed before performing any type of analysis, the parameters were chosen prior to settling on the actual parameters used in the model, and were not the same as the ones used in the analyses.

- An initial connector density of  $c/c$  500mm was chosen
- Mass configuration 1 as per 4.4
- Mass and stiffness properties similar to that of C30 Nordic spruce for the timber elements and B35 for the concrete elements
- Quadrilateral elements with reduced integration
- A single global mesh density

A more sophisticated approach to meshing, such as defining zones around sharp changes in geometry (doors and windows in this context), as well as around the bounding edges of instances would allow a more efficient usage of computing power and memory. This could improve the quality of the mesh within the computing budget at hand.

In a crude attempt to improve mesh efficiency, it was briefly investigated whether it would be beneficial to increase mesh density for instances that had any cut-outs in its geometry, while keeping the mesh for instances with virgin geometry at the coarser base mesh.

However, the improvement of this approach seemed to be negligible. So, for simplicity's sake, a single global mesh size for the entire model was chosen.

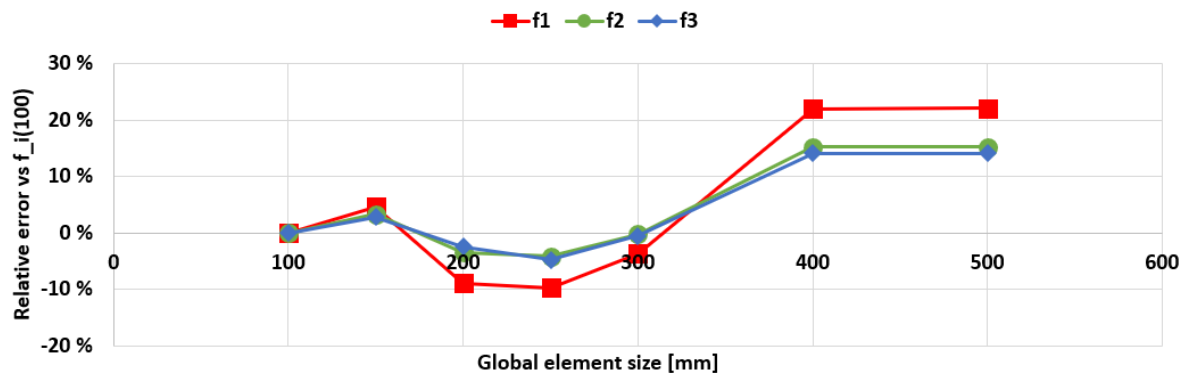


**Figure 4.7:** Investigation regarding choice of mesh density

The results from the densest mesh is assumed to yield an accurate solution. It is however not strictly possible confirm if the results at 100 yield accurate results. For smaller and less complex problems, this could be investigated by increasing the mesh density further, once the converges to some value it is reasonable to assume a correct solution. In this case, however, the limitations of the hardware available in this thesis prevent any denser mesh from being feasible.

So, for this model a global mesh size of 300 was chosen, as that mesh size gives reasonably inexpensive computations, while yielding seemingly accurate results for the frequencies of modes of interest.



## 4.9 Parameter Optimization

A parameter optimization was performed in order to optimize the model parameters so that the modal properties match the results obtained from the physical structures. In general, there are 3 main targets to hit:

- Modal frequency
- Mode shape as evaluated by the MAC-criterion
- Damping ratio

A compliance measure is proposed in (4.3), that makes it possible to weight each mode. It also allows for optimization of an arbitrary number of modes, where it is possible to prioritize the modes and values of the highest interest.

$$Match = 1 - \sqrt{\frac{\sum \left( \frac{X_{FEM,i} - X_{tgt,i}}{X_{tgt,i}} \right)^2 * w_i}{\sum w_i}} \quad (4.3)$$

$X_{FEM,i}$  and  $X_{tgt,i}$  might be the modal frequencies or the damping ratios of the system, while the subscript denotes the numerical and experimental results respectively.  $w_i$  is the weight applied to a specific mode, and the subindices  $i$  indicates which mode it is related to. A match of 1 indicates a perfect fit.

As mentioned in 2.2.2, the mode shapes are influenced by the *distribution* of stiffness and mass, rather than the global sum. From subsection 4.2, it is clear that there are only two modeling parameters adjustable in the optimization process; the sliding- and axial stiffness ratios in connections. When adjusting these ratios, it is the *scale* of stiffness in the connections that changes, not the distribution. This means that it is unnecessary to optimize the model based on the mode shapes (or the MAC-values), because they aren't affected much anyway.

In the case of the buildings in evaluated in this thesis the higher modes are barely excited, and only the three fundamental modes yielded meaningful experimental results. This led to the decision to optimize for these three modes, with equal weighting.

### 4.9.1 Frequency Optimization

First, the models were optimized for frequency compliance. It is possible to optimize for the frequencies without including damping because of the relationship in equation (2.12) seeing as the frequency shift in weakly damped systems such as SML3 and SML5 is negligible.

The frequency optimization procedure was done by performing a series of trials, varying ASR and SSR with regular intervals, and storing the results for each trial. The data from the initial trials was then fed into a MATLAB script **ParameterstudyPlot.m**. A 4th degree polynomial surface interpolation function was generated, on which the peak value and thus the estimated optimized set of ASR - SSR values is estimated.

#### **4.9.2 Damping Optimization**

Secondly, once the optimized connector stiffness values have been determined, a brief damping influence experiment was performed.

Several trials with different combinations of viscous damping values in the axial and sliding direction for connectors were performed, in which:

- ...stiffness and mass properties are held constant
- ...no damping apart from the damping in the connectors are added to the model.

## 5 Results

### 5.1 Empirical Results

In the following section, all the results from the FDD procedure is presented. This is only a presentation of the actual results, as they are further discussed in section 6. The techniques used and the choices taken when performing the FDD is presented in section 3.

### 5.1.1 SML3

#### Frequencies

Table 5.1 shows the seven first natural frequencies, or modal frequencies, of SML3. The first three frequencies were computed by averaging the frequency output from the FDD calculations, whereas the remaining higher modes are estimated from the 24hr PSD in Figure 5.1.

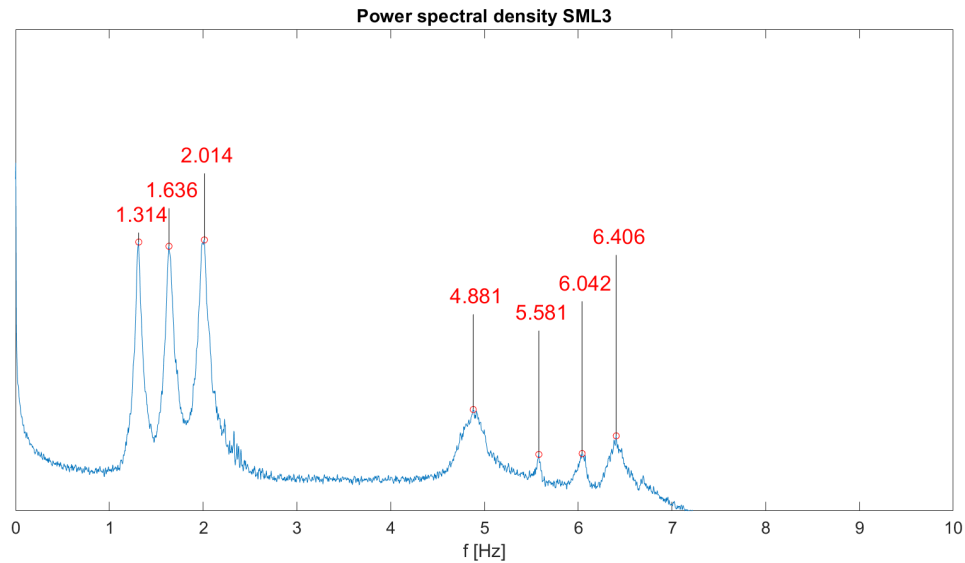


**Figure 5.1:** Estimate power spectral density of SML3, computed over a 24hr time-record. Y-scale is logarithmic.

**Table 5.1:** SML3: Modal frequencies. The modes 1-3 are taken from the FDD analysis, whereas modes 4-7 comes from peak picking on a periodogram

Mode	Frequency [Hz]
1	1.301
2	1.634
3	1.988
4	4.881
5	5.581
6	6.042
7	6.406

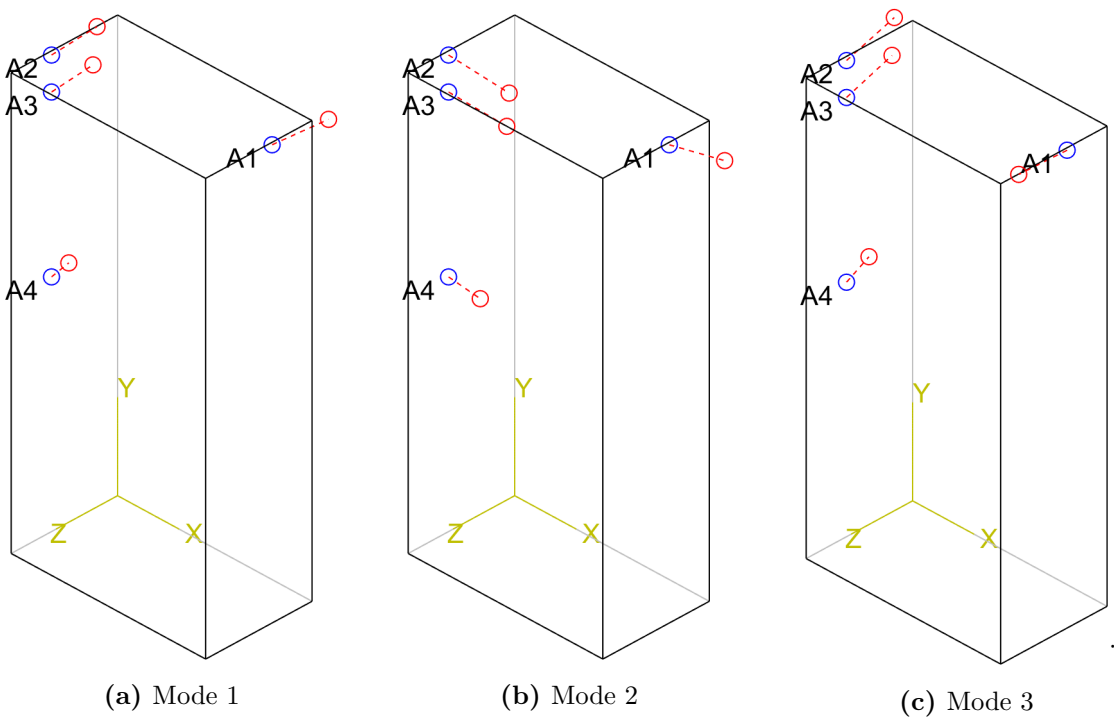
## Mode Shapes

**Table 5.2:** SML3: Computed mode shapes by FDD, grouped by sensors

Mode	A1			A2			A3			A4		
	x	y	z	x	y	z	x	y	z	x	y	z
1	-0.02	-0.07	1.00	0.00	0.04	0.79	0.00	0.05	0.72	0.00	0.05	0.30
2	0.97	0.16	-0.01	1.00	-0.09	0.05	0.95	-0.07	0.06	0.52	-0.07	0.03
3	0.10	0.09	-0.94	-0.17	0.07	1.00	-0.16	0.08	0.95	-0.08	0.09	0.47

**Table 5.3:** SML3: Computed mode shapes by FDD, grouped by axes

Mode	X				Y				Z			
	A1	A2	A3	A4	A1	A2	A3	A4	A1	A2	A3	A4
1	-0.02	0.00	0.00	0.00	-0.07	0.04	0.05	0.05	1.00	0.79	0.72	0.30
2	0.97	1.00	0.95	0.52	0.16	-0.09	-0.07	-0.07	-0.01	0.05	0.06	0.03
3	0.10	-0.17	-0.16	-0.08	0.09	0.07	0.08	0.09	-0.94	1.00	0.95	0.47

**Figure 5.2:** SML3: Computed mode shapes by FDD, plots

## Damping Ratios

**Table 5.4:** SML3: Damping ratios from FDD, N is the number of datapoints that passed the mode excitation threshold of 20

Mode	$\bar{\zeta}$	$\zeta_{0.05}$	$\zeta_{0.95}$	$\sigma_{\zeta}$	N
1	1.536	1.446	1.621	0.156	4072
2	1.438	1.362	1.510	0.134	3987
3	1.617	1.527	1.693	0.144	4114

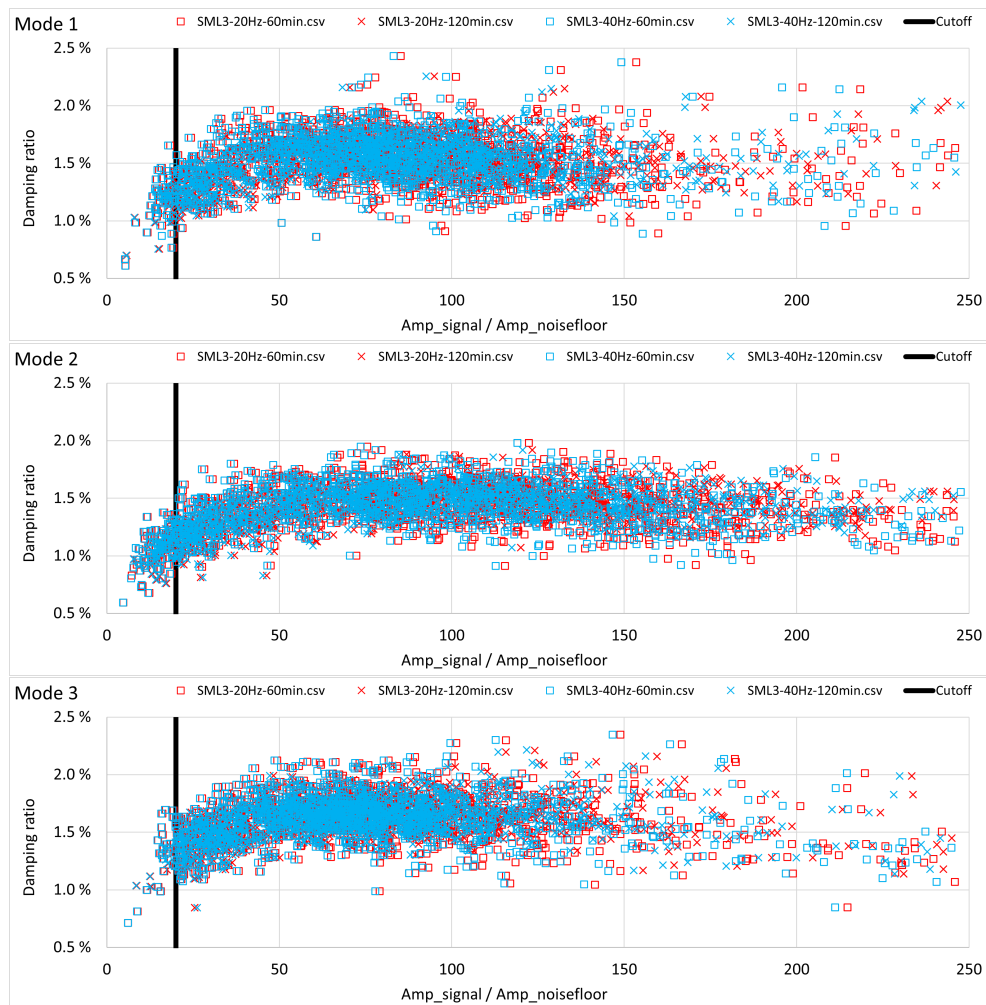


**Figure 5.3:** SML3: Damping ratio estimates from FDD, plotted against signal-to-noise ratio

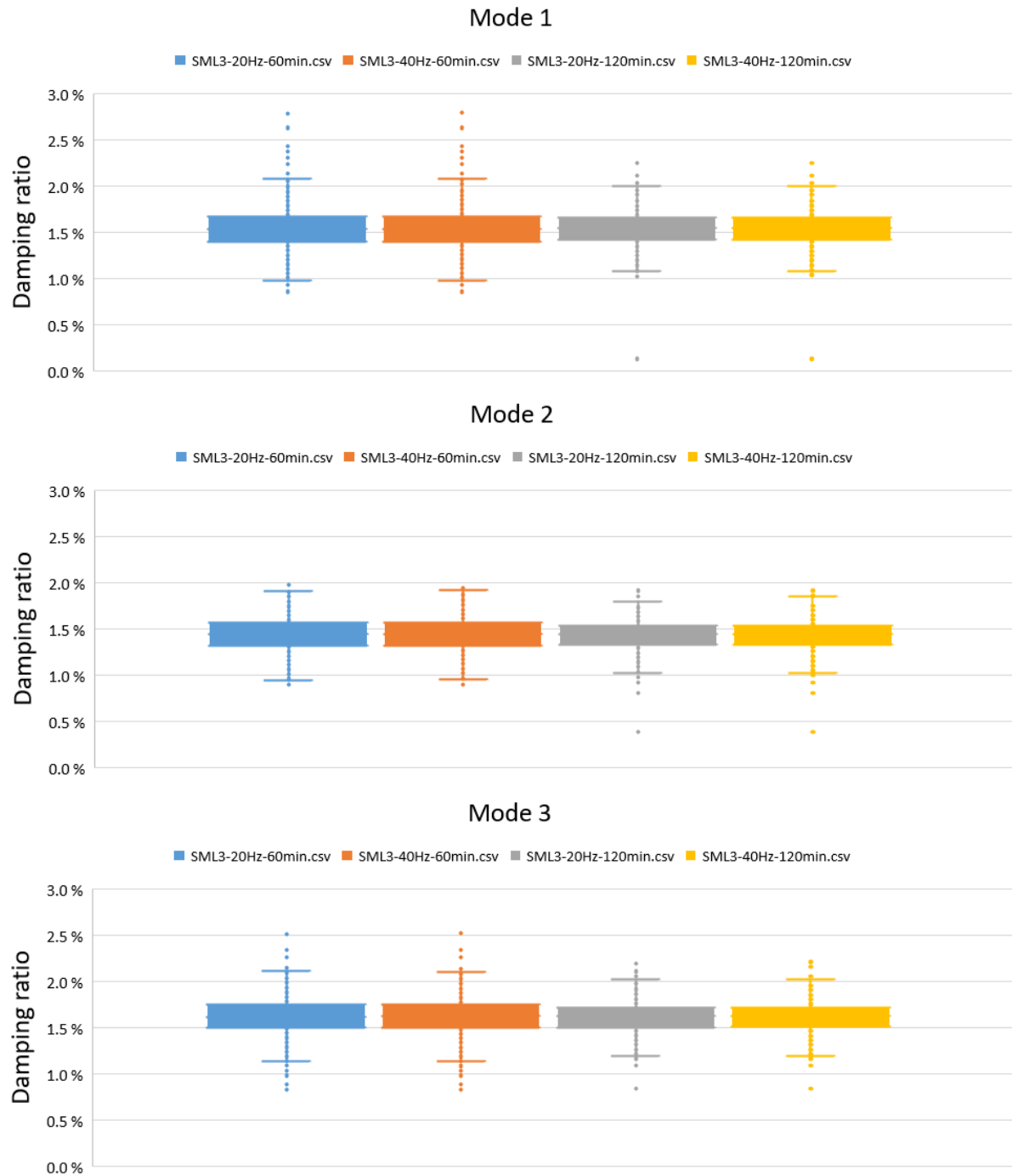


**Figure 5.4:** SML3: Box plot of damping ratio estimates, comparing the different pre-processing routines

## Rayleigh damping approximation

**Table 5.5:** SML3: Rayleigh damping coefficients

	Opt. for mode 1 and 2	Opt. for mode 1 and 3	Compromise
$\alpha$	0.0278	0.0217	0.0214
$\beta$	0.0072	0.0108	0.0105
MSE [%]	0.1170	0.0617	0.0507

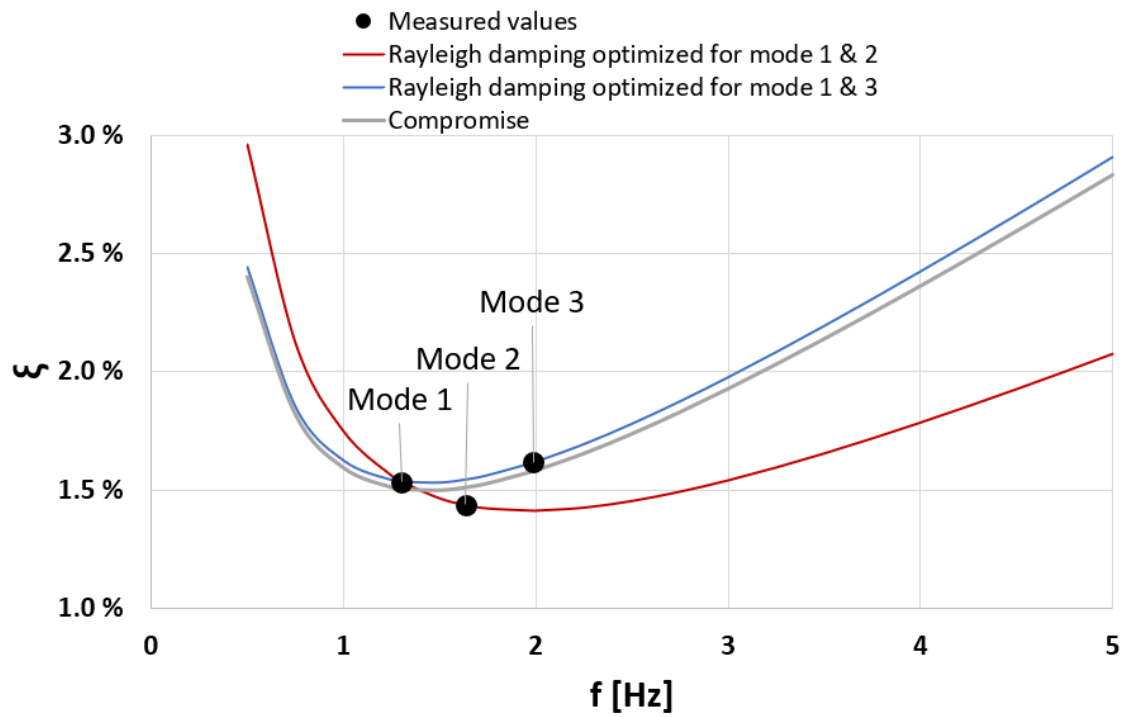


**Figure 5.5:** SML3: Rayleigh approximation of damping behaviour



### 5.1.2 SML5

#### Frequencies

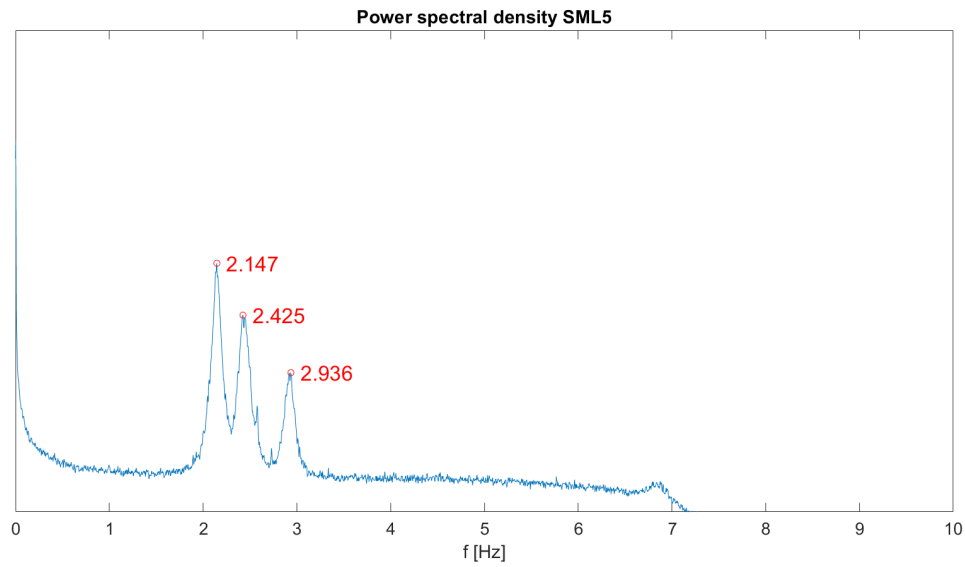


**Figure 5.6:** Estimate power spectral density of SML5, computed over a 24hr time-record. Y-scale is logarithmic.

Table 5.6 shows the identified modal frequency estimates computed by averaging the frequency output from the FDD calculations.

**Table 5.6:** SML5: Modal frequencies

Mode	Frequency [Hz]
1	2.150
2	2.443
3	2.924

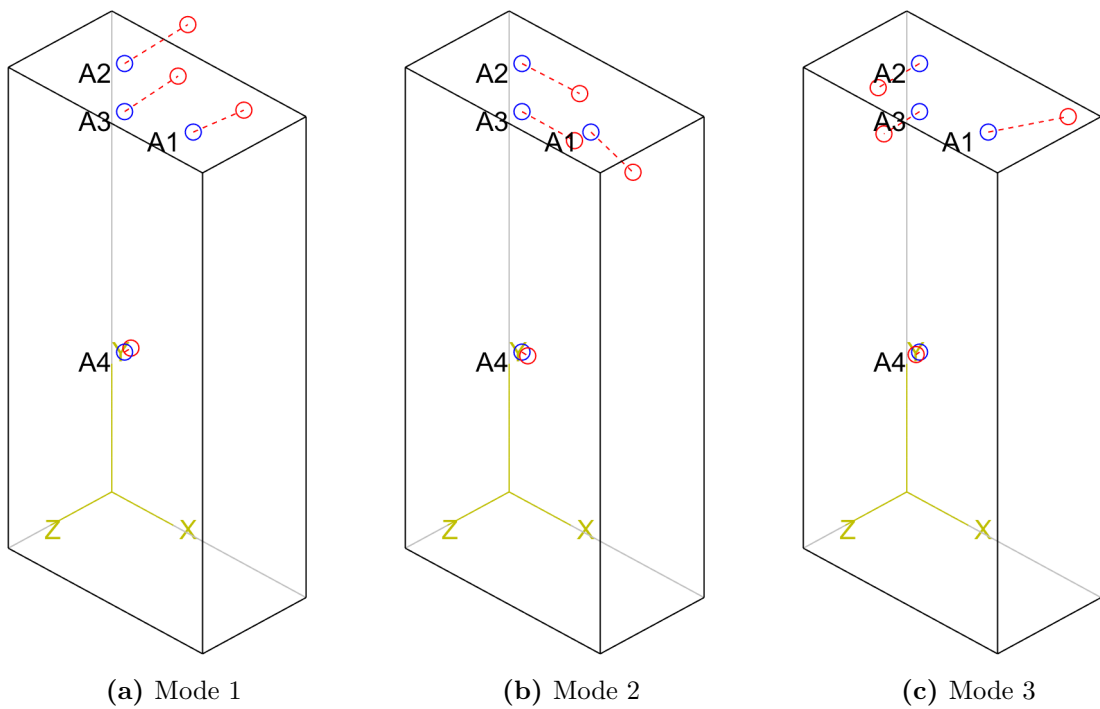
## Mode Shapes

**Table 5.7:** SML5: Computed mode shapes by FDD, grouped by sensors

Mode	A1			A2			A3			A4		
	x	y	z	x	y	z	x	y	z	x	y	z
1	0.07	0.81	-0.01	0.10	1.00	0.09	0.07	0.86	0.09	0.01	0.10	0.01
2	0.95	-0.22	-0.03	1.00	0.00	0.01	0.90	0.01	-0.01	0.11	-0.01	0.00
3	0.39	1.00	-0.03	-0.09	-0.63	-0.06	-0.07	-0.55	-0.06	-0.01	-0.05	-0.01

**Table 5.8:** SML5: Computed mode shapes by FDD, grouped by axes

Mode	X				Y				Z			
	A1	A2	A3	A4	A1	A2	A3	A4	A1	A2	A3	A4
1	-0.02	0.00	0.05	0.79	0.00	-0.07	0.05	0.72	0.00	0.04	1.00	0.30
2	0.97	0.52	-0.07	0.05	1.00	0.16	-0.07	0.06	0.95	-0.09	-0.01	0.03
3	0.10	-0.08	0.08	1.00	-0.17	0.09	0.09	0.95	-0.16	0.07	-0.94	0.47

**Figure 5.7:** SML5: Computed mode shapes by FDD, plots

## Damping Ratios

**Table 5.9:** SML5: Damping ratios from FDD, N is the number of datapoints that passed the mode excitation threshold of 20

Mode	$\bar{\zeta}$	$\zeta_{0.05}$	$\zeta_{0.95}$	$\sigma_{\zeta}$	N
1	1.450	1.122	1.857	0.170	1477
2	1.365	0.827	1.626	0.167	553
3	No results				56

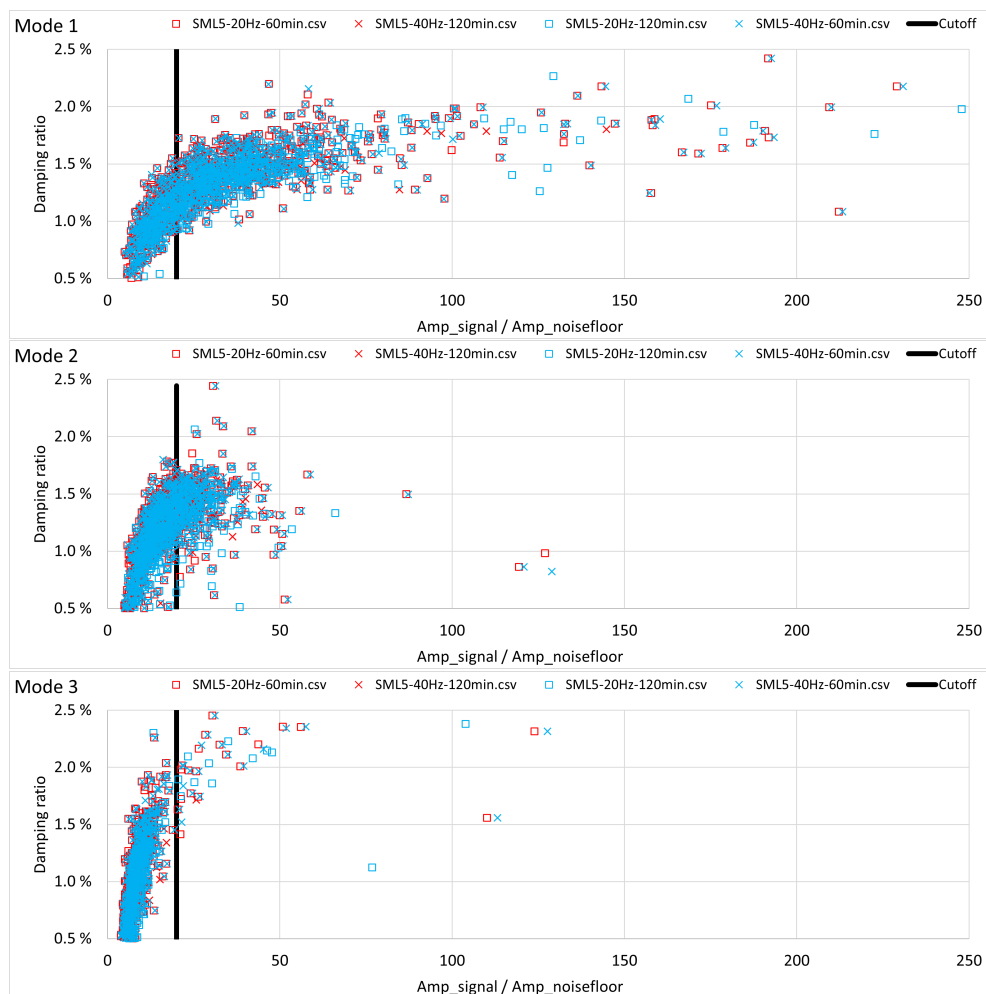


**Figure 5.8:** SML5: Damping ratio estimates from FDD, plotted against signal-to-noise ratio

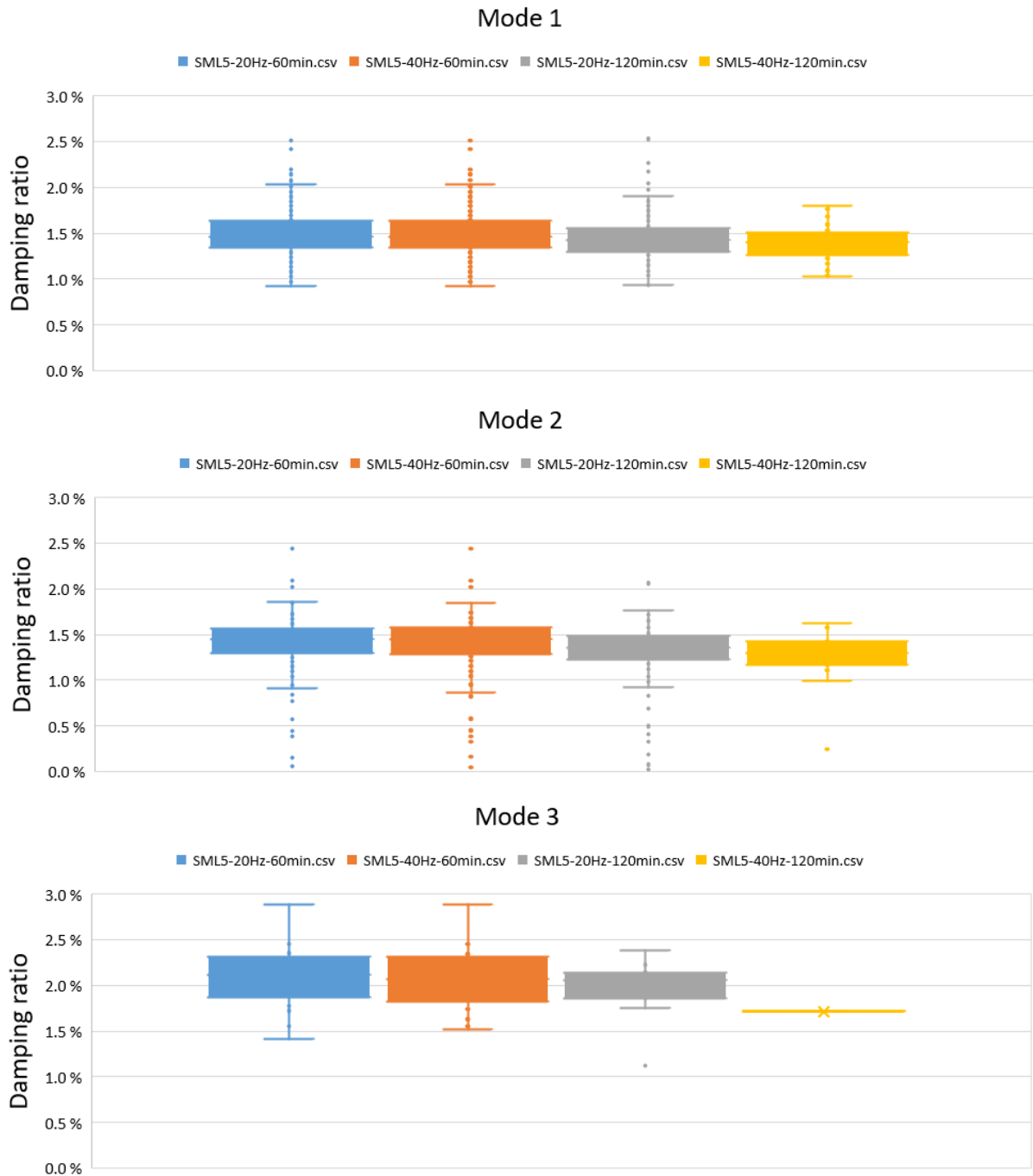


**Figure 5.9:** SML5: Box plot of damping ratio estimates, comparing the different pre-processing routines

Rayleigh damping approximation

Table 5.10: SML5: Rayleigh damping coefficients

	Opt. for mode 1 and 2
$\alpha$	0.0278
$\beta$	0.0072

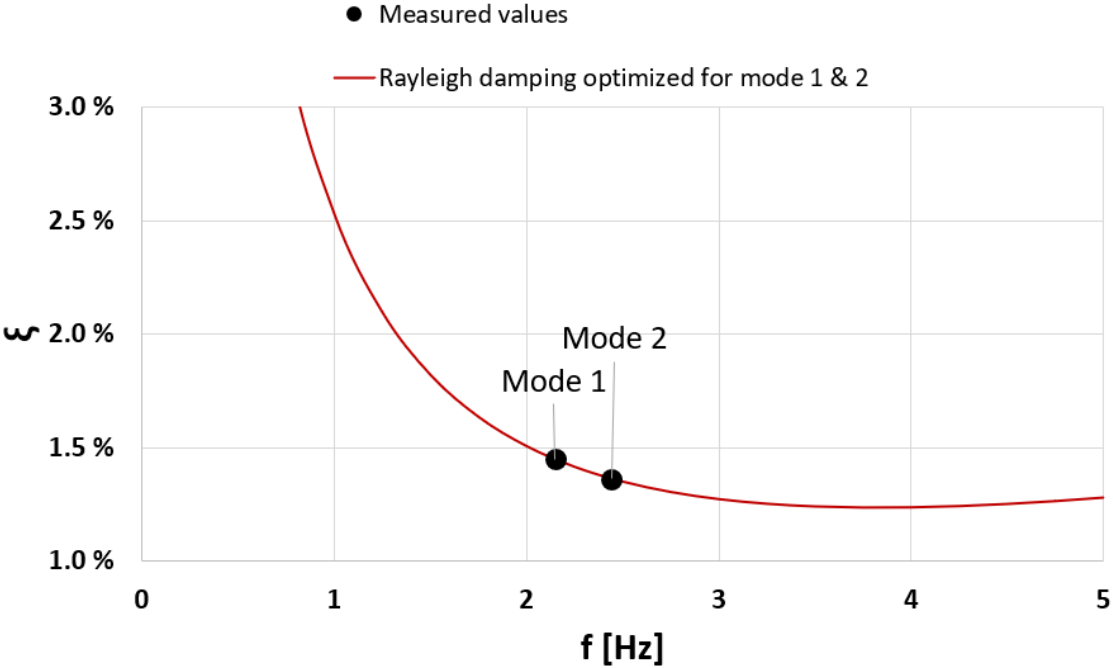
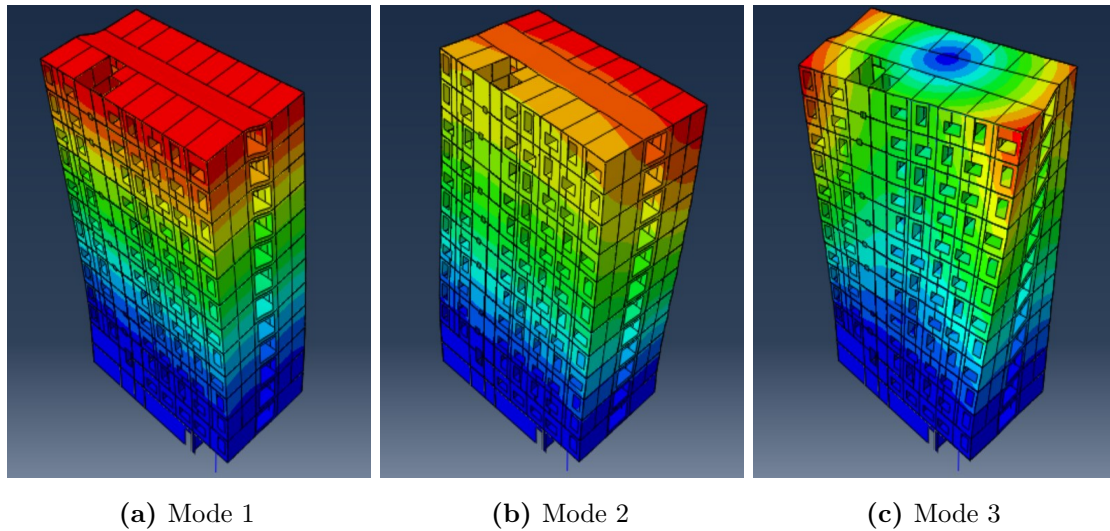


Figure 5.10: SML5: Rayleigh approximation of damping behaviour

## 5.2 Modeling Results

### 5.2.1 SML 3



**Figure 5.11:** The first three mode shapes of SML3

Figure 5.11 shows the first three mode shapes as calculated by Abaqus. Inspection of the plots, along with probing directional displacements and stress values leads to the following qualitative interpretation of the modal results:

- Mode 1: A blend of linear shear and 1st order bending about weak axis
- Mode 2: Mostly linear shear about strong axis
- Mode 3: Torsional rotation

## Frequency Optimization

The frequency optimization was performed for the two different mass configurations as described in subsection 4.9, and the results are presented in Table 5.11 and Figure 5.14. The values called 'Match' in Table 5.11 is calculated from the match criterion in equation (4.3). A comprehensive list of all frequency optimization trial runs can be found in Appendix B.

**Table 5.11:** SML3: Parametric models optimized for frequencies

Description	ASR	SSR	$f_1$ [Hz]	$MAC_1$	$f_2$ [Hz]	$MAC_2$	$f_3$ [Hz]	$MAC_3$	Match
<b>Target</b>			1.301		1.634		1.988		
<b>Mass conf. 1</b>	3.46	11.05	1.296	0.989	1.686	0.882	1.942	0.873	0.9772
<b>Mass conf. 2</b>	3.96	10.64	1.296	0.990	1.675	0.890	1.965	0.877	0.9841

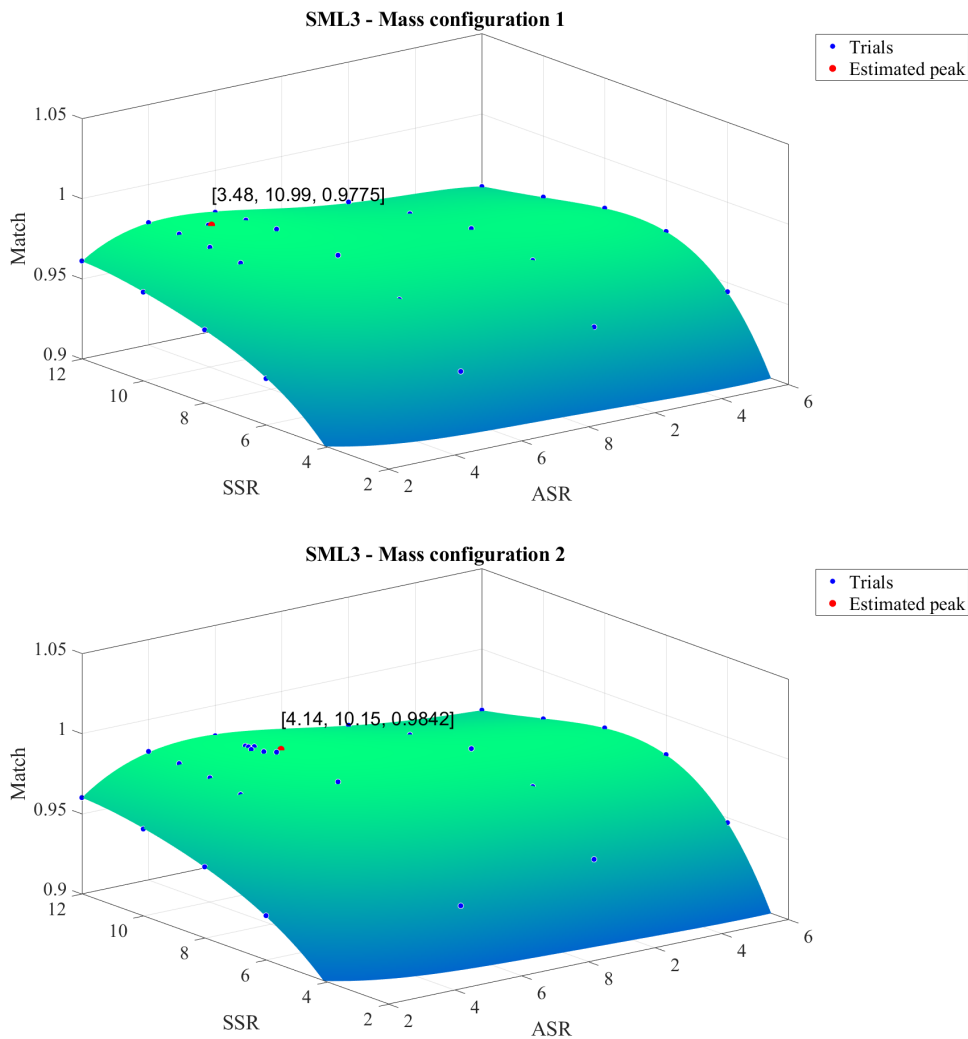


**Figure 5.12:** SML3: Stiffness parameter optimization

## Damping Optimization

The damping optimization was performed like described in subsection 4.9, and the match criterion used for calculating the 'Match'-value in Table 5.14 is given in equation (4.3). A comprehensive list of all damping optimization trial runs can be found in Appendix C.

**Table 5.12:** SML3: Damping optimized model, all damping is limited to viscous damping in connectors

Description	Axial damping	Sliding damping	$\zeta_1$	$\zeta_2$	$\zeta_3$	Match
		$\frac{N}{mm/s}$		%		
<b>Target</b>			1.54	1.44	1.6	
<b>Optimized model</b>	13000	200	1.51	1.55	1.58	0.9527



### 5.2.2 SML 5

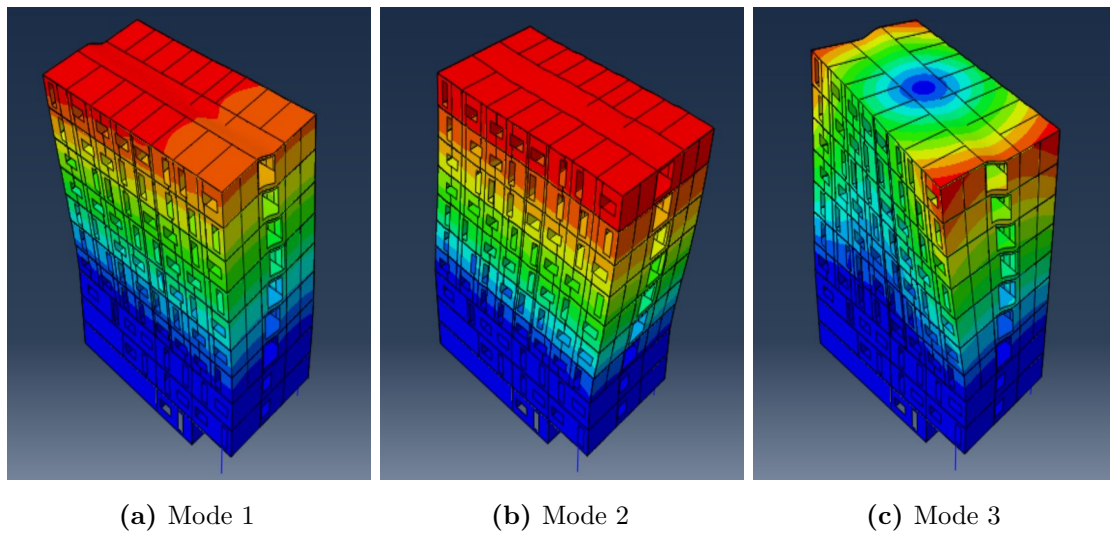


**Figure 5.13:** The first three mode shapes of SML5

Figure 5.13 shows the first 3 computed mode shapes of SML5. As expected, they are very similar in nature to SML3:

- Mode 1: A blend of linear shear and 1st order bending about weak axis
- Mode 2: Mostly linear shear about strong axis
- Mode 3: Torsional rotation

## Frequency Optimization

The frequency optimization was performed for the two different mass configurations as described in subsection 4.9, and the results are presented in Table 5.13 and Figure 5.14. The values called 'Match' in Table 5.13 is calculated from the match criterion in equation (4.3). A comprehensive list of all frequency optimization trial runs can be found in Appendix B.

**Table 5.13:** SML5: Parametric models optimized for frequencies

Description	ASR	SSR	$f_1$ [Hz]	$MAC_1$	$f_2$ [Hz]	$MAC_2$	$f_3$ [Hz]	$MAC_3$	Match
<b>Target</b>			2.150		2.443		2.924		
<b>Mass conf. 1</b>	2.00	4.00	2.162	0.962	2.526	0.981	2.767	0.936	0.9633
<b>Mass conf. 2</b>	2.00	4.00	2.156	0.961	2.532	0.981	2.818	0.934	0.9704

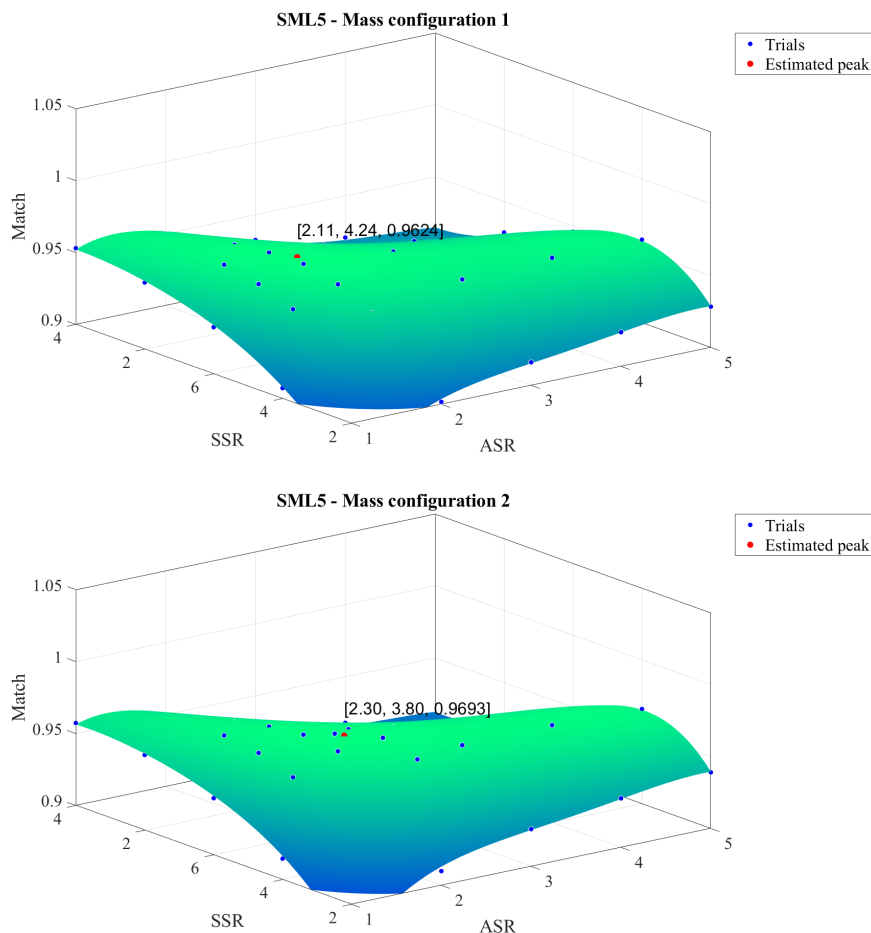


**Figure 5.14:** SML5: Stiffness parameter optimization

## Damping Optimization

The damping optimization was performed like described in subsection 4.9, and the match criterion used for calculating the 'Match'-value in Table 5.14 is given in equation (4.3). A comprehensive list of all damping optimization trial runs can be found in Appendix C.

**Table 5.14:** SML5: Damping optimized model, all damping is limited to viscous damping in connectors

Description	Axial damping	Sliding damping	$\zeta_1$	$\zeta_2$	$\zeta_3$	Match
		$\frac{N}{mm/s}$		%		
<b>Target</b>			1.45	1.37	???	
<b>Optimized model</b>	675	114	1.45	1.37	2.35	0.997

## 6 Discussion

### 6.1 Analysis of Measurements

When analyzing the experimental data with the FDD-method, only the lower modes yielded satisfactory results. Observing the periodograms in Figure 5.1 and Figure 5.6, tall and dominant peaks are observed for the first 3 modes, whereas higher modes are less pronounced for SML3, and outside of the plot range for SML5. Based on these results, it is reasonable to conclude that the structures' dynamic behaviour under normal operating conditions are dominated by the first three modes. This applies to both SML3 and SML5, which is to be expected, considering their similar shape, structural system and location. The results achieved for SML3 are relatively good. Natural frequencies, mode shapes and damping ratios for all 3 dominant modes are found with satisfactory accuracy. For SML5 however, the results are of significantly poorer quality compared to SML3: Only the mode 1 yields satisfactory results for damping ratios, mode 2 gives uncertain estimates, and the results for mode 3 are so poor that they practically are of no value at all.

The poor quality of the data-analysis results for SML5's damping ratios is thought to be due to the structure's dimensions and layout. As the first three floors have bearing walls comprised of concrete walls of 200mm and 250mm thickness, SML5 is essentially equivalent to a 7-story CLT-building. With a cross-section of roughly 14m x 25m, this gives a *height-to-width ratio* of approximately 1.5 and 0.8 for the weak and strong axes respectively, which is not particularly slender in the context of structural dynamics. This stubbiness likely means the building simply does not get significant modal excitation during normal operation in ambient wind conditions.

The assumed explanation for SML5's issues with quality of results suggests that instrumenting CLT structures that are as stubby as SML5 might be a waste of time if the goal is to determine damping ratios by means of OMA. However, it may be possible to use an experimental modal analysis (EMA) to determine the damping ratios of shorter buildings like SML5, but this has not been attempted on either SML3 or SML5. The estimation of mode frequencies and mode shapes does not require the same quality of data as the damping ratios, and these values are therefore significantly more reliable.

### 6.1.1 Comparison of Pre-processing Schemes

Analysing the plots in Figure 5.3, Figure 5.4, Figure 5.8, and Figure 5.9, it is clear that there is not much difference between the different pre-processing schemes.

There seems to be little to no benefit from choosing a higher down-sampled frequency. This is likely due to both sets having a frequency comfortably above the modes of interest. Choosing a higher than necessary down-sampled frequencies do not seem to meaningfully increase quality of results.

The choice of time series length does have an impact. While the benefit is small, there are clearly fewer outliers and in general, a tighter box plot. This strongly suggests that there is some merit in choosing longer time series, when performing the FDD-analysis.

## 6.2 Comparison of Empirical Results With Other Structures

Considering the measured base frequencies of the buildings and comparing them with predicted frequencies using the proposed trend in Figure 1.2 [12], a remarkably close fit is achieved. If one also considers that the concrete walls also have some degree of flexibility, the "effective" height of the buildings in the table would be slightly taller than just the height of the main CLT section. This slight increase in effective height would make the predictions even closer to the empirical measurements. All in all, it is fair to say that the base frequencies of both SML3 and SML5 are well within the expected range.

**Table 6.1:** Comparison of measured frequencies vs predicted frequencies by the trend proposed by [12]

Building	Number of CLT-storeys	Effective CLT height	$f_{meas}$	$f_{est} = 46/h$	Diff
SML3	11	33m	1.301 Hz	1.394 Hz	6.92%
SML5	7	21m	2.150 Hz	2.190 Hz	1.86%

As for damping, when looking at the trend in Figure 1.2, the expected values are approximately 1.6% and 1.8% for mode 1 for SML3 and SML5 respectively. While SML3 has a relatively good match with the expected value, the measured damping ratio for SML5 is significantly lower than the expected value. This does not necessarily invalidate the mode damping results for SML5; it could for instance be partly due to the increased effective slenderness in mode 1, as discussed in 6.3.1. As the trend in the data set in Figure 1.2 suggests that taller, and in turn more slender, structures have lower damping ratios, the increased "effective" height would lower the expected damping ratios somewhat. However, keeping in mind the poor results for mode 3 and to some extent mode 2 for SML5, it is

entirely possible that the correct explanation is that the computed damping ratio is off by some amount.

## 6.3 Modeling

### 6.3.1 Comments on Mode Shapes

**Mode 1** in both buildings have a computed mode shape that seems to be a blend of bending and linear shear. A possible explanation is that the buildings have a quite high effective slenderness about the weak axis. For both SML3 and SML5, the weak axis is significantly less stiff than what the outer dimensions of the structures normally would suggest. This is in part due to them both having a hallway running down the entire length of the building, as can be seen on Figure 1.4. Only the outer walls span the entire width of the building to create wide continuous shear walls. However, due to the large cutouts in each end, these outer walls effectively have nearly the same stiffness as two shorter separate shear walls. The result is a quite high apparent slenderness about the weak axis. For this reason a larger amount of bending in the mode shape for mode 1 is to be expected in both buildings.

Regarding **mode 2**, both buildings continuous shear walls running the entire length of the buildings, not only in the outer walls, but also along the central hallways. Also keeping in mind the rather low height-length ratio for both buildings, a shear dominated mode is to be expected.

**Mode 3** is a torsional mode, with rotation that increases roughly linearly with height above the concrete sections. This is essentially what one would expect from the 1st order rotational mode. One observation is that the centre of rotation for SML3 is shifted slightly away from the centre of the geometry. There are two main sources of asymmetry in the prepared model of SML3. First, the walls around the elevator shaft and main stairway have increased cross sectional dimensions. One would expect that this would attract the rotational centre towards the increased stiffness section. Second, the floors have cutouts for the elevator and stairs, without the mass of these installations being specifically compensated in these locations. As the floors in the model have quite high amounts of smeared dead-weight due to the concrete screed, this would cause a shift in mass centre in the same direction that the rotational centre has shifted. It would seem that this shift in mass distribution has a much more powerful effect than the increased stiffness around the elevator shaft.

SML5 was modeled without any cut outs in the floors, and there were no increased cross-sections around shafts, and unsurprisingly, there is no rotational asymmetry for SML5.

### 6.3.2 The Modeling Approach

While the modeling approach yielded sensible results with relatively good compliance with measured modal properties after parameter optimization, it made for a very cumbersome modeling experience. Handling and navigating through the high number discrete parts and connectors, is impractical, and thus this modelling approach is only practical in a parametric approach with scripts.

**Geometry creation,** the process of creating wall and floor parts; cutting out windows; doors and other openings; creating nodes to attach connectors to; and creating the connectors themselves, is a very slow process in Abaqus, even when completely automated. This may be because of a weakness in the Abaqus software, or it may just be unreasonable to expect any-FEM software to swiftly do this amount of work in this way. A work-around to this is to pre-generate the geometry and connections, and only changing the stiffness or mass properties between runs. While this saves a massive amount of time per run, this means that the model in its current implementation, is unfit for performing any parametric model updating that involves multiple changes in geometry.

**Running the FEM-analysis** did not take unreasonably long. For SML3, with a mesh element size of approx 300mm, this produces a mesh with around 220k elements. A complete modal frequency analysis, along with post processing of the results, took around 2 minutes on a 4-core desktop computer from around 2015.

### 6.3.3 Modeling Floors as a Single, Continuous Part

As mentioned in 5.2.1 and 5.2.2, both buildings have a very slender weak axis, which causes mode 1 to have a contribution from bending about the weak axis. Because the floors are modeled as single part, this creates additional stiffness in the bending modes, this effect is clearly visible from the bending of the floor part in ??Figure 5.13. This stiffness contribution from the floor parts increases the computed natural frequency for mode 1.

The widths of both SML3 and SML5 are relatively small ( $< 15m$ ), and it is possible that the floors are constructed using long CLT-floor elements spanning the entire width of the building. This would make the single part floors a valid modeling approach as the 2nd and 3rd modes are shear- and sliding dominated, and would not be affected by floors to the same degree as mode 1.

Specific details of how the floors are constructed were not available during work for this thesis, so it is difficult to conclude whether or not modeling the floors as a single part is wrong or not. A possible approach to investigate the significance of this decision is to

create a copy of the model with discrete floor parts spanning between the lengthwise walls, and compare the results. Unfortunately there was not enough time to explore this further in this thesis.

#### 6.3.4 The Use of Connectors

Using discrete connectors to model the connections between elements creates a believable model as the connectors to some degree represent the physical screws and brackets. In addition to this, it opens the possibility of operating with a more physically compatible values for the stiffness in connections; either as some stiffness per meter, or stiffness per fastener.

The practicality of such an approach is enticing. A designing engineer could predetermine some ASR and SSR that satisfy some modal criteria, and directly get the design stiffness to be used CLT-joints in construction that would satisfy the criteria. The values related to the sliding stiffness of connections are essentially directly transferable, but the axial stiffness is transferable, because this stiffness value captures both the compressive contact forces between the CLT-elements as well as the stiffness in the connectors themselves. This is the reason for the high values for the resulting optimized stiffness value by multiplying ASR with values in Table 4.1. The stiffness values are in the order of  $100kN/mm$  per connector which is without a doubt much higher than any normal type of fastener used for joining CLT-elements.

#### 6.3.5 Frequency Optimization

The parameter optimizations yield quite good results for both buildings, but the stiffness ratios ASR and SSR are quite different between the buildings. This is somewhat bad news regarding the predictive ability of the modeling approach proposed in this thesis. While this does not necessarily invalidate a discrete connector-based modeling technique, it does suggest that some refinement to the approach is needed, for instance coming up with a better scheme for the way connector stiffness is computed and distributed.

An observation is that both buildings yielded (marginally) better closer matches for frequency optimization when the non-structural mass was distributed only across floor faces, as opposed to when estimated outer wall mass from cladding, windows etc. was smeared across outer walls. This is surprising because one would expect that a finer control of the distribution of non-structural mass would give more accurate results. It is difficult to say whether this applies in general, but the experience from this thesis is at least that it might not be worthwhile to spend time dividing non-structural mass between walls and floors; gathering it per storey and smearing it across floors seems to work just fine.



As can be observed in the list of trial runs in Appendix B, ASR is more powerful for influencing mode 1, while SSR is more powerful for mode 2 and 3. This is thought to be due to the bending contribution to the mode shape in mode 1. A bending of the structure would induce compressive and tensile stress in the connectors between storeys, especially along the outer walls running the length of the building. A higher axial stiffness ratio in connectors would then increase the stiffness in this mode, whereas mode 2 and 3 would be less affected, so this observation fits expectations.

### 6.3.6 Damping Optimization

As mentioned in 4.2.2, the damping values of connectors are globally constant across the entire model, and do not scale with stiffness in connections of the cross sections they are attached to. This means that lowering ASR and SSR will increase the modal damping values, since a larger amount of structural deformation is happening in connectors, and thus a larger amount of movement is subjected to the constant viscous damping effect.

Following the damping optimization, one would therefore expect significantly lower optimized viscous damping values in SML5, compared to SML3. This is because in the frequency optimization process, lower optimized ASR and SSR was found for SML5 compared to SML3. This effect is indeed seen in the resulting optimized damping values. One should note that since no result was found for mode 3 damping in SML5, only the damping ratios mode 1 and 2 was included in the optimization for SML5.

Despite being very simple, the implementation using constant, global viscous damping values might not be the most accurate nor elegant. Instead, a different approach defining some percentage damping ratios, and letting a script compute which amount of viscous or structural damping value to add to each set of connectors might be better. Future refinement of the modeling approach using such a damping scheme could be worth looking at, if a convenient solution can be found.

## 7 Conclusions and Further Work

### 7.1 Conclusions

The ultimate goal for work done on this thesis was to obtain satisfactory estimates of the natural frequencies, mode shapes and damping ratios of the two CLT-buildings SML3 and SML5 in Tromsø, as well as developing a parametric model in order to explore the possibility of the modeling such structures using discrete parts and connectors.

#### 7.1.1 Data analysis by FDD

The results of the frequency domain decomposition (FDD) analysis indicates that the first three modes that dominates the behaviour of both buildings in operational conditions. The higher modes were not excited enough in the measurements to be able to gain accurate results, suggesting these modes are not particularly influential in the dynamic behaviour of these buildings in normal conditions.

While frequencies and mode shapes estimates seem reasonably reliable, damping ratios proved to be more tricky to extract, suggesting a higher demand for data quality and degree of modal excitation for damping estimation by means FDD. As is hinted at in the discussion, this might imply that instrumenting and measuring stubby buildings could be a waste of time, at least when analysing for if trying to determine damping ratios by FDD.

#### 7.1.2 Modeling with discrete connectors

The modeling technique is able to represent the actual behaviour of the structure reasonably well. The mode shape - compliance as measured by the MAC-values between measured mode shapes and computed mode shapes is quite good, despite not having influencing mode shapes this during model updating. After model updating 2 stiffness parameters and 2 damping parameters, both models are able to reproduce frequencies, mode shapes and damping for the first 3 modes reasonably well.

The predictive ability of the modeling approach as implemented in this thesis, might not be particularly strong. This is hinted from the discrepancy in the optimized parameters for the two models. Refinements to the implementations, especially related to how individual connectors are assigned stiffness, are likely necessary for this approach to have practical use in design.

## 7.2 Further Work

### 7.2.1 Data analysis

The technique performed for analysis the data for modal property extraction is by no means the only way to analyse the data. Other algorithms such as the time-domain based *Covariance based stochastic subspace identification*, *data driven stochastic subspace identification* and more exists. Other techniques might prove better suited for modal extraction on the data, and might even yield reliable results for higher modes. Furthermore, having results from various techniques will assist in proving (or disproving) the validity of the results and the FDD-implementation used in this thesis.

In the original data collected by NTNU and made available for this thesis, there have also been made wind measurements. This wind data has not analysed in any way during this thesis. There is great potential for more statistical analysis of this data. Correlations between the wind excitation, both amplitude and spectral composition, and structural response comes to mind.

Higher quality modal property estimates, and likely also results for higher modes than the first 3, can be achieved by performing shaker-experiments on the buildings. This would of course incur extra costs for NTNU for re-instrumentation of the structures and mounting shakers, but the data extracted will allow for a much greater understanding of the modal behaviour of SML3 and SML5.

### 7.2.2 Modeling

A possible next step in developing the modeling approach is refining the implementation, such as coming up with different and hopefully improved schemes to control connector stiffness and damping in connectors.

# Bibliography

- [1] Birgit Östman. “Fire safety in timber buildings”. In: Seminário Casas de Madeira, 2013.
- [2] Birgit Östman, Daniel Brandon, and Håkan Frantzich. “Fire safety engineering in timber buildings”. In: *Fire Safety Journal* 91 (2017).
- [3] Lizhen Huang et al. “Carbon emission of global construction sector”. In: *Renewable and Sustainable Energy Reviews* 81 (2018).
- [4] Francesca Pierobon et al. “Environmental benefits of using hybrid CLT structure in midrise non-residential construction: An LCA based comparative case study in the US Pacific Northwest”. In: *Journal of Building Engineering* 26 (2019), p. 100862.
- [5] Swedish wood. *The CLT Handbook*. Swedish wood, 2019.
- [6] Reinhard Brandner. “Production and Technology of Cross Laminated Timber (CLT): A state-of-the-art Report”. In: Focus Solid Timber Solutions - European Conference on Cross Laminated Timber (CLT), 2013.
- [7] R. Harris. *Wood Composites*. Woodhead Publishing, 2015.
- [8] Matteo Izzi et al. “Seismic behaviour of Cross-Laminated Timber structures: A state-of-the-art review”. In: *Engineering structures* 170 (2018).
- [9] Sayigh Ali. *The Importance of Wood and Timber in Sustainable Buildings*. Springer, 2022.
- [10] Enrico Lazzarini et al. “Comfort assessment of high-rise timber buildings exposed to wind-induced vibrations”. In: *Progress in Structural Engineering and Materials* (2021).
- [11] “State-of-the-Art Review on Damping in Wood-Frame Shear Wall Structures”. In: *Journal of Structural Engineering* 144 (2018).
- [12] Thomas Reynolds et al. “Design Parameters for Lateral Vibration of Multi-Storey Timber Buildings”. In: Conference: INTER International Network on Timber Engineering Research 2016, 2016.
- [13] Rune Abrahamsen et al. “Dynamic response of tall timber buildings under service load - the DynaTTB research program”. In: XI international conference on structural dynamics, 2021.

- [14] Norway's arctic student welfare organization. *Samskipnaden*. 2021. URL: <https://samskipnaden.no/en/housing/vare-boliger/dramsvegen-panorama> (visited on 05/26/2022).
- [15] Econor. *Smørbukkliia studentboliger 3*. 2021. URL: [https://econoras.no/no/prosjekter-view/boligbygg\\_afb7/smorbukklia-studentboliger-3\\_3673.html](https://econoras.no/no/prosjekter-view/boligbygg_afb7/smorbukklia-studentboliger-3_3673.html) (visited on 06/02/2022).
- [16] Econor. *Smørbukkliia studentboliger*. 2017. URL: [https://econoras.no/no/prosjekter-view/boligbygg\\_afb7/smorbukklia-studentboliger\\_5fc8.html](https://econoras.no/no/prosjekter-view/boligbygg_afb7/smorbukklia-studentboliger_5fc8.html) (visited on 06/02/2022).
- [17] Robert Halse Lervik and Sondre Kristiansen. "Assessing Wind Induced Dynamic Properties of Two Tall CLT Buildings in Tromsø". 2021.
- [18] Henrik Børde Elstrand and Håvard Nummedal Os. "A Parametric Study of Connection Modeling in Tall CLT Structures". 2021.
- [19] Swedish wood. *Design of timber structures*. Swedish wood, 2016.
- [20] *NS-EN 338:2016 Konstruksjonstrevirke - Fasthetsklasse*. Standard. 2016.
- [21] Isaac M. Daniel and Ori Ishai. *Engineering mechanics of composite materials*. Oxford university press, 2006.
- [22] MD Shahnevez, Marjan Popovski, and Tannert Thomas. "Deflection of cross-laminated timber shear walls for platform-type construction". In: *Engineering structures* (2020).
- [23] Jagmohan L. Humar. *Dynamics of structures, 2nd edition*. A.A. Balkema, 2002.
- [24] Joseph Tedesco, William G McDougal, and C Allen Ross. *Structural dynamics*. Pearson Education London, UK, 2000.
- [25] DA Rade and V Steffen Jr. "Structural dynamics and modal analysis". In: *EOLSS-Encyclopedia of Life Support* (2008).
- [26] A.L Kimball and D.E Lovell. "Internal friction in solids". In: *Physical Review* (1927).
- [27] Anil K. Chopra. *Dynamics of structures: Theory and Application to Earthquake engineering*. Pearson, 2017.
- [28] Rune Brincker and Carlos Ventura. *Introduction to Operational Modal Analysis*. Wiley, 2015.
- [29] Carlo Rainieri and Giovanni Fabbrocino. *Operational Modal Analysis of Civil Engineering Structures Modal Analysis of Civil Engineering Structures*. Springer, 2014.
- [30] The SciPy community. *SciPy Documentation*. 2022. URL: <https://scipy.org> (visited on 04/28/2022).
- [31] John Dempster. *The Laboratory Computer A Practical Guide for Physiologists and Neuroscientists*. Academic Press, 2001.
- [32] Gerhardt Heinzl, Albrecht Rudiger, and R. Schilling. "Spectrum and spectral density estimation by the Discrete Fourier transform (DFT)". In: *Max Planck Inst* (2002).

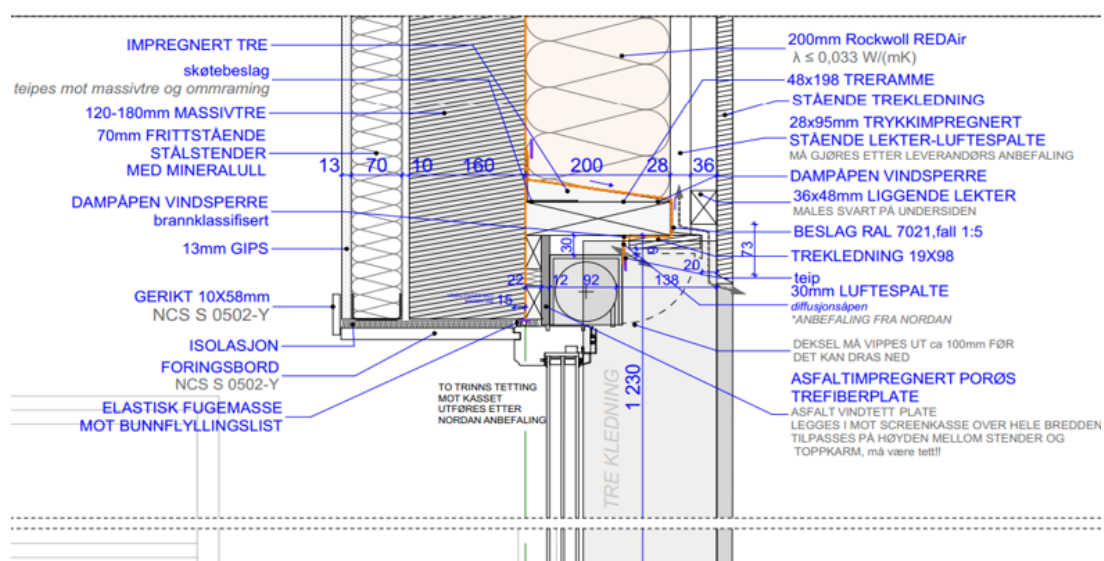
- [33] Fredric J. Harris. “On the Use of Windows for Harmonic Analysis With the Discrete Fourier Transform”. In: *Proceedings of the IEEE* (1978).
- [34] Peter D. Welch. “The Use of Fast Fourier Transform for the Estimation of Power Spectra: A Method Based on Time Averaging Over Short, Modified Periodograms”. In: *IEEE TRANSACTIONS ON AUDIO AND ELECTROACOUSTICS* (1967).
- [35] Rune Brincker, Carlos E Ventura, and Palle Andersen. “Damping Estimation by Frequency Domain Decomposition”. In: Proceedings of IMAC 19, 2001.
- [36] Kolbein Bell. *Finite Element Analysis of linear structural mechanics problems, 3rd edition*. Fagbokforlaget, 2013.
- [37] John O.Dow. *A Unified Approach to the Finite Element Method and Error Analysis Procedures*. Academic Press Inc, 1999.
- [38] Ted Belytschko et al. “Hourglass control in linear and nonlinear problems”. In: *Computer Methods in Applied Mechanics and Engineering* (1984).
- [39] O.C. Zienkiewicz, R.L. Taylor, and David Fox. *The Finite Element Method for Solid and Structural Mechanics (Seventh Edition)*. Butterworth-Heinemann, 2014.
- [40] Abaqus Inc. *Abaqus Analysis User’s Guide, chapter 23.6.2*. 2016. URL: <https://abaqus-docs.mit.edu/2017/English/SIMACAEELMRefMap/simaelm-c-shellelem.htm> (visited on 03/15/2022).
- [41] Abaqus Inc. *Abaqus Theory Manual, chapter 3.6.1*. 2013. URL: <http://130.149.89.49:2080/v6.13/books/stm/default.htm> (visited on 05/16/2022).
- [42] The NumPy community. *NumPy Documentation*. 2022. URL: <https://numpy.org> (visited on 04/28/2022).
- [43] Adam Reeve. *npTDMS Documentation*. 2022. URL: <https://pypi.org/project/npTDMS/> (visited on 04/28/2022).
- [44] Mathworks. *Signal processing toolbox*. 2021. URL: <https://mathworks.com/help/signal/> (visited on 04/28/2022).
- [45] Angelo Aloisio et al. “Dynamic identification and model updating of an eight-storey CLT building”. In: *Engineering Structures* 213 (2020).
- [46] Francesco Mirko Massaro et al. *Timber structures 2, lecture notes*. notes. 2021.
- [47] Abaqus Inc. *Common difficulties associated with contact modeling in Abaqus/Standard*. 2017. URL: <https://abaqus-docs.mit.edu/2017/English/SIMACAEITNRefMap/simaitn-c-contacttrouble.htm> (visited on 06/01/2022).
- [48] *NS 3470-1:1999 Prosjektering av trekonstruksjoner - Beregnings- og konstruksjonsregler - Del 1: Allmenne regler*. Standard. 1999.
- [49] *NS-EN 1992 1-1:2004+NA:2008 Eurokode 2 Prosjektering av betongkonstruksjoner Del 1-1: Allmenne regler og regler for bygninger*. Standard. 2008.
- [50] *NS-EN 1993-1-1:2005+A1:2014+NA:2015 Eurokode 3: Prosjektering av stålkonstruksjoner Del 1-1: Allmenne regler og regler for bygninger*. Standard. 2015.

# Appendices

# A Mass Configuration



## A.1 Estimation of Outer Wall Dead Mass



15mm trekledning	6.0 kg/m <sup>2</sup>
36x48 lekter cc 600	1.2 kg/m <sup>2</sup>
23x48 sløyfe cc 600	0.7 kg/m <sup>2</sup>
48x198 ramme + rockv	14.3 kg/m <sup>2</sup>
70mm isolasjon	1.2 kg/m <sup>2</sup>
13mm gips	9.0 kg/m <sup>2</sup>
<b>Sum</b>	<b>32.4 kg/m<sup>2</sup></b>

## A.2 SML3 Mass Calculations

### A.2.1 Mass Configuration 1

Floor data		Outerwall data	
Width	1.39E+04 mm	Outer wall area pr floor	2.35E+08 mm <sup>2</sup>
Length	2.53E+04 mm	Window area	5.50E+08 mm <sup>2</sup>
Area_g	3.51E+08 mm <sup>2</sup>	Window density	30 kg/m <sup>2</sup>
Cutout	1.84E+07 mm <sup>2</sup>	Window mass	16.5 T
Area_n	3.32E+08 mm <sup>2</sup>	Wall mass to distribute	3.90E-08 T/mm <sup>2</sup>

*Structural mass from abaqus*

Floor	Floor mass	Wall mass	Total mass	Lervikmass	Mass to add pr floor	Wall mass distributed	Mass pr area floor
	T	T	T	T	T	T	T/mm <sup>2</sup>
14	22.3		36.1	180.4	144.3	9.15	4.1E-07
13	22.3	27.6	51.0	143.3	92.35	9.15	2.5E-07
12	22.3	29.7	52.1	144.6	92.5	9.15	2.5E-07
11	22.3	29.9	53.0	145.7	92.75	9.15	2.5E-07
10	22.3	31.4	53.7	146.6	92.9	9.15	2.5E-07
9	22.3	31.4	54.5	146	91.55	9.15	2.5E-07
8	22.3	32.9	56.6	149.3	92.7	9.15	2.5E-07
7	22.3	35.7	58.1	151.4	93.35	9.15	2.5E-07
6	22.3	35.8	58.8	150.4	91.6	9.15	2.5E-07
5	22.3	37.2	60.7	153.1	92.4	9.15	2.5E-07
4	22.3	39.6	62.0	155	93.05	9.15	2.5E-07
3	191.0	39.7	320.7	398.4	77.7	9.15	2.1E-07
2	191.0	219.7	380.6	484.5	103.9	9.15	2.9E-07
1		159.5					

### A.2.2 Mass Configuration 2

Floor data	
Width	1.39E+04 mm
Length	2.53E+04 mm
Area_g	3.51E+08 mm <sup>2</sup>
Cutout	1.84E+07 mm <sup>2</sup>
Area_n	3.32E+08 mm <sup>2</sup>

*Structural mass from abaqus*

Floor	Floor mass	Wall mass	Total mass	Lervikmass	Mass to add pr floor	Wall mass distributed	Mass pr area floor
	T	T	T	T	T	T	T/mm <sup>2</sup>
14	22.3		36.1	180.4	144.3	0.00	4.3E-07
13	22.3	27.6	51.0	143.3	92.35	0.00	2.8E-07
12	22.3	29.7	52.1	144.6	92.5	0.00	2.8E-07
11	22.3	29.9	53.0	145.7	92.75	0.00	2.8E-07
10	22.3	31.4	53.7	146.6	92.9	0.00	2.8E-07
9	22.3	31.4	54.5	146	91.55	0.00	2.8E-07
8	22.3	32.9	56.6	149.3	92.7	0.00	2.8E-07
7	22.3	35.7	58.1	151.4	93.35	0.00	2.8E-07
6	22.3	35.8	58.8	150.4	91.6	0.00	2.8E-07
5	22.3	37.2	60.7	153.1	92.4	0.00	2.8E-07
4	22.3	39.6	62.0	155	93.05	0.00	2.8E-07
3	191.0	39.7	320.7	398.4	77.7	0.00	2.3E-07
2	191.0	219.7	380.6	484.5	103.9	0.00	3.1E-07
1		159.5					

## A.3 SML5 Mass Calculations

### A.3.1 Mass Configuration 1

Floor data		Outerwall data	
Width	1.35E+04 mm	Outer wall area pr floor	2.33E+08 mm <sup>2</sup>
Length	2.53E+04 mm	Window area	3.40E+08 mm <sup>2</sup>
Area_g	3.42E+08 mm <sup>2</sup>	Window density	30 kg/m <sup>2</sup>
Cutout	1.84E+07 mm <sup>2</sup>	Window mass	10.19631 Tonne
Area_n	3.24E+08 mm <sup>2</sup>	Wall mass to distribute	3.62E-08 T/mm <sup>2</sup>

*Structural mass from abaqus*

Floor	Floor mass	Wall mass	Total mass	Lervikmass	Mass to add pr floor	Wall mass distributed	Mass pr area floor
	T	T	T	T	T	T	T/mm <sup>2</sup>
11	17.2		28.2	102.8	74.57	8.43	2.0E-07
10	20.6	22.0	44.4	137.1	92.75	8.43	2.6E-07
9	20.6	25.5	47.2	138.8	91.65	8.43	2.6E-07
8	20.6	27.6	49.1	138.7	89.6	8.43	2.5E-07
7	20.6	29.4	49.0	139.6	90.6	8.43	2.5E-07
6	20.6	27.4	48.2	139.8	91.6	8.43	2.6E-07
5	20.6	27.8	50.0	140.7	90.75	8.43	2.5E-07
4	20.6	30.9	153.3	426.8	273.55	8.43	8.2E-07
3	150.0	234.4	380.2	520.2	140.05	8.43	4.1E-07
2	150.0	225.9	350.0	423.7	73.75	8.43	2.0E-07
1		174.0					

### A.3.2 Mass Configuration 2

Floor data	
Width	1.35E+04 mm
Length	2.53E+04 mm
Area_g	3.42E+08 mm <sup>2</sup>
Cutout	1.84E+07 mm <sup>2</sup>
Area_n	3.24E+08 mm <sup>2</sup>

*Structural mass from abaqus*

Floor	Floor mass	Wall mass	Total mass	Lervikmass	Mass to add pr floor	Wall mass distributed	Mass pr area floor
	T	T	T	T	T	T	T/mm <sup>2</sup>
11	22.9		33.9	102.8	68.9	0.00	2.1E-07
10	22.9	22.0	46.7	137.1	90.45	0.00	2.8E-07
9	22.9	25.5	49.5	138.8	89.35	0.00	2.8E-07
8	22.9	27.6	51.4	138.7	87.3	0.00	2.7E-07
7	22.9	29.4	51.3	139.6	88.3	0.00	2.7E-07
6	22.9	27.4	50.5	139.8	89.3	0.00	2.8E-07
5	22.9	27.8	52.3	140.7	88.45	0.00	2.7E-07
4	22.9	30.9	155.6	426.8	271.25	0.00	8.4E-07
3	22.9	234.4	253.1	520.2	267.15	0.00	8.3E-07
2	188.0	225.9	388.0	423.7	35.75	0.00	1.1E-07
1	188.0	174.0					

# B Parameter Optimization Results

## B.1 SML3

### B.1.1 Mass Configuration 1

Weight ->		1	0	1	0	1	0		
Target ->		1.301	1	1.634	1	1.988	1		
AxStiff	SIStiff	f1	MAC1	f2	MAC2	f3	MAC3	Match	
3.46	11.05	1.2959	0.9894	1.6859	0.8820	1.9422	0.8727	0.9772	
4.00	10.00	1.3065	0.9895	1.6833	0.8823	1.9379	0.8724	0.9772	
3.00	12.00	1.2836	0.9893	1.6854	0.8817	1.9429	0.8730	0.9763	
3.00	11.00	1.2803	0.9893	1.6767	0.8817	1.9321	0.8728	0.9760	
4.00	11.00	1.3105	0.9896	1.6935	0.8823	1.9505	0.8725	0.9760	
4.00	8.00	1.2960	0.9895	1.6571	0.8826	1.9056	0.8721	0.9746	
3.00	10.00	1.2765	0.9893	1.6666	0.8817	1.9196	0.8727	0.9746	
4.00	12.00	1.3140	0.9896	1.7024	0.8823	1.9615	0.8727	0.9740	
6.00	8.00	1.3293	0.9897	1.6750	0.8836	1.9258	0.8720	0.9737	
3.00	9.00	1.2719	0.9893	1.6549	0.8818	1.9049	0.8725	0.9716	
6.00	10.00	1.3403	0.9898	1.7017	0.8832	1.9584	0.8722	0.9692	
8.00	8.00	1.3476	0.9899	1.6848	0.8842	1.9368	0.8719	0.9688	
8.00	6.00	1.3304	0.9898	1.6450	0.8853	1.8884	0.8718	0.9680	
6.00	6.00	1.3126	0.9896	1.6357	0.8846	1.8777	0.8718	0.9676	
6.00	12.00	1.3482	0.9898	1.7211	0.8830	1.9823	0.8724	0.9627	
8.00	10.00	1.3590	0.9900	1.7116	0.8837	1.9697	0.8721	0.9620	
2.00	12.00	1.2316	0.9890	1.6553	0.8811	1.9108	0.8737	0.9612	
4.00	6.00	1.2801	0.9894	1.6184	0.8835	1.8580	0.8719	0.9607	
2.00	10.00	1.2251	0.9890	1.6371	0.8809	1.8878	0.8734	0.9555	
8.00	12.00	1.3671	0.9900	1.7312	0.8835	1.9937	0.8723	0.9548	
2.00	8.00	1.2158	0.9890	1.6121	0.8809	1.8564	0.8729	0.9457	
8.00	4.00	1.3005	0.9895	1.5786	0.8879	1.8081	0.8718	0.9442	
6.00	4.00	1.2835	0.9894	1.5698	0.8870	1.7978	0.8718	0.9398	
4.00	4.00	1.2526	0.9892	1.5537	0.8856	1.7792	0.8717	0.9297	
2.00	6.00	1.2019	0.9889	1.5751	0.8813	1.8102	0.8725	0.9291	
2.00	4.00	1.1777	0.9888	1.5133	0.8829	1.7338	0.8720	0.8987	
8.00	2.00	1.2315	0.9885	1.4357	0.8948	1.6379	0.8724	0.8727	
6.00	2.00	1.2165	0.9885	1.4283	0.8937	1.6289	0.8722	0.8675	
4.00	2.00	1.1890	0.9884	1.4146	0.8918	1.6124	0.8720	0.8572	
2.00	2.00	1.1219	0.9881	1.3801	0.8879	1.5721	0.8718	0.8298	

## B.1.2 Mass Configuration 2

		Weight ->	1	0	1	0	1	0		
		Target ->	1.301	1	1.634	1	1.988	1		
AxStiff	SIStiff	f1	MAC1	f2	MAC2	f3	MAC3	Match		
3.96	10.64	1.2956	0.9899	1.6745	0.8898	1.9652	0.8767	0.9841		
3.90	10.80	1.2948	0.9899	1.6752	0.8898	1.9662	0.8767	0.9839		
3.90	10.70	1.2944	0.9899	1.6743	0.8898	1.9650	0.8767	0.9840		
3.85	10.50	1.2924	0.9899	1.6716	0.8897	1.9617	0.8767	0.9842		
4.00	10.00	1.2940	0.9899	1.6683	0.8899	1.9574	0.8766	0.9847		
3.90	10.20	1.2924	0.9899	1.6692	0.8898	1.9586	0.8766	0.9844		
4.00	12.00	1.3014	0.9899	1.6872	0.8897	1.9812	0.8768	0.9811		
6.00	8.00	1.3166	0.9901	1.6602	0.8915	1.9452	0.8763	0.9830		
3.00	12.00	1.2713	0.9897	1.6704	0.8890	1.9624	0.8771	0.9801		
6.00	10.00	1.3275	0.9902	1.6865	0.8909	1.9781	0.8765	0.9778		
3.00	11.00	1.2680	0.9897	1.6618	0.8890	1.9515	0.8769	0.9794		
8.00	8.00	1.3348	0.9903	1.6698	0.8921	1.9564	0.8763	0.9783		
3.00	10.00	1.2642	0.9897	1.6518	0.8891	1.9389	0.8768	0.9774		
4.00	8.00	1.2836	0.9899	1.6424	0.8904	1.9248	0.8764	0.9799		
8.00	10.00	1.3460	0.9903	1.6964	0.8916	1.9895	0.8764	0.9702		
6.00	12.00	1.3353	0.9902	1.7058	0.8907	2.0022	0.8766	0.9701		
3.00	9.00	1.2597	0.9897	1.6401	0.8892	1.9241	0.8767	0.9738		
8.00	6.00	1.3177	0.9902	1.6304	0.8933	1.9075	0.8761	0.9754		
6.00	6.00	1.3000	0.9900	1.6211	0.8926	1.8966	0.8761	0.9731		
8.00	12.00	1.3540	0.9904	1.7158	0.8913	2.0137	0.8766	0.9620		
2.00	12.00	1.2198	0.9893	1.6405	0.8878	1.9300	0.8776	0.9602		
4.00	6.00	1.2679	0.9898	1.6040	0.8913	1.8768	0.8762	0.9630		
2.00	10.00	1.2133	0.9893	1.6225	0.8878	1.9068	0.8773	0.9543		
2.00	8.00	1.2042	0.9893	1.5977	0.8880	1.8751	0.8770	0.9445		
8.00	4.00	1.2881	0.9899	1.5645	0.8959	1.8265	0.8762	0.9467		
6.00	4.00	1.2713	0.9898	1.5559	0.8951	1.8161	0.8761	0.9415		
2.00	6.00	1.1904	0.9893	1.5611	0.8887	1.8285	0.8767	0.9278		
4.00	4.00	1.2406	0.9896	1.5399	0.8936	1.7973	0.8761	0.9301		
2.00	4.00	1.1664	0.9892	1.4999	0.8905	1.7513	0.8763	0.8973		
8.00	2.00	1.2199	0.9891	1.4230	0.9025	1.6548	0.8766	0.8727		
6.00	2.00	1.2050	0.9891	1.4156	0.9015	1.6456	0.8765	0.8671		
4.00	2.00	1.1777	0.9890	1.4020	0.8997	1.6289	0.8763	0.8565		
2.00	2.00	1.1112	0.9887	1.3679	0.8959	1.5882	0.8761	0.8285		

## B.2 SML5

### B.2.1 Mass Configuration 1

Weight ->		1	0	1	0	1	0		
Target ->		2.150	1	2.443	1	2.924	1		
AxStiff	SIStiff	f1	MAC1	f2	MAC2	f3	MAC3	Match	
2.00	4.00	2.1624	0.9619	2.5256	0.9805	2.7673	0.9361	0.9633	
2.11	4.23	2.1807	0.9612	2.5466	0.9807	2.7886	0.9343	0.9628	
2.00	4.50	2.1811	0.9609	2.5589	0.9805	2.8013	0.9340	0.9625	
1.50	4.50	2.1208	0.9605	2.5266	0.9792	2.7566	0.9372	0.9607	
2.00	5.00	2.1982	0.9604	2.5879	0.9807	2.8343	0.9325	0.9593	
3.00	4.00	2.2287	0.9617	2.5617	0.9818	2.8135	0.9319	0.9587	
4.00	3.00	2.2056	0.9632	2.4890	0.9821	2.7348	0.9342	0.9583	
5.00	3.00	2.2287	0.9632	2.5019	0.9826	2.7526	0.9329	0.9577	
2.00	3.50	2.1362	0.9620	2.4841	0.9801	2.7160	0.9375	0.9576	
3.00	3.00	2.1697	0.9630	2.4691	0.9814	2.7074	0.9362	0.9565	
1.50	4.00	2.1017	0.9610	2.4933	0.9789	2.7187	0.9388	0.9558	
1.00	6.00	2.0563	0.9587	2.5448	0.9772	2.7641	0.9390	0.9530	
4.00	4.00	2.2668	0.9619	2.5827	0.9825	2.8425	0.9298	0.9517	
2.00	6.00	2.2254	0.9598	2.6348	0.9810	2.8879	0.9302	0.9498	
1.50	3.50	2.0786	0.9616	2.4533	0.9787	2.6735	0.9406	0.9469	
2.00	3.00	2.1057	0.9627	2.4343	0.9799	2.6594	0.9397	0.9464	
1.00	5.00	2.0337	0.9593	2.5004	0.9767	2.7140	0.9411	0.9463	
5.00	4.00	2.2914	0.9620	2.5964	0.9829	2.8614	0.9284	0.9461	
3.00	5.00	2.2688	0.9608	2.6262	0.9821	2.8874	0.9287	0.9457	
4.00	5.00	2.3085	0.9610	2.6481	0.9828	2.9178	0.9265	0.9355	
1.50	3.00	2.0499	0.9623	2.4045	0.9784	2.6182	0.9428	0.9333	
1.00	4.00	2.0025	0.9603	2.4408	0.9762	2.6467	0.9439	0.9324	
3.00	6.00	2.2980	0.9602	2.6742	0.9823	2.9425	0.9263	0.9323	
5.00	5.00	2.3340	0.9611	2.6623	0.9832	2.9374	0.9251	0.9283	
5.00	2.00	2.1254	0.9651	2.3509	0.9822	2.5797	0.9396	0.9283	
4.00	2.00	2.1046	0.9651	2.3392	0.9817	2.5637	0.9407	0.9238	
4.00	6.00	2.3389	0.9604	2.6967	0.9830	2.9737	0.9240	0.9209	
3.00	2.00	2.0721	0.9650	2.3212	0.9808	2.5390	0.9426	0.9161	
5.00	6.00	2.3652	0.9605	2.7113	0.9834	2.9940	0.9225	0.9131	
1.00	3.00	1.9560	0.9616	2.3550	0.9755	2.5503	0.9477	0.9073	
2.00	2.00	2.0151	0.9652	2.2903	0.9795	2.4988	0.9459	0.9017	
1.00	2.00	1.8781	0.9638	2.2177	0.9747	2.3965	0.9532	0.8621	

## B.2.2 Mass Configuration 2

		Weight ->	1	0	1	0	1	0		
		Target ->	2.150	1	2.443	1	2.924	1		
AxStiff	SIStiff	f1	MAC1	f2	MAC2	f3	MAC3	Match		
2.00	4.00	2.1560	0.9610	2.5318	0.9808	2.8183	0.9339	0.9704		
2.24	3.86	2.1705	0.9613	2.5323	0.9811	2.8219	0.9334	0.9703		
2.50	3.50	2.1706	0.9619	2.5120	0.9813	2.8010	0.9339	0.9702		
1.50	4.50	2.1151	0.9601	2.5334	0.9798	2.8117	0.9351	0.9678		
4.00	3.00	2.2026	0.9629	2.4961	0.9824	2.7917	0.9331	0.9678		
2.50	4.00	2.1959	0.9613	2.5533	0.9815	2.8488	0.9322	0.9676		
2.00	3.50	2.1317	0.9616	2.4910	0.9806	2.7712	0.9356	0.9674		
2.00	4.50	2.1760	0.9605	2.5659	0.9809	2.8577	0.9325	0.9674		
3.00	3.00	2.1662	0.9627	2.4761	0.9817	2.7634	0.9347	0.9671		
5.00	3.00	2.2259	0.9630	2.5091	0.9828	2.8100	0.9320	0.9659		
1.50	4.00	2.0963	0.9606	2.5000	0.9796	2.7733	0.9365	0.9643		
2.50	3.00	2.1392	0.9626	2.4614	0.9812	2.7425	0.9359	0.9638		
3.00	4.00	2.2246	0.9614	2.5688	0.9820	2.8710	0.9309	0.9627		
2.00	5.00	2.1928	0.9601	2.5949	0.9810	2.8912	0.9312	0.9618		
1.00	6.00	2.0492	0.9582	2.5512	0.9781	2.8181	0.9362	0.9573		
2.00	3.00	2.1015	0.9623	2.4412	0.9804	2.7138	0.9376	0.9565		
1.50	3.50	2.0735	0.9612	2.4600	0.9794	2.7273	0.9381	0.9559		
4.00	4.00	2.2631	0.9616	2.5900	0.9826	2.9010	0.9292	0.9536		
1.00	5.00	2.0270	0.9589	2.5069	0.9778	2.7673	0.9382	0.9523		
2.00	6.00	2.2196	0.9594	2.6419	0.9812	2.9455	0.9292	0.9492		
5.00	4.00	2.2880	0.9618	2.6038	0.9830	2.9205	0.9280	0.9469		
3.00	5.00	2.2642	0.9605	2.6334	0.9822	2.9460	0.9281	0.9454		
1.50	3.00	2.0451	0.9619	2.4112	0.9792	2.6713	0.9400	0.9422		
1.00	4.00	1.9963	0.9598	2.4472	0.9774	2.6991	0.9407	0.9394		
5.00	2.00	2.1237	0.9649	2.3579	0.9825	2.6344	0.9378	0.9390		
4.00	2.00	2.1026	0.9648	2.3461	0.9821	2.6178	0.9388	0.9341		
4.00	5.00	2.3043	0.9608	2.6555	0.9828	2.9773	0.9263	0.9340		
3.00	6.00	2.2930	0.9599	2.6815	0.9824	3.0019	0.9260	0.9301		
5.00	5.00	2.3302	0.9609	2.6698	0.9832	2.9976	0.9251	0.9263		
3.00	2.00	2.0697	0.9647	2.3280	0.9814	2.5923	0.9402	0.9259		
4.00	6.00	2.3344	0.9601	2.7042	0.9830	3.0341	0.9241	0.9179		
1.00	3.00	1.9505	0.9612	2.3613	0.9769	2.6013	0.9440	0.9145		
2.00	2.00	2.0111	0.9644	2.2963	0.9800	2.5474	0.9429	0.9099		
5.00	6.00	2.3610	0.9602	2.7189	0.9833	3.0550	0.9229	0.9098		
1.00	2.00	1.8737	0.9634	2.2239	0.9764	2.4453	0.9489	0.8692		



# C Damping Optimization Results

## C.1 SML3

		Weight ->	1	1	1		
		Target ->	1.54 %	1.44 %	1.63 %		
AxDam	SI Damp	$\zeta_1$	$\zeta_2$	$\zeta_3$	Match		
13000	200	1.51 %	1.55 %	1.58 %	0.9527		
13000	150	1.48 %	1.49 %	1.52 %	0.9513		
14000	100	1.57 %	1.53 %	1.54 %	0.9501		
15000	100	1.68 %	1.63 %	1.64 %	0.9061		
12000	400	1.48 %	1.68 %	1.80 %	0.8867		
10000	500	1.31 %	1.59 %	1.75 %	0.8865		
15000	200	1.72 %	1.75 %	1.79 %	0.8473		
15000	300	1.76 %	1.86 %	1.94 %	0.7803		
15000	400	1.81 %	1.98 %	2.10 %	0.7099		
2000	1000	0.65 %	1.37 %	1.71 %	0.6635		
5000	500	0.76 %	1.09 %	1.25 %	0.6489		
1000	1000	0.54 %	1.27 %	1.61 %	0.6183		
100	100	0.05 %	0.13 %	0.16 %	0.0734		
0	0	0.00 %	0.00 %	0.00 %	0.0000		

## C.2 SML5

		Weight ->	1	1	0		
		Target ->	1.45 %	1.37 %	1.50 %		
AxDam	SI Damp	$\zeta_1$	$\zeta_2$	$\zeta_3$	Match		
675	114	1.45 %	1.37 %	2.35 %	0.9970		
675	113	1.44 %	1.36 %	2.33 %	0.9948		
675	115	1.45 %	1.38 %	2.36 %	0.9922		
690	115	1.47 %	1.39 %	2.37 %	0.9855		
750	110	1.49 %	1.37 %	2.34 %	0.9824		
700	115	1.48 %	1.39 %	2.38 %	0.9807		
800	100	1.46 %	1.31 %	2.22 %	0.9705		
800	110	1.53 %	1.40 %	2.38 %	0.9573		
900	100	1.55 %	1.37 %	2.31 %	0.9532		
1000	100	1.64 %	1.41 %	2.39 %	0.9065		
100	100	0.83 %	0.95 %	1.66 %	0.6284		
0	0	0.00 %	0.00 %	0.00 %	0.0000		
1000	1000	8.29 %	9.51 %	16.66 %	-4.3796		

